FACULDADE DE ENGENHARIA DA UNIVERSIDADE DO PORTO

Design of an Electric Powertrain for an All-Terrain Vehicle

Gabriel Vicente Cerqueira Ribeiro

DISSERTATION

FINAL REPORT

DISSERTATION

Supervisor: Prof. Dr. Adriano da Silva Carvalho

October 2016

Resumo

O principal objetivo desta dissertação é o desenvolvimento e implementação de um sistema de tração elétrica totalmente operacional para um veículo todo-o-terreno (VTT).

O documento inicia com uma introdução ao tema, onde está apresentada a motivação para o projeto, seguida de uma análise das tarefas que foram desenvolvidas durante o tempo de execução desta dissertação. Este documento apresenta o veículo tornado elétrico e analisa a sua construção mecânica, resultando deste estudo os cálculos necessários nas fases mais avançadas do projeto.

Os requisitos mínimos que o veículo todo-o-terreno deve cumprir estão especificados pelo autor da dissertação e devidamente justificados no mesmo capítulo.

Com os requisitos prévios em mente, é executado um estudo das diferentes tipologias de motores adequados à implementação de sistemas de tração elétrica, culminando o capítulo numa escolha justificada do tipo de motor a estudar e implementar.

É depois executada uma breve análise de baterias, com o objetivo de escolher o tipo e os aspetos de projeto do "pack" de baterias a utilizar, de modo a cumprir totalmente com os requisitos.

Após se ter decidido relativamente ao motor e "pack" de baterias, são estudados os conversores implementados para realizar os andares de conversão de potência. As tipologias mais comuns são comparadas, com o intuito de optar pelas mais vantajosas para a aplicação em mãos.

O motor a desenvolver e utilizar na fase de implementação do projeto é estudado e projetado, com foco nos componentes utilizados na sua criação.

O controlo do conversor responsável pela operação do motor é um dos fatores com maior influência no funcionamento do VTT. Com isto em conta, são apresentados ao leitor os tipos de controlo existentes e o funcionamento do motor. Um dos métodos é escolhido, simulado e implementado.

Todos os componentes utilizados na implementação do sistema, tal como plataformas de controlo, sensores, conexões elétricas, entre outros, são apresentados num capítulo específico.

A dissertação termina com uma conclusão, onde está presente uma discussão dos resultados e uma análise incidente no trabalho que poderá ser executado no futuro de modo a melhorar a operação e fiabilidade do sistema.

Abstract

The main goal of this dissertation is the development and implementation of a fully electric functional traction system for an All-Terrain Vehicle (ATV).

The dissertation starts with an introduction, where the motivation for the project is exposed. It is then presented an overview of the tasks that were developed over the time at which this dissertation was created. This document presents the vehicle that was made electric and analyses its mechanical construction, providing the calculations needed.

The minimum requirements of the electric ATV are calculated and presented. These requirements are specified by the author of the dissertation and are justified in the same chapter.

With the previous determined requirements in mind, there is a study of the different topologies of rotary motors that can be used in traction systems, culminating in a justified choice of the type of motor to study and implement.

An analysis of the batteries is made, in order to choose the type of batteries and the main project aspects that these need to have, in order to fulfil the requirements completely.

Having been decided the motor and battery pack, a discussion is presented on the power converters used. The most common power converters are pondered, based on their advantages and disadvantages, achieving a decision on which to employ in this given application.

The motor used in the implementation is studied and designed. Its components were created and assembled, so as to achieve a final motor that is used in the validation phase of the project.

The control of the converter responsible for the operation of the motor is one of the most influential aspects in the response of the ATV. That said, it is presented to the reader the detailed operation of the motor and various methods of control. One method is chosen and simulated, before being implemented.

Everything related to the physical implementation of the system, such as control platforms, sensors, connections, among others, is presented in a chapter specifically dedicated for that effect.

The dissertation ends with a discussion of the results achieved in the implementation and an overview of the work that can be done in the future to improve the system.

Acknowledgements

Poderia mentir e dizer que não devo nada a ninguém, que gerei todo este trabalho sozinho e sem qualquer tipo de contributo por parte de quem me rodeia. Mas não se deve mentir. Isso foi uma das coisas que os meus pais me ensinaram, entre oportunidades dadas e sacrifícios vividos. É a eles que devo o primeiro "muito obrigado". Completamente indispensável na minha educação e desencaminhamento dos estudos em dias soalheiros, mostra alguma da loucura em mim impingida. A minha irmã é outra das pessoas a quem devo imenso. Expresso desta forma, o meu total orgulho em ser sua cobaia e agradeço todo o permanente apoio. Numa última nota de agradecimento para a família, não posso passar sem mencionar gente como Mindinha, Isidro, Célia, Ricardo, Diogo, Conceição, Milheiro, os meus padrinhos e os já típicos "tios e primos de Fraumssa".

Muito obrigado aos meus amigos de Rubras City, Ana Isabel, Kiko Mauzão, Vítor, Ana, Maria, Robinho, já são mais de 11 anos de aulas, cafés, gozo mútuo e tudo o resto que nos faz ter uma idade mental de 8 anos de cada vez que estamos juntos. Que nunca acabe.

Posso dizer que o curso instruiu-me em várias áreas do conhecimento, mas não posso dizer que espere que tal conhecimento tenha nem metade da longevidade que vejo algumas das amizades que fiz na FEUP terem. Muito obrigado Faíscas Pataniscas, principalmente a gente como Ramos, Correu, Bilassa, Bender, Marciana, MPT, Inhes, Tenas, Xóninhas, Cámones. Tenho a certeza que para o ano ou a ideia da autocaravana ou a casa no Alentejo vai acontecer. Um grande obrigado também à Risoliana, uma madrinha e amiga espetacular. Sei que sem vocês, não teria chegado tão longe no curso, tão depressa.

À malta com quem fui morcego, foi um prazer e um privilégio ser discriminado convosco.

Tenho dever de agradecer à malta da 02, robótica e 104 por todos os conselhos e ajuda no projeto, verdadeiramente cruciais para que a dissertação evoluísse e chegasse ao patamar que chegou (isto escalou, raios!). Um obrigado muito sincero ao Ricardo e ao Tiago Pereira, parceiros de crime no maior desfalque financeiro algum dia registado nas contas da FEUP ("E daquela vez que entreguei ao Isidro uma fatura de 4500€ em bobines?").

Um muito obrigado também para o meu orientador, professor Adriano Carvalho, não só pela orientação neste projeto e amizade demonstrada, mas também por me fazer aperceber do que é preciso para se ser engenheiro e pela oportunidade de poder entrar no mercado de trabalho já na minha área de especialização.

Ao engenheiro Rui Pinho e ao grupo PPRR, um muito obrigado por terem impulsionado a evolução deste projeto, principalmente na construção do "Scrappy".

Só sinto que os agradecimentos estarão completos com uma grande palavra de apreço a certas pessoas que normalmente passam despercebidas a muita gente, no dia-a-dia, mas que fazem trabalhos da mais alta importância e sem as quais nada da parte da implementação seria possível. Falo de pessoas como Isidro Ribeiro, Pedro Alves, Rui Carvalho.

Muito obrigado e um bem-haja a todos,
Gabriel

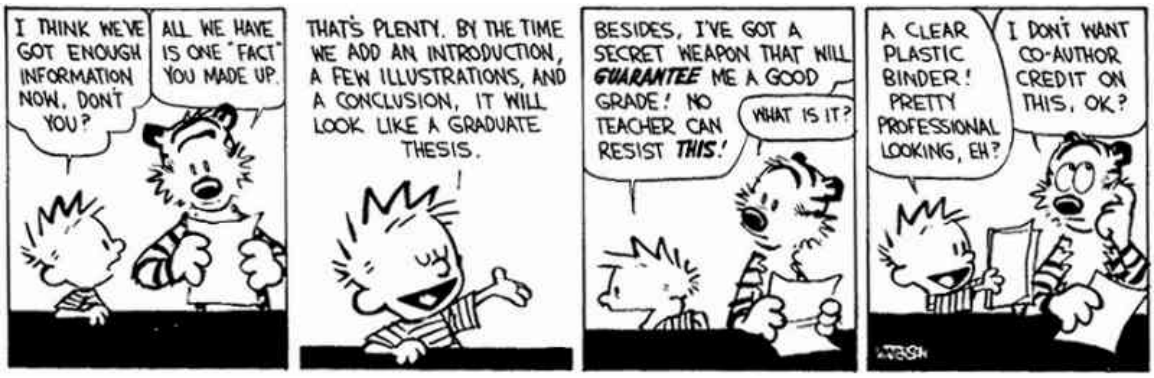

Bill Watterson, in *Calvin and Hobbes*

Contents

List of Figures

List of Tables

Abbreviations and Symbols

ADC	Analog Digital Converter
ATV	All-Terrain Vehicle
CAD	Computer Aided Design
CAM	Computer Aided Manufacturing
DAC	Digital Analog Converter
DC	Direct Current
DITC	Direct Instantaneous Torque Control
EMF	Eletromotive force
EMI	Electromagnetic Interference
EV	Electric Vehicle
FEA	Finite Element Analysis
ICE	Internal Combustion Engine
IM	Induction Motor
LED	Light Emitting Diode
PDI	Preparação da Dissertação
PMSM	Permanent Magnet Synchronous Motor
RMS	Root Mean Square
RPM	Revolutions per minute
SPC	Single Pulse Control
SRM	Switched Reluctance Motor
TSF	Torque Sharing Function
VTT	Veículo Todo-o-Terreno

ω_m	Angular velocity of the motor
V_{DC}	Voltage of the DC bus
η	Efficiency
θ_r	Angular position of the rotor
R_s	Resistance of the stator windings
T_e	Electromagnetic Torque
T_l	Torque Load
λ	Flux Linkage
L_u	Unaligned inductance
L_a	Aligned inductance
θ_{ON}	Commutation ON angle
θ_{OFF}	Commutation OFF angle
R_p	Number of rotor poles
S_p	Number of stator poles

Chapter 1

Introduction

Starting by a contextualization, where the author presents what is the scope of the dissertation and the overall system, this chapter will evolve and show the reader the motivation for the study and design of the proposed topic. The chapter will then conclude with the goals set up for completion during the time in which this dissertation is developed, as well as the structure of the final dissertation document.

1.1 Context

This dissertation was developed by the author during the second semester of the academic year of 2015/2016 and aims to design and implement a complete, fully electric power train for an All-Terrain Vehicle. Particularly, the vehicle in which this dissertation focuses is the HONDA FOURTRAX 250cc, existing in FEUP.

This topic implies a study and project that covers several areas of electrical and mechanical engineering. So, in a way to contextualize the reader for the problem that is going to be approached, the following lines show what are the main aspects that will be debated along this dissertation. To make the understanding of the topic easier, they are divided in two areas, mentioned previously: one electrical and one mechanical.

Starting with the mechanical area, it can be said that it is crucial in two stages of the project: in the start of the project, when requirements need to be established, and in the later stages of the project, when the implementation starts to take part. All of the mechanical analysis is to be done so to keep at all times the maximum of safety for the user, at the same time that a prototype of an ATV with better performance and superior characteristics than before is achieved.

This can only be done after an analysis of the components constituting the vehicle and after a mechanical transformation, so to assure that the space, although small, is used efficiently for the fixation of the motor, controller, batteries and electronics. Having also in mind more sensible aspects of the electrical part of the project, a strategic assembly of the components will be accomplished, so to reduce electric cables and exposed connectors and components, and assure the

safety of the user. Being an ATV, its imperative that the electric conductors and components are thoroughly isolated from dust and humidity.

As one can expect, the electrical component of the project is the most focused during this document. In a starting analysis, it is expected that this component of the project will be constituted by, at least, some of the following key systems:

- Battery Pack
- DC/DC Converter
- Motor Control Converter
- Electrical Motor
- Control Platform

The electrical component of the project comprehends a detailed analysis on the functioning and parameters of the motor, including several calculations for its construction. The control of the DC/DC and motor control power converters and consequentially, of the electrical machine, will be fulfilled with the purpose to obtain the highest efficiency possible, and with a motor response that is adequate and capable of creating an enjoyable experience for the user, implying that torque ripple must be minimized. This is one of the main challenges of the dissertation.

All the subsystems for the acquisition and conditioning of the signal were carefully implemented and all the power sources for the electronics needed for the correct operation of the system, as for example, sensors and even the control platform, were either created or bought.

In order to power the motor, there is a battery pack associated with the power train. The most common types of batteries are presented, but the emphasis is set on the functional requirements and not on the control and balance of the pack, seeing as this is not the main focus of the dissertation.

1.2 Motivation

An internal combustion engine is traditionally the main responsible for the motion of any typical automobile. These motors make use of the explosion of fossil fuels inside cylinders, creating the torque that will be used for moving the car.

Due to the constant rise in fossil fuel price, driven by the scarcity of these materials, it has become of crucial importance to find a sustainable alternative to their use, in the millions of vehicles that exist all around the world and that travel the roads everyday.

Nowadays, electrical engines are, more and more, being seen as a viable and safe alternative to conventional combustion engines, not only for not depending directly on fossil fuels to operate, but also because they produce zero emissions of pollutant gases, like carbon monoxide and dioxide, harmful to living beings and responsible for greenhouse effect. Electric motors also have advantages when compared to ICE in terms of acoustic pollution, as the electrical motor doesn't have so many mobile parts as an ICE and don't have the need for an exhaust system.

One of the most significant advantages of the electric motors when compared to ICEs is their efficiency. According to [2], an ICE-based vehicle presents an efficiency of around 20%, which is much lower than the 75% achieved by the EV, as indicated in the same reference.

In ICE-based vehicles, due to the torque characteristic that these provide, there is the need to use a gearbox, with the purpose to convert the velocity of rotation of the rotor, in a superior or inferior velocity, as desired. This system allows the obtention of high speed rotation at low torque, and low speed with high torque. This enables the operation of the motor to be executed in a zone that maximizes performance, over a wide range of speeds. These mechanisms, beside representing an additional cost for the power train and an extra risk of failure, reduce the overall efficiency of the system.

Some topologies of electric motor are capable of developing a constant torque over a wide range of speeds, which makes the previous mentioned mechanism unnecessary, being, by that fact, an alternative that presents potential advantage.

The main motivation for the development of this dissertation is the interest to study, explore the control and validate the use, in electric vehicle applications, of a recent market-emerging type of motor, the switched reluctance motor [3]. It is a type of electrical motor that exists for about two centuries, but, for technological reasons, such as limitations posed by the semiconductors and micro controllers, it wasn't possible, until recently, to control effectively the operation of such motors.

There are many reasons why the switched reluctance motor presents an attractive solution in electrical vehicle applications, and those are to be addressed in a comparative analysis with other existing solutions, in the second chapter of the present dissertation.

1.3 Objectives

There are several objectives that were set at start, as there was the need to define exactly what was the scope of the dissertation and what was possible to obtain in the period of development of such project.

The list of objectives to fulfil is as follows:

- Design of a switched reluctance machine
- Simulation and implementation of a state of the art control algorithm for switched reluctance machines
- Creation of a switched reluctance machine prototype
- Simulation and implementation of a DC/DC bidirectional converter
- Assembly of a test bench for the prototype electric machine

1.4 Structure of the dissertation report

This dissertation document is composed by the Introduction and the chapters that are here presented.

On chapter 2, a presentation is done on the state of the art of the different subsystems that take part of the power train.

The chapter 3 has the calculations for the expected requirements to be fulfilled by the ATV.

The full explanation on the working principle of the SRM, along with a detailed analysis of the machine is done in chapter 4.

An analysis on the DC/DC bidirectional converter and a discussion on the control of the power flow in both directions is presented in chapter 5.

In the sequence of the study on the SRM, there is a chapter focused just on the control of said electrical machine, chapter 6.

The practical implementation of the system is analysed in chapter 7, which is specially created for that effect, where the components are presented and the set up is described.

The dissertation then converges on the final chapter, the Conclusion, chapter 8, where there is a discussion on the work that was developed and the goals achieved. Future work will also be proposed.

Chapter 2

Bibliographic Review

2.1 Introduction

The main goal of this chapter is to, at first, overview the system to be dimensioned and implemented, so that the work done in this dissertation can be clear.

There is a comparative analysis on the different electric motors available and adequate for traction purposes.

A review on DC/DC converters used in electric vehicle applications is done, in order to choose the most appropriate for the application in hands.

Next, the control power converters referred in the literature for the motor chosen are presented, pondering advantages and disadvantages of the different topologies.

The control strategies for the motor control converter are also exposed in this chapter, but a greater study on this subject is done in chapter 6.

The types of batteries typically used for EV purposes are analysed and the best one for this application is chosen accordingly.

2.2 System Overview

The whole system can be overviewed as composed by the blocks depicted in figure 2.1.

The battery pack is the first block of the figure, and is responsible for generating ideally constant DC voltage, with enough capacity for powering the electric powertrain during the required time, under the determined circumstances.

Next on the electric powertrain, a DC/DC converter can be employed, for boosting the battery voltage level to the desired value before the motor control converter, which in turn will establish the bridge between the DC/DC converter and the motor windings. The DC/DC converter enables the electric power to flow bidirectionally. Furthermore, the use of this DC/DC converter allows

The gate control of the semiconductors present on the power converters is assured by the control platform, the XMC 4500 by Infineon®. The board is then connected to position, voltage and current sensors, responsible for providing feedback needed for the control of the electric machine.

The motor has its shaft output power delivered to a mechanical transmission mechanism, responsible for delivering the rotational movement to the vehicle's wheels.

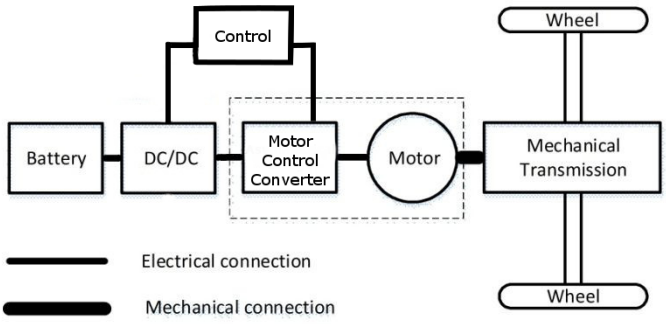

Figure 2.1: Typical Powertrain of a Full Electric Vehicle

2.3 Rotational Electric Machines

The performance of an electric vehicle greatly depends on the type of motor used to propel it. In the present case, an electrical vehicle requires certain characteristics from the electric motor, to make it excel when compared to ICE vehicles. The high power density, the high torque output obtained at low speed, the high range of speed of operation and the high efficiency are the main aspects from the motor that confer advantages to electric vehicles [4].

As can be seen in figure 2.2, for vehicle traction applications, the ideal performance characteristic of a powertrain is a constant power output over the full speed range. Consequently, the torque varies with speed hyperbolically. With this ideal profile, the maximum power of the powertrain will be achievable at any vehicle speed, making possible the obtention of optimal vehicle performance [5]. This constant power characteristic will provide the vehicle with high torque at low speeds, where demands for acceleration and effort are high.

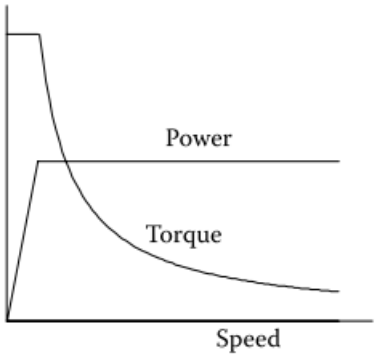

Figure 2.2: Ideal Characteristic of Powertrain

Nowadays, ICE are the most commonly motors used in powertrains for land vehicles. Typical characteristics of an ICE are shown in Figure 2.3, which has torque–speed curves far from the ideal performance characteristic shown before. ICE starts operating smoothly around the idle speed. Good combustion quality and maximum torque are reached at an intermediate engine speed. As the speed further increases, the torque decreases due to a reduction in the air introduced in the cylinders and the additional power losses caused by mechanical friction and hydraulic viscosity [5].

Power output, however, increases to its maximum at a certain higher speed. Beyond this speed,the engine power starts declining. Due to the torque-speed characteristic, a multi gear transmission is usually employed.

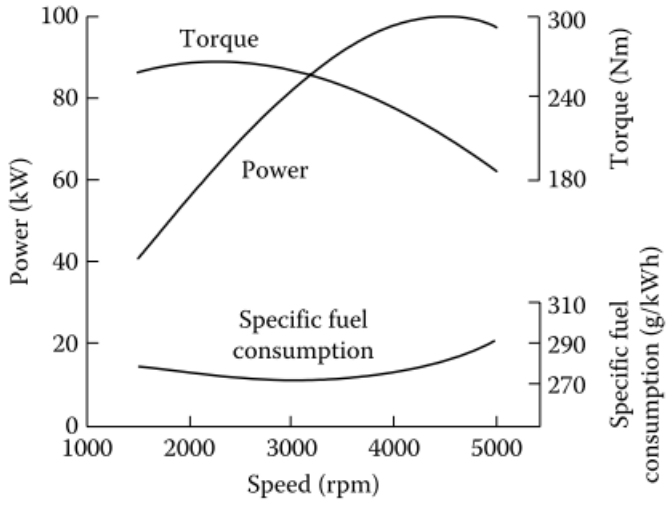

Figure 2.3: Typical Characteristic of ICE Powertrain [1]

The electric motor is another candidate as a vehicle power traction machine, and is becoming more and more important with the rapid development of electric, hybrid electric, and fuel

cell vehicles. Electric motors with good speed adjustment control usually have a speed-torque characteristic that is much closer to the ideal, as shown in figure 2.4.

Generally, the electric motor starts from zero speed and presents a constant output power while the torque declines hyperbolically with speed. Since the speed-torque profile of an electric motor is close to the ideal, a single-gear or double-gear transmission may be employed to meet the performance requirements.

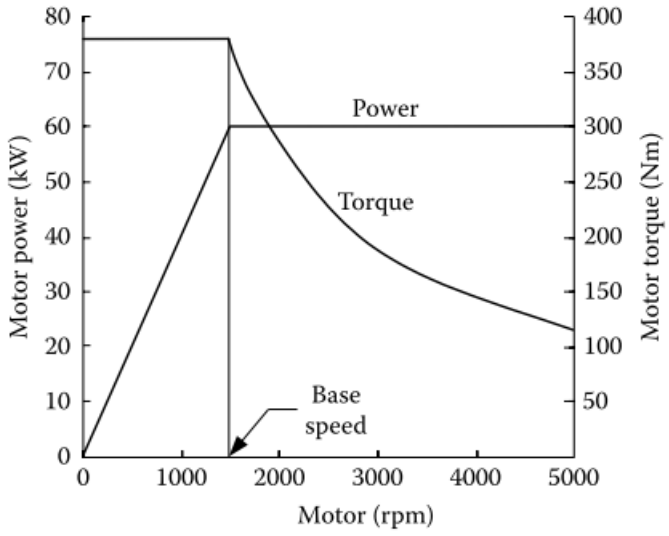

Figure 2.4: Typical Characteristic of EV Powertrain [1]

The advance in technology made the option of AC motor drives much more desirable than most DC machines, specially in traction applications, seeing as these are more reliable, have more power density and require less maintenance [6].

A brief comparison of electrical machines is now presented, with an analysis of the main advantages and disadvantages of the most common types of AC motor drives: asynchronous motor and synchronous motor. From these types of machines, the Induction Motor with Squirrel Cage rotor and the Permanent Magnet Synchronous Motor were the ones used for the mentioned comparison, due to their popularity.

Another motor that is presented in literature as a strong candidate in traction systems is the switched reluctance motor. It is a DC motor, with salient poles on both the rotor and stator and its operation is based on magnetic reluctance, as can be seen in chapter 4.

The electrical machine comparison is done in certain topics, as listed:

- **Power Density**

  The machine capable of possessing the highest power density is the PMSM, due to the employment of "rare earths" in it's construction, that not only help achieve the high power density, but also to reduce the operation losses. SRM possess a power density that is lower than the PMSM, but superior to IM [6].

- **Efficiency**

In terms of efficiency, the PMSM is again the best choice to take. Due to the lack of rotor coils, there are no Joule losses on the rotor side of the machine. The same can be said about the SRM, leaving the IM in the last place, when concerning efficiency.

- **Control**

The most complex control to implement is the one needed to power the SRM, due to the need to obtain, with a high level of precision, the position of the rotor, along with the variation of the inductance, responsible for the creation of torque, as explained in chapter 4. The IM and PMSM machines have their means of control well documented, with the use of vector control, in a similar manner.

- **Reliability**

When reliability comes to terms, the IM is said in the literature to be one of the best options. It is a motor known to have very little need for maintenance, at the same time that is capable of operating even in harsh environments. The SRM is also a very reliable machine, being capable of operating correctly with a fault in one of the phases (although with power losses). The PMSM is the least reliable, when one thinks of the risk that these motors present, in terms of loss of magnetization and loss of synchronism.

- **Cost**

The cost is the worst characteristic of the PMSM, due to the necessity to employ "rare earths" in its construction, alloys that are characterized by their capability to present a very high intensity, permanent magnetic field. The SRM excels in this point, due to the simplicity of construction and materials used, as the reader can see in chapter 4.

The SRM is the electrical machine to be studied and implemented in this dissertation, not only because the advantages described, but also due to the interest in studying and developing the control of an electrical machine that, although less common, can be a good and powerful option for creating new, cost effective solutions for vehicle traction applications.

2.4 Switched Reluctance Motor

2.4.1 Mechanical Construction and Operation Principle

The rotary Switched Reluctance Motor (SRM) is an electrical machine composed by a rotor and a stator, both of which have a rather simple construction, made essentially of the phase windings (on the stator) and agglomerated laminations of magnetic steel 2.5. Switched reluctance refers to the switching of phase currents, which is an essential aspect of the operation, as will be presented.

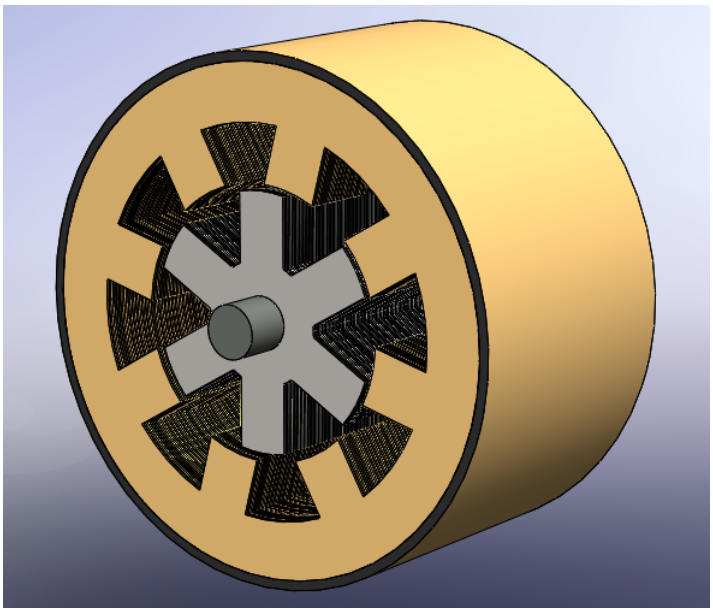

Figure 2.5: 3D Simulated visual aspect of SRM's stator and rotor

Both the stator and rotor have salient poles, and the number of stator poles is different than that of the rotor. The quantity of poles in stator and rotor are related to the number of phases of the electric machine. Typically, three phase SRMs have 6 stator and 4 rotor poles, whereas 4 phase SRMs have 8 stator and 6 rotor poles, or multiples of these values. The typical form used in the literature for designating this aspect of the SRM is as follows: S_p/R_p. Since the design of the prototype SRM is made having as starting point a previously existing 500W motor (see chapter 4) and the laminations of the motor are cut using a pneumatic press, the SRM used in this dissertation is a four phase machine with 8 stator and 6 rotor poles, so, a 8/6 SRM, as presented in figure 2.6.

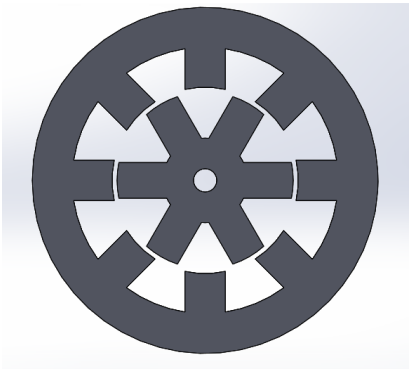

Figure 2.6: Laminations of SRM

There are coils of an electric conductor, typically copper, around the stator poles. Each phase of the SRM consists on two of these coils, placed in geometrically opposed poles. The windings

on the stator operate in the same manner as an inductor with a ferromagnetic core, so the idea is to generate two aligned electromagnets on the stator. When one of the phases is turned ON and the current rises in the corresponding coils (figure 2.7a), magnetic flux is generated and both of the poles act as an electromagnet. This in turn creates a force that causes the physical alignment of two geometrically opposed rotor poles with the excited stator poles (figure 2.7b), generating torque, in a way that the created magnetic circuit possesses the least reluctance possible [7]. This occurs due to the high difference of magnetic permeability existing between the air and the magnetic steel.

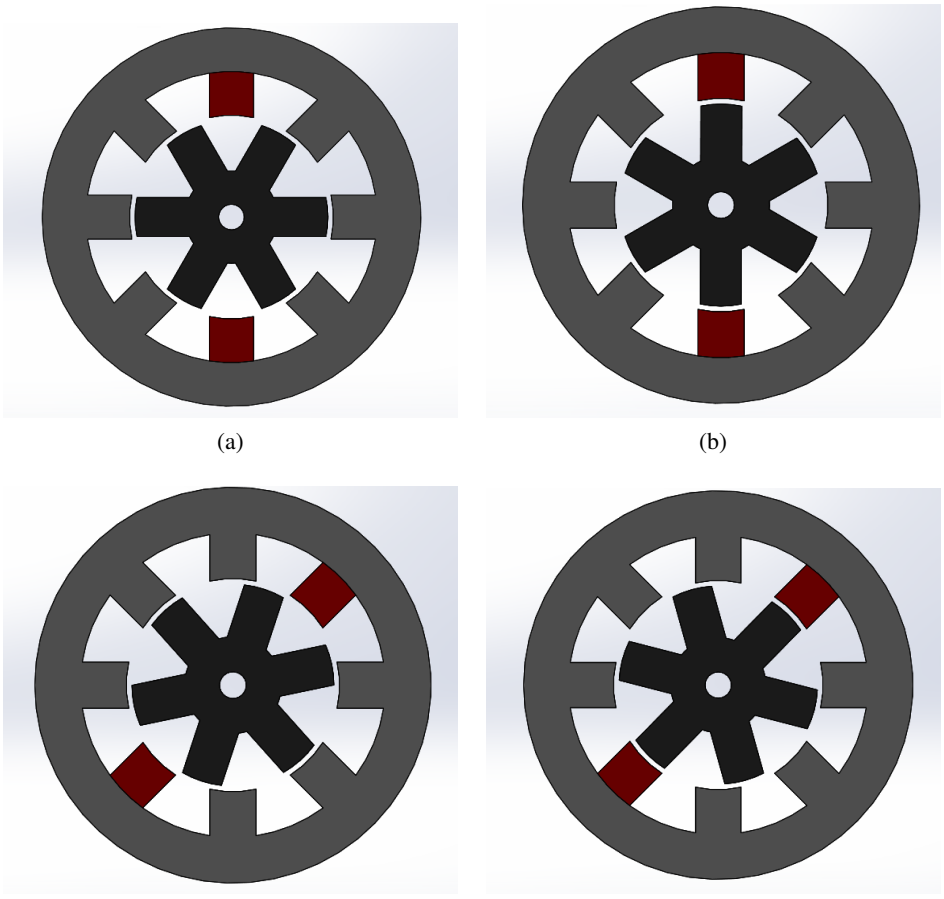

(a) (b)

(c) (d)

Figure 2.7: Sequential excitation of SRM's phases

The difference in number of stator and rotor poles exists for a reason. Due to this difference, at the same time that two pole pairs (one stator pair and one rotor pair) are aligned, two others are misaligned. Commutating OFF the voltage in the phase when a pole pair is aligned, at the same time that the phase where another pole pair is misaligned is commutated ON (figure 2.7c), will cause the alignment of this set of poles (figure 2.7d). Executing correctly and successively this operation, a rotational movement of the rotor can be achieved.

It is important to note that the torque generated changes signals when crossing the poles'

aligned position. If a phase is ON and the rotor pole position exceeds the aligned position, due to its momentum, there will be negative torque being generated, so to keep the rotor pole from departing the aligned position, where the magnetic circuit has the least reluctance path. In order to avoid this phenomenon, it becomes crucial to command the turning OFF of each of the phases at the correct moment and with that, demagnetize the stator poles before negative torque is produced. Output torque ripple can be greatly diminished with a correct control of the turn ON and OFF of the motor's phases.

In the figure 2.8, extracted from [7], it is possible to see the ideal variation of the inductance of a phase of the motor with the rotor's position variation. While the rotor pole is aligning with the stator pole, the inductance of the phase is increasing, and positive torque is being generated. In the aligned position, the inductance is maximum and the torque generated reverses, starting the motor to produce braking torque. In motoring operation, it is desired that the phase current is zero when the rotor pole is starting to separate itself from the stator pole, so as not to create negative torque. When using the SRM as a generator, the phases are excited while the rotor pole is departing the aligned position, that is, in the negative torque zone.

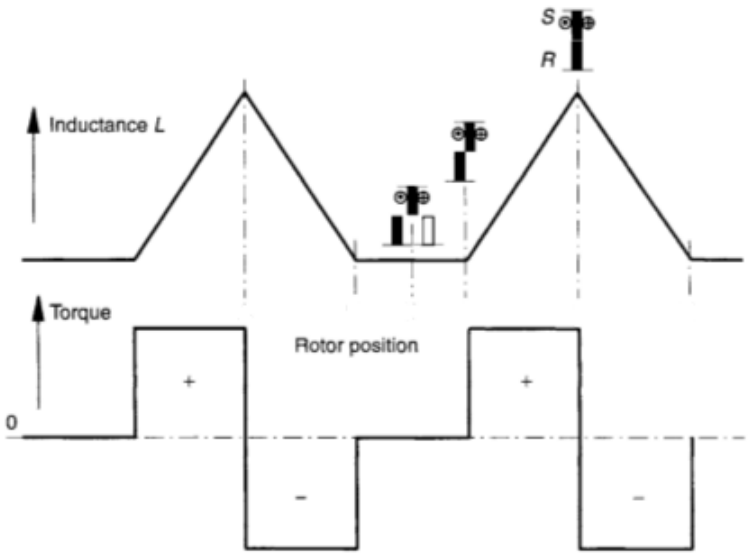

Figure 2.8: Ideal inductance and torque variation of a phase

In figure 2.9, it is possible to see the typical curves of inductance for a real SRM, and their variation with the rotor's position, as well as with the phase current. It is clear that they are very distinct from the ideal ones presented. As a consequence, some control algorithms make use of lookup tables, with values obtained either from finite element analysis (FEA) or measurements realized, as an attempt to estimate the value of the inductance, for each rotor position and current value.

With the stated before, one can conclude that high precision in the determination of the rotor's position is crucial for the correct operation of this motor. This is often done with the use of an

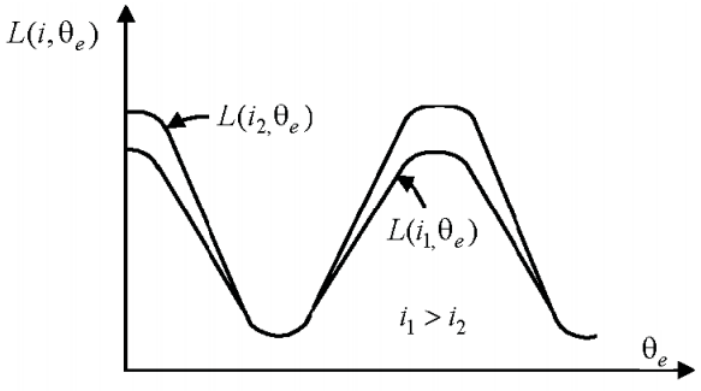

Figure 2.9: Inductance variation of a phase

encoder, coupled to the shaft of the motor, as is done in this dissertation and explained in chapter 4.

2.5 SRM Control Converter

The converter used to control the operation of a SRM has to fulfil some basic requirements, as follows [7]:

- Each phase of the Switched Reluctance motor should be able to conduct independently. This means that one phase has at least one switch for motor operation.
- The converter should be able to demagnetize the phase before it steps into the generating region, if the machine is operating as a motor.

To improve the performance, the converter should be able to utilize the demagnetization energy from the outgoing phase in a useful way either by feeding it back to the source (DC- link capacitor) or by using it in the incoming phase. Another way to improve performance is to have the converter create a high negative voltage for the outgoing phase in order to reduce demagnetization time.

2.5.1 Asymmetrical Bridge

The Asymmetrical Bridge is the most common converter in the literature for the control of the operation of a SRM. It uses 2 transistors and 2 diodes for each phase of the motor. For the case depicted in figure 2.10, the converter is set to command the operation of a 4 phased SRM, with the inductors seen in the image being the coils of each of the phases of the motor. If the motor were to have 5 phases, one would only need to add another module of 2 diodes and two transistors, as presented on each of the phases in the image. A brief explanation on the working principle of the converter is given below.

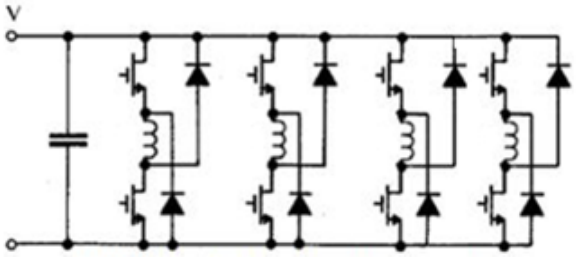

Figure 2.10: Asymmetrical Bridge for 4 phase SRM

The asymmetrical bridge converter allows an independent excitations of each of the motor phases. With the ON command of both the transistors of a phase simultaneously, a voltage of V_{DC} is applied to the phases' terminals, and the phase current will rise.

When any of the transistors of said phase is commanded OFF, the voltage across the phase will be equal to 0 V, being called the freewheeling stage of the converter.

When both the transistors are commanded OFF, the voltage across the phase is $-V_{DC}$ and the current will drop quickly until it reaches 0 A, time at which the diodes stop it from flowing in the opposite direction.

The described operation is visible in figure 2.11. Extracted from [8], the waveforms produced can be seen in image 2.12. By order of appearance, the phase inductance is depicted, increasing as the poles align and then decreasing when they depart. In the region where the inductance is increasing, positive torque can be produced (explained in chapter 4) and the current reference $i*_a$ is set to the desired value of I_p. The real value of the current generated can be seen as being controlled by hysteresis, with a window of $2 \times \Delta i$, with the signals used for the control of the semiconductors and phase's applied voltage appearing as the last two graphs in the image.

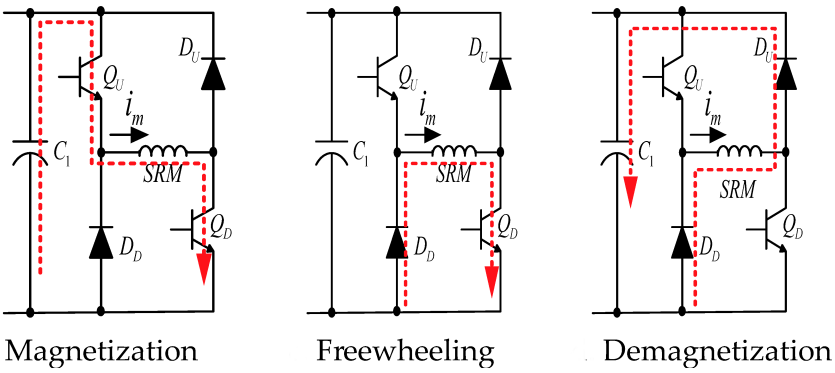

Figure 2.11: Operation Asymmetrical Bridge

Seeing as the motor has 4 phases, the transistors on the different phases are commanded ON only one quarter of the cycle of operation. This leaves opportunity to reduce the number of power electronic elements employed, as is analysed in the next subsection.

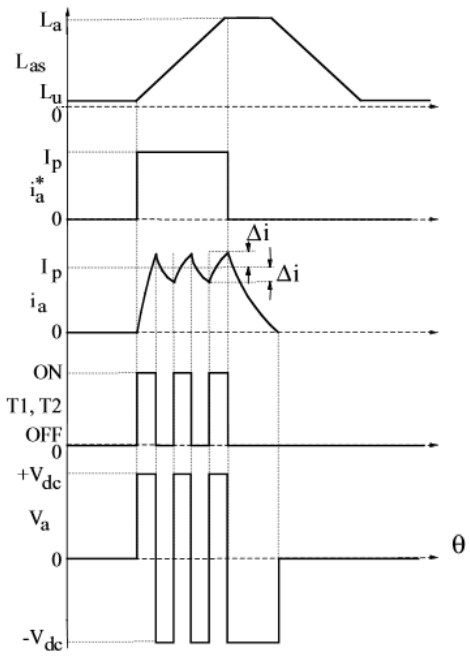

Figure 2.12: Waveforms related to an Asymmetrical Bridge and SRM

2.5.2 1.5 Diode and Transistor Configuration

The Asymmetrical Bridge fitted in a class named ”2 Diodes and Transistors Configuration” , due to having, associated with each phase of the SRM, two transistors and two diodes. The ”1.5 Diode and Transistor Configuration” is very similar to the Asymmetrical Bridge, but it aims at lowering the number of power electronics components in the converter. In order to do that, this topology uses one transistor and one diode that are connected not to one phase of the SRM, but to two phases, as seen in figure 2.13 , original from [8].

Figure 2.14 is a scheme of the typical waveforms of this configuration and shows that the converter can have the same capability of operation as the asymmetrical bridge, with the only down side of having a higher RMS current in two diodes and two transistors, that are shared by two of the motor’s phases, meaning that these semiconductors will be ON during half of the cycle of operation. Compared to the asymmetrical bridge, this converter has two less transistors and diodes, reducing the cost, weight and the volume of the converter. These are the factors that led the author to the choice of implementing this topology.

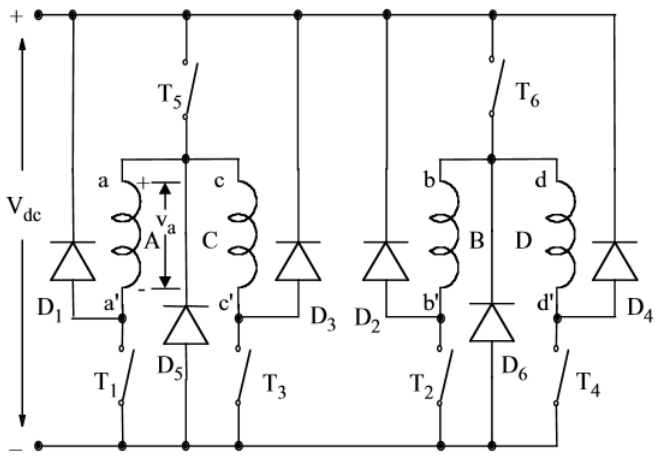

Figure 2.13: 1.5 Configuration for 4 phase SRM

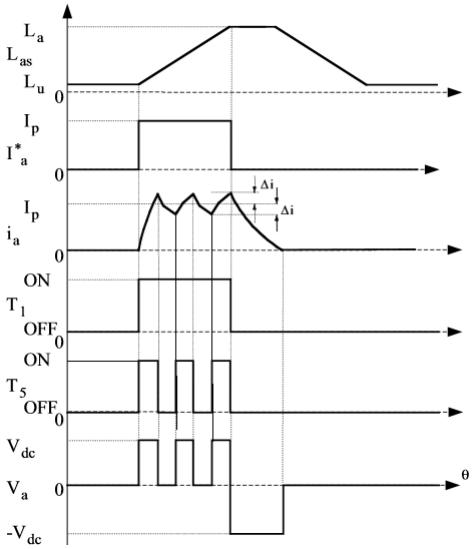

Figure 2.14: Waveforms of 1.5 Configuration for 4 phase SRM

2.6 SRM Control

In an EV, when the user steps on the accelerator pedal, it is requesting torque from the electric machine. This is the main interaction between the user and the powertrain. When the user wishes that the ATV accelerates, he sends a signal to the control platform that calculates and commands the operation of the motor. The way that the control algorithm adapts the operation of the SRM to this input can be made in several, very distinct ways. Ultimately, the control algorithms are the key for an operation with high efficiency and minimum torque ripple.

As mentioned before, torque is generated by successively commutating ON and OFF the transistors of the phases of an SRM, in a way that causes a rotational movement from the rotor.

However, this torque can present high ripple and even zero torque zones, due to the highly non linear torque generation principle [8].

2.6.1 Single Pulse Control

The most basic control that can be used is named single pulse control (SPC). This type of control is characterized by not having control over the phase current. It consists on an algorithm, with a position feedback loop, that verifies if the rotor position is between two angles, θ_{ON} and θ_{OFF}, for each of the SRM's phases. The algorithm then turns ON the power switches when the rotor's position is equal to θ_{ON} and only commutates them OFF when the rotor's angular position has the value of θ_{OFF} 2.15.

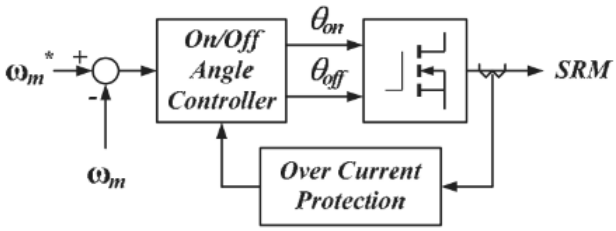

Figure 2.15: Single pulse control diagram

This simple algorithm has a major drawback, that is much more noticeable at low speed. Since there is only one ON command and one OFF command of the phases' semiconductors per stroke of the motor, the phase current of the SRM will have a peak value dependant on the ON and OFF commutation angles. This means that, if the ON angle is too small, the current will rise quickly, due to the low inductance value of the phase at this time. This can cause over current states in the semiconductors and lead to faults in the system (curve A of 2.16). The solution to this problem could be retarding the ON commutation angle. However, this can pose as a problem too, as the phase current may take substantially longer to reach the intended value. If the phase current doesn't reach the desired value in the defined time interval, the maximum motor torque will consequentially be lower than expected (curve B of 2.16). Likewise, the variation of the OFF commutation angle can cause negative torque (if too delayed) or can reduce the maximum value of the torque generated (if too advanced).

This type of control has large torque ripple issues and, when using small windows of phase excitation, "dead zones" in torque generation might appear, ranges of angles where zero torque is produced (curve C of 2.16). This, combined with a high load applied on the shaft, can cause an irregular operation of the motor, along with great mechanical stress on the rotor's shaft.

Normally, either a calculation of turn ON and turn OFF angles in real time or a lookup table is needed, in order to adapt these angles to the velocity of the motor. This can be explained by the variance of inductance of the motor's phases. In low velocities, the ON angle is delayed, since the current has the time to rise to the desired value, before the poles align. At higher velocities, this

is not true. The ON angle has to be advanced, so that the phase is excited while the inductance is low, and so the current has sufficient time to reach the needed value.

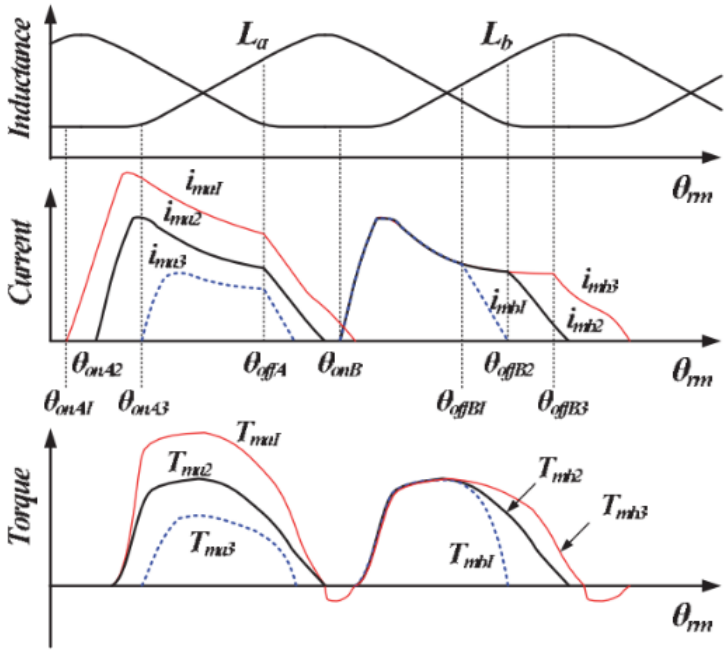

Figure 2.16: Single pulse control, for distinct commutation angles

2.6.2 Current Control

Increasing the complexity of the control algorithm, the use of a feedback loop in the motor's current allows for a better and smoother operation of the electrical machine 2.17. Since the electromagnetic torque is approximated by $T_e = \frac{i^2}{2} \cdot \frac{dL}{d\theta}$ [8], large variations on the phase current cause large torque ripple, as seen in the previous subsection.

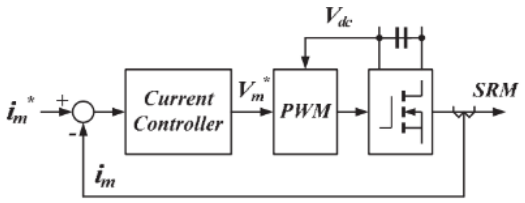

Figure 2.17: Hysteretic current control diagram

Combining the feedback loop of current with a hysteresis control for the switching of the semiconductors, the waveforms depicted in figure 2.18 can be achieved. Here, a reference signal for the current is given for each phase of the motor. The hysteresis window dictates the ripple magnitude of the current. The working principle is quite simple: If the current measured in a given phase is less than the reference minus half the hysteresis window value, the semiconductors

of said phase are turned ON, causing an increase in current. With the same philosophy, when the current measured is superior to the sum of the reference value with half the hysteresis window, the semiconductors are turned OFF, causing the decrease in current.

The current reference, in this control, is the key element for a good operation of the motor [9]. The use of ON and OFF commutation angles is inherently present in this algorithm, as the current reference is always equal to 0 while the rotor's angle isn't between the position where the phase is to be excited.

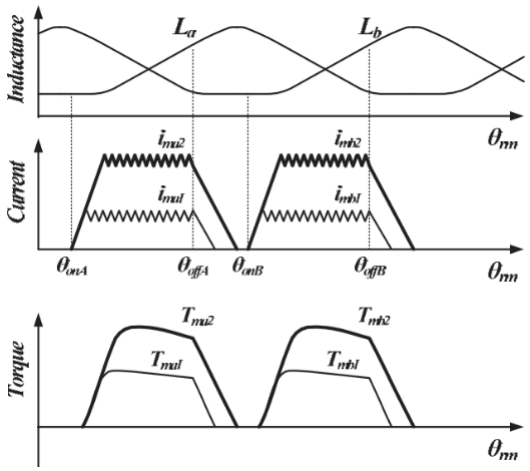

Figure 2.18: Hysteretic current control waveforms

2.6.3 Direct Instantaneous Torque Control

In Direct Instantaneous Torque Control (DITC), the previous shown control algorithms are employed, as well as some new concepts, which are here presented. Apart from sensorless and control using methods like fuzzy rules and genetic algorithms or neural networks, this is currently the most commonly mentioned algorithm when it comes to the control of an SRM, with torque ripple optimization [10].

As seen before, the machine produces discrete pulses of torque with each successive phase excitation. The total torque of the SRM is the sum all the torques produced by each of the phases, and according to [8] with proper design of overlapping inductance profile, it is possible to produce a near constant torque.

For a good and fast torque response, unlike the previously presented control algorithms, multi-phase switching is necessary. Multiphase switching is characterized by commuting ON more than one phase at the same time. A way to achieve this is by controlling the torque based on distribution functions to guarantee a linear torque out of the SRM drive.

These torque sharing functions (TSF), as they are known, are functions that are set to generate the torque references. For each angle of the rotor, these functions calculate a value, that is to serve as reference for the control, for each of the phases. There are several types of these functions, the most commonly found in the literature are Linear, Sine, Cosine and Exponential TSF [7]. The last

three TSF mentioned fall into the non linear classification. The difference in the types of TSF is well seen on the overlap angle of two phases, which is defined as the zone where two phases are turned ON, in order to achieve a more constant torque response [11].

The linear TSF is the most simple TSF and the one that requires less computational time. It is called linear, as it assumes that the torque produced by the phases during phase commutation is changing linearly with the rotor position. This is obviously not accurate, since, as seen before, the inductance variation with rotor position is also highly non linear. The reference generated by this function can be seen in figure 2.19.

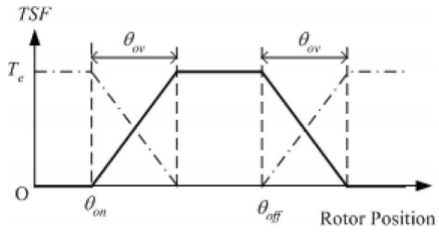

Figure 2.19: Torque references from linear TSF

In an attempt to better adjust the torque reference to the actual developed electromagnetic torque, other, non linear TSF appeared. As the name of each one of these functions suggest, expressions with sine, cosine and exponential functions are used for the generation of the references, during the overlap of the SRM's phases. In figure 2.20, a typical waveform is presented.

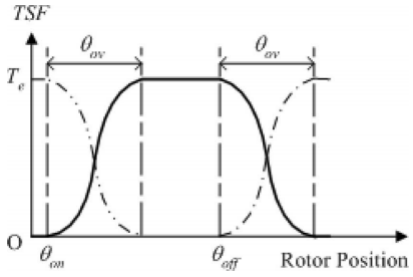

Figure 2.20: Torque references from non linear TSF

Recapitulating, in a RL circuit, as are the inductor coils around the stator poles, a current can't instantaneously rise to the desired value. This phenomenon, along with the thought that it is crucial to have the the desired current in the phase at the instant that the inductance starts to rise, in order to obtain instantaneous torque production, makes evident that the phase must have voltage applied to it's terminals before the poles start to overlap. In other words, there is the need to employ voltage in advance to the stator's phase, as well as turn OFF the voltage before the poles are aligned, so that the current has time to drop to zero, and doing that, avoiding the generation of braking torque, due to the start of a negative slope of the inductance.

The strategy is to apply voltage to the phase winding in advance by a certain number of degrees and the current turn-off is initiated in advance by another. These angles are dependent on the magnitude of the peak winding current I_p and the rotor speed [7]. In a DITC algorithm, the TSF has as inputs a torque reference value, T_e^*, the rotor's position θ, and the ON and OFF commutation angles θ_{ON} and θ_{OFF}. The output of the TSF is the torque reference for each of the phases of the SRM. From there, a torque error is calculated, as being the difference from the reference torque and the torque generated by a phase at that given moment.

The torque generated at a given moment is function of the position of the rotor and the phase current. Normally, the phase current and position are measured (using current sensors and an encoder) and the torque is estimated, either by analytical calculation, or lookup tables. Usually, lookup tables are employed, as they can reduce the time the algorithm takes to run on a micro controller.

A hysteresis control is made to keep the torque error for each of the phases between the permissible value of the hysteresis window, and from there, PWM signals are generated, for the control of the commutation of the converter's semiconductors.

This is the operation of the DITC algorithm, which is also presented in figure 2.21. This algorithm is simulated in chapter 6 and the results obtained are discussed.

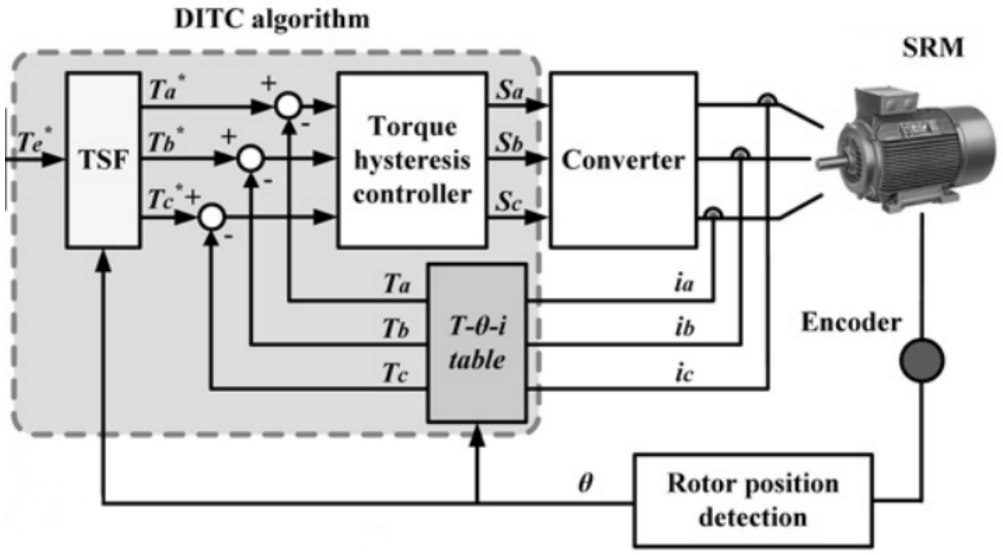

Figure 2.21: Direct instantaneous torque control of a SRM

The main drawback of this algorithm lays with the time that it takes the micro controller to run one cycle of it. This is where the single pulse algorithm begins to look interesting. At higher speeds of rotation, the time for computation becomes increasingly a problem and single pulse control becomes a better option for control of the SRM than DITC. So, when implementing, it is frequent to employ not one, but two control algorithms, DITC for low and medium speed operation and SPC for high speeds, extracting the best characteristics of both the methods [12].

2.7 DC/DC Bidirectional Power Converter

Between the battery pack and the power converter responsible for controlling the SRM operation, the powertrain has a DC/DC bidirectional power converter, responsible for increasing the voltage from the battery pack, as well as allowing more efficient energy conversion when employing regenerative braking [13]. Such operation analysis is explained in chapter 6.

The main advantage of having a boost converter before the motor control converter, is enabling a fast rise and fall in the phase current of the SRM. As seen before, that is of great importance in order to achieve a good output torque, with the lowest ripple possible.

The most typical converter topologies for these types of applications, in EV, can be divided into isolated and non isolated topologies. Isolated topologies have the advantage of providing isolation from the power source to the SRM control converter. The advantages of using non isolated converters are listed as follows [14]:

- Simple and less bulkier structure
- High efficiency
- Low cost
- High reliability

Due to the application in which this converter is to be used and pondering the trade-off between the two types of bidirectional DC/DC converters, the author has chosen to implement a non isolated topology. The main topologies of bidirectional DC/DC non isolated converters are compared in [14], for a 10kW application. Those topologies are listed next:

- **SEPIC**

  The SEPIC converter is a good option for applications of lower power. Due to the difficulty associated with correctly synchronizing the commutation command of the transistors [15], it becomes impracticable to implement this converter in such a small interval of time, without having any major advantages over the other topologies. In fact, it is predicted that this converter would be more expensive than the rest, derived from the number of passive elements. The topology is presented in figure 2.22.

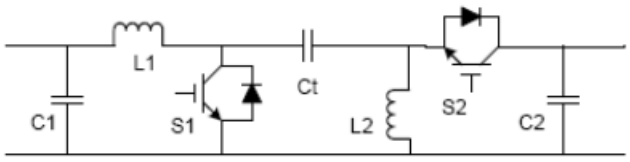

Figure 2.22: SEPIC Converter

- **Half Bridge**

  The half bridge converter 2.23 is based on the typical Buck and Boost topology combined. Where the Boost converter normally has a diode, the Half Bridge has a transistor, and it's freewheeling diode serves the same purpose that the one present of the Boost converter. It has a very simple structure and is well documented in the literature, having an efficiency of around 94 % for a 10 kW application [14]. Furthermore, it doesn't have many components, so the converter can be compact and adequate for the project.

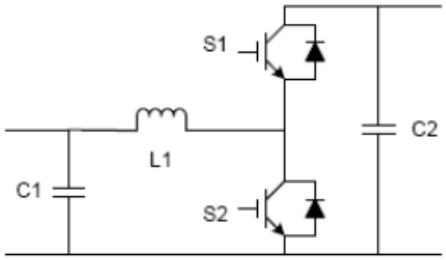

Figure 2.23: Half Bridge Converter

- **Three Level**

  The three level converter presented in figure 2.24 has the double of the number of semiconductors when compared to the half bridge topology, as well as an extra capacitor. This makes the converter heavier and with a higher cost, therefore, less suitable for the application. The advantage of this converter when compared to the half bridge one, is the $2-3\%$ of improved efficiency that it can develop, for the same application [14].

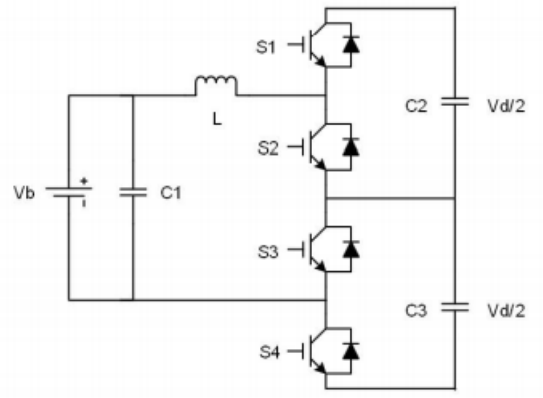

Figure 2.24: Three Level Converter

With this in mind, the author decided to study and design, for later implementation, of a half bridge topology, buck boost bidirectional converter. As mentioned before, the buck boost topology shown

here, when in boost operation, is exactly the same as a traditional DC boost converter. This means that the equations or the calculation of the inductor's current, current ripple and inductance, the capacity of the output capacitor, the ratings of the semiconductors can all be calculated as in a normal boost converter. The aspect that needs special attention is the capacitor, that will have to be able to deal with large currents in small intervals of time, caused by the demagnetization of the phases of the SRM.

2.8 Battery Analysis

Batteries tend to be one of the biggest disadvantages of the electric vehicles. The low autonomy they offer, as well as long charging time and price of acquisition, more than justify the growing interest in studying and discovering new types of batteries. There are some concepts that need to be fully understood before comparing the most common types.

Capacity: the capacity of a battery is expressed in A.h and it gives information on what is the current that can be extracted from a fully charged battery, during an interval of time.

Specific Energy: specific energy defines the battery's amount of energy per unit of mass (J/kg).

Specific Power: specific power determines what is the maximum power capable of being extracted from the battery. The internal resistance of the battery greatly affects this parameter.

C-rate: the C-rate of a battery indicates the current at which a battery is to be charged or discharged. Discharging a battery at 1C means that the battery is being charged with the current specified by the capacity and will take the indicated time to discharge. Example: If a battery indicates 1 A.h of capacity and is being fully discharged at a constant current of 1 A, it is expected that the discharge will last 1 hour. However, if it is discharged at a constant current of 0.5 A, it will last 2 hours.

The most commonly found batteries are listed below, each one with a list of pros and cons [16].

Nickel-Cadmium Battery

Pros: Is capable of fast charge, high number of charging cycles, capable of enduring several full discharges without loss of performance and is economical.

Cons: Has low energy density, it isn't environmentally friendly, has high self discharge and has the "memory effect", which is a phenomenon that causes the loss of capacity of the battery.

Nickel-Metal Hydride Battery

Pros: Comparing to Nickel-Cadmium, these batteries possess higher energy density and experience much less the "memory effect". They are also environmentally friendly.

Cons: These battery's performance is greatly reduced if they are repeatedly discharged completely. The same happens to these batteries if they are subjected to high discharge currents and operate at high temperatures. The self discharge is also high.

Lead Acid Battery

Pros: This type of batteries is very economical, allows high discharge rates, doesn't suffer the "memory effect" and has low self discharge.

Cons: These batteries have low energy density and are only capable of a limited number of full discharge cycles. Furthermore, they are harmful to the environment.

Lithium Ion Battery

Pros: The Lithium Ion Batteries have high energy density, low self discharge and no "memory effect".

Cons: This type of batteries are sensible to high temperatures, which affects greatly their performance, and are expensive to produce.

Taking all the above into consideration, the Lithium Ion batteries appear to represent the best choice for this application. These are the types of batteries to be used in the implementation of this dissertation.

In Lithium Ion batteries, electrical energy is obtained from the combination of a lithium carbon and a metal oxide to form carbon and lithium metal oxide.

According to [1] and [16], Lithium ion batteries are a highly attractive candidate for future electric vehicle, due to their low weight advantage and high specific energy. Their major drawback is their production cost.

2.9 Final Solution

Adding up all the topics covered before, the powertrain to be implemented will be constituted by the following major subsystems:

- Lithium Ion batteries, connected to create a pack with the characteristics set on chapter 3
- DC/DC Buck Boost Half Bridge Bidirectional Converter
- SRM Control Converter, based on ”1.5 Diode and Transistor Configuration”
- Control platform
- Electric machine, a SRM with the design made in chapter 4

Chapter 3

Requirements

3.1 Introduction

In order to assure the ATV will be able to operate effectively and without compromising the mechanical structure or the safety of the user, there exists the need to set, at start, several operational requirements. It is vital to make sure the motor is capable of generating enough torque to start the movement of the system ATV plus user, in the worst predictable conditions, as well as achieving the top speed, seeing as the ATV will not need a gearbox when operating as an electric vehicle.

3.2 Overall Requirements

According to [17], the ATV used in this project has a gear ratio of $3.69:1$ in the differential and another reduction, of $2:1$, in the fixed transmission from the motor to the differential, which sums up to a total reduction, i:

$$i = 2 \times 3.69 = 7.38:1 \tag{3.1}$$

In the next calculations, for worst case scenario approach, an efficiency, η , of 90% was assumed for the total transmission [18].

3.2.1 Starting torque

To establish this requirement, it was defined that the ATV must be able to start its movement, with the extra weight of the driver, presumed to be around 70 kg, in a 15 % slope, according to figure 3.1, with the restraint that the ATV must be capable of reaching a speed of 10 km/h in a maximum time of 2 seconds.

Some of the parameters were present in the owner's manual, such as the vehicle's weight, the radius of the wheels, among others. All the relevant calculations for the estimation of the starting torque are as follows:

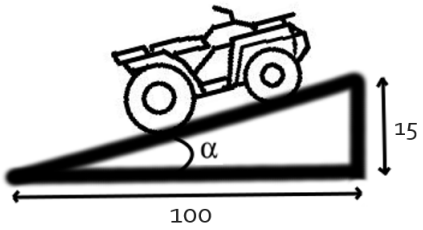

Figure 3.1: Vehicle on 15% slope

$$Mass_{ATV} = 196kg \qquad R_{wheel} = 27.94\ cm \qquad Mass_{user} = 70kg$$

$$\alpha = \arctan\left(\frac{15}{100}\right) = 8.53^{\circ} \tag{3.2}$$

Naming the required acceleration that the vehicle must achieve in order to fulfil the requirements a, the following expression derives:

$$a = \frac{(v_{final} - v_{initial})}{\Delta t} = \frac{\frac{10\times10^3}{3600}}{2} = 1.38\ m/s^2 \tag{3.3}$$

This acceleration results in a force, calculated according to Newton's second law of motion:

$$F_{acc} = \left(Mass_{ATV} + Mass_{user}\right) \times a = (196+70) \times 1.38 = 367.08\ N \tag{3.4}$$

The gravitational force that acts on the ATV can be calculated as follows, being g the gravitational acceleration:

$$F_{gravity} = \left(Mass_{ATV} + Mass_{user}\right) \times g \times \sin(\alpha) = (196+70) \times 9.8 \times sin(8.53) = 386.66\ N \tag{3.5}$$

The friction force that acts on the ATV's wheels, F_f, must be calculated for a worst case scenario. Here, it is assumed that the worst case is for a start executed in a gravel road, is calculated taking in account the rolling resistance coefficient, C_{rr}, as seen in [5], in equation 3.6:

$$F_f = C_{rr} \times \left(Mass_{ATV} + Mass_{user}\right) \times g \times \cos(\alpha) = 0.02 \times 266 \times 9.8 \times \cos(8.53) = 51.56\ N \tag{3.6}$$

The force executed by the air resistance acts in the whole frontal area of the vehicle, and its value is calculated according to equation 3.9, where ρ_{air} is the air density, C_x is the aerodynamic resistance coefficient, C_d is the air drag coefficient and A_t is the vehicle's frontal area, calculated as being approximately the area of a rectangle, according to the dimensions indicated in the owner's manual [17]. C_d presents a typical value of around 1.6 for a motorcycle and rider application [18]. The velocity of the vehicle is v^2 and equal to 10 km/h or 2.78 m/s.

$$A_t = Height_{front} \times Width_{front} = 0.7925 \times 1.0338 = 0.8193\ m^2 \tag{3.7}$$

$$C_x = C_d \times A_t = 1.6 \times 0.8193 = 1.31 \tag{3.8}$$

$$F_{air} = \frac{\left(\rho_{air} \times C_x \times v^2\right)}{2} = \frac{\left(1.22 \times 1.31 \times 2.78^2\right)}{2} = 6.18\ N \tag{3.9}$$

The total force executed on the vehicle at the defined starting conditions, is the sum of the previous calculated

$$F_{total} = F_{acc} + F_{gravity} + F_f + F_{air} = 369.74 + 386.66 + 51.56 + 6.18 = 814.14\ N \tag{3.10}$$

The total force applied to the vehicle enables the calculation of the torque that the wheels require to start the movement and reach the requested speed, in the determined time.

$$T_{wheel} = F_{total} \times R_{wheel} = 227.47\ Nm \tag{3.11}$$

As stated before, there exists a fix gear relation of 7.38 : 1 between the motor shaft and the wheels of the vehicle. That results in a minimum torque generated by the motor, in order to fulfil the requirements, of 34.25 Nm, result obtained by employing the equation 3.12.

$$T_{motor} = \frac{T_{wheel}}{i \times \eta_{gears}} = 34.25\ Nm \tag{3.12}$$

3.2.2 Maximum Motor RPM

The next requirement to set is the maximum rpm at which the the motor will operate, in order to make the vehicle achieve maximum velocity, in a road with 0 % slope.

The original vehicle is capable of achieving a top speed of 80 km/h, 22.22 m/s, without compromising its physical integrity or the safety of the driver. With that in mind and for safety reasons, the author decided that the maximum speed of the electric vehicle would be equal to that of the original vehicle. Also, the rated power of the all-terrain

vehicle's previously existing internal combustion engine is of 8kW. In order to not compromise the safety of the user and mechanical structure of the all-terrain vehicle, that is the power used for the following calculations. The calculations executed are as presented, where Per_{Wheel} is the perimeter of the wheel:

$$R_{wheel} = 27.94\ cm \Rightarrow\ Per_{wheel} = 2 \times \pi \times 27.94\ = 175.55\ cm \tag{3.13}$$

$$v_{wheelm/s} = \frac{\frac{rpm_{motor}}{i \times \eta}}{60} \times Per_{wheel} \Rightarrow\ rpm_{motor\ max} = 5608\ rpm \tag{3.14}$$

This results in a torque at maximum speed that must be equal to 13.6 $N.m$, according to equation 3.15.

$$T_{max\ rpm} = \frac{P_m}{\frac{2 \times \pi}{60} \times rpm_{motor\ max}} = 13.6\ N.m \tag{3.15}$$

3.2.3 Capacity Required from the Battery Pack

The battery pack's capacity is expressed in $A.h$ and gives information on which current can be extracted from a fully charged battery, during a certain period of time [19]. For example, if a battery's capacity is set at 11 $A.h$, the user can expect that the battery is able to power a load that requires 11 A to operate, during 1 hour.

It becomes imperative to analyse the battery pack's capacity, in order to predict if it is capable of matching the requirements set. Seen as the original motorcycle has a fuel tank of 9.1 l [17], and the average fuel consumption is 8 $l/100\ km$, the range of the vehicle will be of, approximately, 120 km. The system will be designed to be able to reach the same autonomy. It was defined that the author, that an acceptable route would be composed by 90 km, with an average speed of 50 km/h and 30 km with an average speed of 80 km/h.

The capacity calculation to meet the requirements is as follows, where C_{bat} is the battery pack's capacity, P_{motor} is the electric power consumption of the motor, D is the distance that the ATV will travel, V_{source} is the voltage at the motor's phases (the value of 600V was used, consequence of the design of the electrical machine, as is done in 4)and v is the velocity at which the ATV moves [20].

$$C_{bat} = \frac{P_{motor} \times D}{V_{source} \times v} = \frac{8000 \times 90}{600 \times 50} + \frac{8000 \times 30}{600 \times 80} = 29\ A.h \tag{3.16}$$

The battery packs to be used are already created and available. The Lithium Ion battery cells have a capacity of 11 $A.h$ and a operating voltage range that is between 4.2 V and 3.2 V, being 3.7 V their nominal value.

The voltage of the total battery pack is dictated by the number of battery cells connected in series. The capacity of the pack, on the other side, is dependent on the number of battery cells connected in parallel.

In order to design a pack that is able to match the capacity required, it is understandable that the number of battery cells has to be at least 3, which corresponds to a capacity of 33 $A.h$.

The number of battery cells (N_{cells}) connected in series is calculated by the following expression:

$$N_{cells} = \frac{V_{pack}}{V_{cell}} \tag{3.17}$$

Where V_{pack} is the desired voltage of the battery pack and V_{cell} is the voltage of each of the cells. The voltage desired for the pack was decided pondering the trade off between the dimensions of the resulting pack and the need to achieve a high voltage, while still keeping the 3 battery parallel.

This analysis resulted in 36 blocks of batteries connected in series, each one constituted by 3 battery cells in parallel, as seen in figure 3.2. This results in an output voltage for the pack of around 140 V.

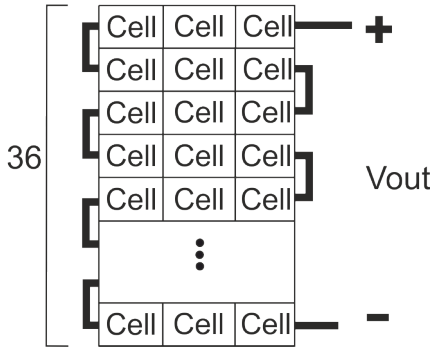

Figure 3.2: Battery Pack Cell Connection

3.3 Conclusion

In this chapter the core requirements for the design of the ATV's power train were calculated. These are of upmost importance, in order to assure the system is able to respond to the user's needs and equal the performance of the common, ICE powered ATV.

With the main requirements for the application set, it became possible to advance to the next step in the creation of the ATV's power train, the design of the core element, the electric motor. This design is presented and thoroughly explained in the next chapter.

Chapter 4

Switched Reluctance Motor

For this dissertation, an 8kW, 8/6 switched reluctance motor was designed and manufactured, having as base a previously existing 500W switched reluctance motor, that was subject to a redesign.

For the theoretical design some calculations presented in this chapter were made and then the resulting motor was simulated using FEA software, particularly Infolytica's Motorsolve ®.

The several components of the motor were designed and assembled in 3D CAD software, in order to establish the needed parts and assure correct fixation and assembly of the final motor.

The manufacturing process was mainly done by the author, and most of the materials used were scavenged from existing motors, that didn't pass the quality control or had one, or several, manufacturing defects. This resulted in a final motor that is presented at the end of this chapter and is named "Scrappy" or "Sucatinhas", in Portuguese.

4.1 Design and Simulation

In order to better understand the operation of the motor and the correlation between the variables that define its response, in a first stance of this section, a linear and a non linear analysis is done. The major equations for the design of the SRM are then presented and the existing constraints for the manufacturing of the motor are discussed. From there, it is then possible to suggest a starting point in parameters for the FEA simulation.

4.1.1 Motor Analysis

4.1.1.1 Linear

Neglecting mutual inductances between phases and magnetic saturation, a simple equivalent circuit of the SRM can be calculated as done in [8]. Analysing the voltage

applied to a phase, one can derive that it is equal to:

$$V = R_s \times i + \frac{d\lambda(\theta,i)}{dt} \tag{4.1}$$

Where R_s is the resistance of the phase, i is the current, θ is the rotor position and λ is the flux linkage given by:

$$\lambda = L(\theta,i) \times i \tag{4.2}$$

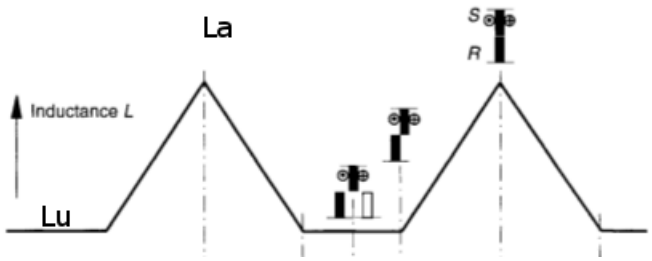

Figure 4.1: Inductance variation with rotor position

L is the inductance, that varies with the rotor position and phase current (in figure 4.1, L_u is the unaligned inductance, L_a the aligned). The previous equations can be transformed in the following expression:

$$V = R_s \times i + L(\theta,i) \times \frac{di}{dt} + i \times \frac{d\theta}{dt} \times \frac{dL(\theta,i)}{d\theta} = R_s \times i + L(\theta,i) \times \frac{di}{dt} + \frac{dL(\theta,i)}{d\theta} \times \omega_m \times i \tag{4.3}$$

ω_m is the speed of the rotation of the SRM. The terms in equation 4.3 represent, in the order depicted, the resistive voltage drop of the phase, the inductive voltage drop and an induced emf. This allows the conclusion that an SRM can be electrically approximated by the circuit present in figure 4.2 [21].

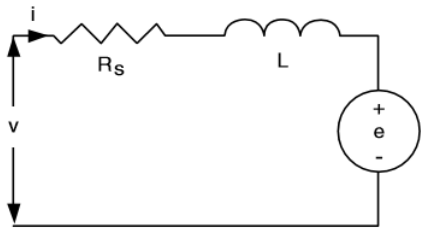

Figure 4.2: Equivalent circuit of a phase of an SRM

$$P_i = V \times i = R_s \times i^2 + i^2 \times \frac{dL(\theta,i)}{dt} + L(\theta,i) \times i \times \frac{di}{dt} \tag{4.4}$$

The rate of change of magnetic stored energy at any instant is given by:

$$\frac{d}{dt} \times \left(\frac{i^2}{2} \times L \times i^2 \right) = \frac{i^2}{2} \times \frac{dL}{dt} + L \times i \times \frac{di}{dt} = \frac{i^2 \times \omega_m}{2} \times \frac{dL}{d\theta} + L \times i \times \frac{di}{dt} \tag{4.5}$$

Noting the law of conservation of energy, the mechanical power conversion $P = \omega_m \times T_e$ (T_e is the electromagnetic torque) is equal to the difference between the power input, $v \times i$ and the sum of the resistive loss $R_s \times i^2$ and the rate of change of magnetic stored energy.

From the junction of the precious equations, one is able to write that:

$$T_e = \frac{P}{\omega_m} = v \times i - R_s \times i^2 - \frac{d\left(\frac{1}{2} \times L \times i^2\right)}{dt} \tag{4.6}$$

Resulting in an electromagnetic torque that is equal to:

$$T_e = \frac{i^2}{2} \times \frac{dL}{d\theta} \tag{4.7}$$

This is the approximate equation used for the computation of torque created by a SRM. It varies with the current intensity and with the variation of inductance in the motor phase.

4.1.1.2 Non-Linear

In [7], the limitations of the linear model are presented. The same method is here exposed, extracted from the reference.

When the phase switches are turned ON, the phase voltage starts to build up phase current. At this time, one part of the input energy will be stored in the magnetic field. With the increasing inductance, the magnetic field energy will increase until the switches are turned OFF. The input energy will be used to not only build up the magnetic field energy 4.3, but it will also be converted to mechanical work and loss [22].

Beginning with the consideration that immediately before the aligned position is reached, the magnetic stored energy ($\frac{L_a \times i^2}{2}$) must be returned to the power supply. When saturation doesn't exist, this magnetic energy has a great value, since L and i are at their maximum values.

The plot of flux linkage versus current for this situation is in figure 4.4. As depicted, the slope of OA is the aligned inductance and the slope OJ is the unaligned inductance. OJAO defines a complete stroke (execution of this loop) of the rotor, in motoring operation.

Along OJ, the energy defined by OJC must be supplied to the magnetic circuit, which is equal to $\frac{L_u \times i^2}{2}$. Along JA the electromechanical energy conversion is OJA:

$$OJA = W = T_e \times \Delta\theta = \frac{i_m^2 \times (L_a - L_u)}{2} \tag{4.8}$$

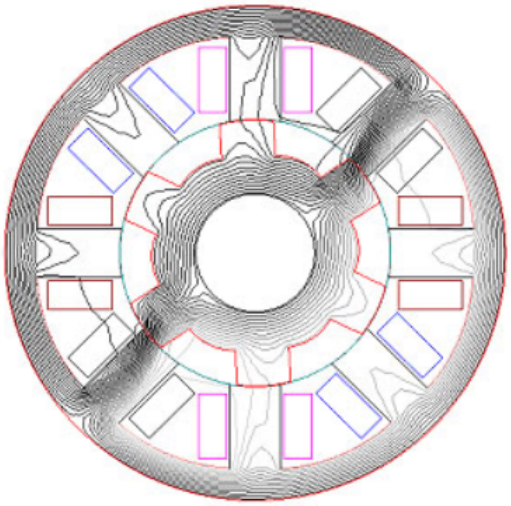

Figure 4.3: Magnetic field distribution

Along JA, the back-EMF absorbs energy equal to ABCJ:

$$ABCJ = i_m^2 \times \omega_m \times \frac{dL}{d\theta} \times \frac{\Delta\theta}{\omega_m} = i_m^2 \times (L_a - L_u) \tag{4.9}$$

The total energy supplied to the phase is then the sum of both areas, OCJ and ABCJ, which is OJAB:

$$OJAB = i_m^2 \times (L_a - L_u) + \frac{i_m^2 \times L_u}{2} \tag{4.10}$$

Reference [7] then shows a way to compare non saturating and saturating operation, by using the energy ratio (Q), as being:

$$Q = \frac{energy\ converted}{energy\ supplied} = \frac{W_c}{W_c + W_f} = \frac{OJA}{OJAB} = \frac{\frac{i_m^2 \times (L_a - L_u)}{2}}{i_m^2 \times (L_a - L_u) + \frac{i_m^2 \times L_u}{2}} \tag{4.11}$$

This energy ratio, is comparable to the power factor of AC machines. So, the higher value achieved for the energy ratio, the higher the output power, for the same energy provided to the motor.

During the JA part of the stroke, the energy is divided equally between the energy used for developing mechanical work (W_c) and energy that is stored in the magnetic field (W_f). The energy ratio would then be 0.5, except there is the need to store the field energy OJC before the torque zone JA, meaning the energy ratio is less than 0.5.

Real switched reluctance machines have higher energy ratios, but are magnetically non linear. In order to express correctly the electromagnetic energy conversion, one must analyse the motor based on magnetization curves, such as the ones seen in figure 4.5, that relate the flux linkage and current for a certain rotor position.

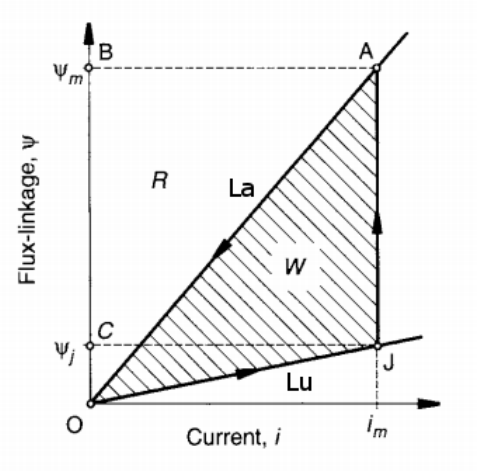

Figure 4.4: Flux linkage versus current for non saturating operation

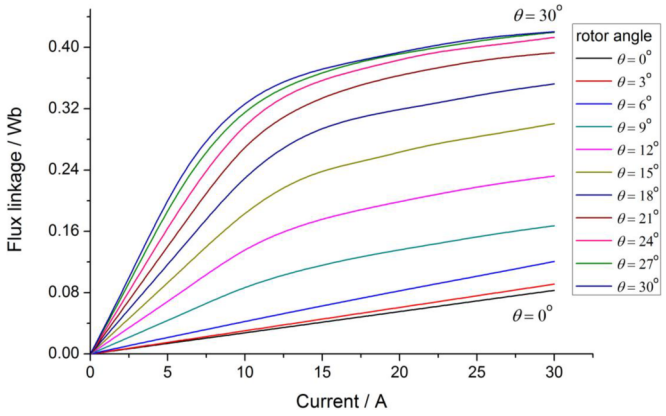

Figure 4.5: Example of magnetization curves

Graphically, the stored magnetic energy W_f and the co-energy W_c are represented in image 4.6. Mathematically, they are calculated as in equations 4.12 and 4.13

$$W_f = \int i\, d\psi \tag{4.12}$$

$$W_c = \int \psi\, di \tag{4.13}$$

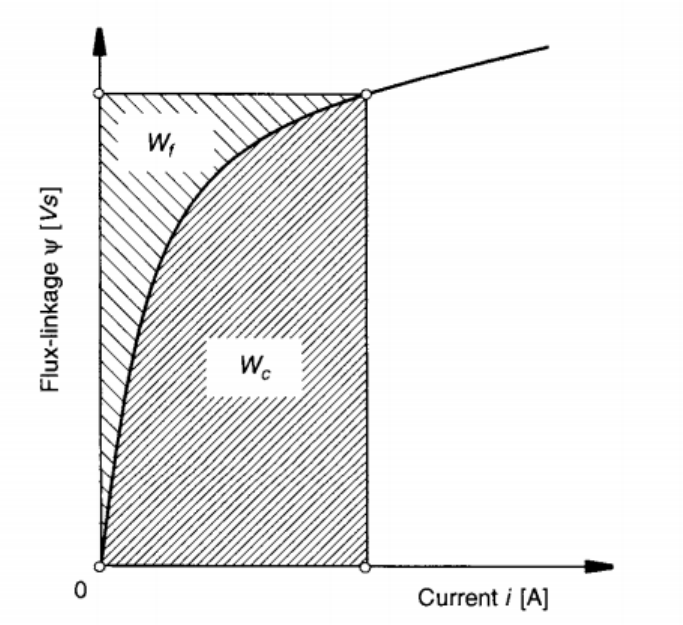

Figure 4.6: Stored field energy W_f and co-energy W_c

Magnetic saturation causes the magnetic stored energy, W_f, to be less than the co-energy W_c. Saturation in a switched reluctance motor is bound to happen in two occasions:

- When the overlap between the poles is small and the flux concentrates in the corners of the poles, because the area of ferromagnetic material is small.

- When the poles are in aligned position, the magnetic core can saturate, at high levels of current.

When displacing the poles by $\Delta\theta$ (AB), at constant current, there occurs an exchange of energy with the power supply that is determined by the following equation:

$$\Delta W_e = \int i \times \frac{d\psi}{dt} dt = ABCD \tag{4.14}$$

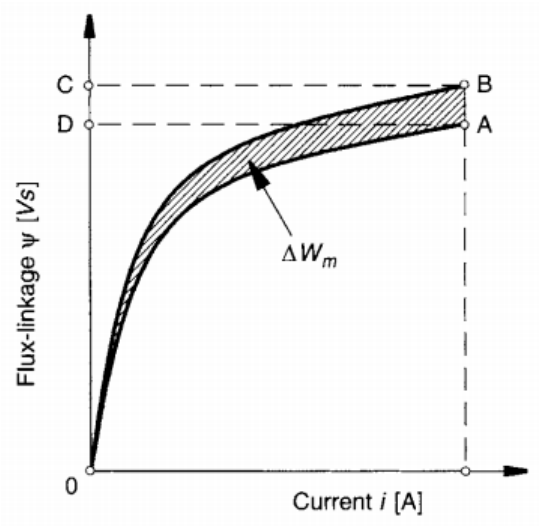

Figure 4.7: Mechanical work for a variation of rotor position

This exchange of energy causes a change in magnetic stored energy:

$$\Delta W_f = OBC - OAD \tag{4.15}$$

Seeing as the total variation of energy is equal to the sum of the variation of mechanical work with the variation of mechanical work done, one can conclude that the mechanical work is equal to OAB:

$$\begin{aligned} \Delta W_f &= \Delta W_e - \Delta W_f \\ &= ABCD - (OBC - OAD) \\ &= OABCD - OBC \\ &= OAB \end{aligned} \tag{4.16}$$

The mechanical work is equal to $T_e\ \Delta\theta$, and when, at the limit, $\Delta\ \theta$ tends to 0, the following expression for the computation of torque can be achieved:

$$T_e = \frac{d\,W_c}{dt}|_{i=const} \tag{4.17}$$

The saturation effect causes the energy ratio to increase, since one achieves lower levels of stored energy and higher levels of co-energy, which, according to 4.17, means higher torque capability. However, causing high levels of saturation leads to difficulties later on, regarding the control of the switched reluctance motor.

In the next section, the design of the SRM to be used in this thesis is presented. As can be seen, it is done taking into consideration what was exposed in this section, as the

motor is designed to reach the magnetic field intensity which saturates the steel used.

4.1.2 Design

The design of an electric motor is often a slow, recursive process, with several calculations and considerations that represent trade-off situations. The case of an SRM is not an exception to the rule.

The SRM designed in this dissertation was created in cooperation with a company that possesses the materials and machinery required for manufacturing a 500W switched reluctance motor.

Since the process of creating these motors is elaborated for mass production, there are several restraints to the design of the motor that must be kept. With that in mind, the first step in designing the new motor is knowing which constructive parameters are used for the design of an SRM, followed by an analysis on the parameters that can be changed and those which need to be kept equal to the original motor.

4.1.2.1 Power Developed

The design of the SRM was made accordingly with the represented in [8]. Starting with the output power calculation, which is presented as:

$$P_{out} = \eta \times k_d \times k_1 \times k_2 \times B \times A_s \times D^2 \times L \times \omega \tag{4.18}$$

Where P_{out} is the motor power, aimed to be maximum around 8kW, η is the efficiency of the motor, that is predicted to be around 90% and k_d is the duty cycle of current conduction angle, in relation to each inductance profile, here assumed equal to 1. The value of k_1 is constant and equal to $\pi^2/120$. k_2 is calculated in 4.20 using the defined ratios in 4.19.

$$\sigma_s = \frac{L_a^s}{L_a^u} \qquad \sigma_u = \frac{L_a^u}{L_u} \tag{4.19}$$

$$k_2 = 1 - \frac{1}{\sigma_s \times \sigma_u} \tag{4.20}$$

L_a^s is the saturated aligned inductance, L_a^u is the aligned unsaturated inductance and L_u is the unaligned inductance. k_2 depends on the operation point of the motor and here, it will be calculated to extract the maximum output power from the SRM, therefore, at the maximum stator current.

Focusing again on equation 4.18, B is the magnetic field intensity, D is the diameter of the stator bore, A_s is the specific electric loading (equation 4.21), L is the axial length of the stator and ω is the speed of the motor.

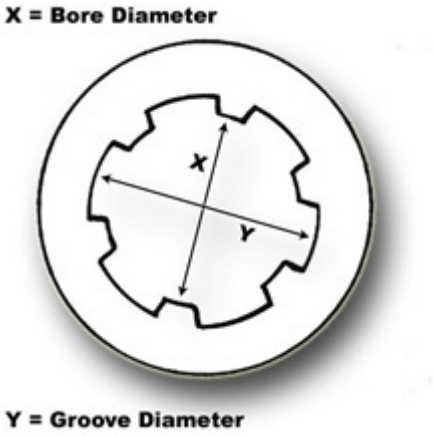

Figure 4.8: Bore and groove diameter

$$A_s = \frac{2 \times T_{ph} \times i \times m}{\pi \times D} \tag{4.21}$$

This parameter A_s, the specific electric loading as it is denoted, expresses the number of armature conductors per meter of armature periphery at the air gap. The torque developed by the motor can be obtained from equation 4.22, being calculated as follows:

$$T = \eta \times k_d \times \frac{\pi}{4} \times k_2 \times B \times A_s \times D^2 \times L \tag{4.22}$$

4.1.2.2 Mechanical Constraints

As mentioned earlier, the design of the SRM must take into account that the manufacturing process has limitations. In various moments during the creation of the motor, the machinery available proved to be difficult or even impossible to adapt for the creation of Scrappy.

The cut of the magnetic steel was the most notorious limitation for the design of the motor. Since the cut is made not by laser but by a pneumatic press, there are several dimensions of both rotor and stator that had to be set at start as unchangeable:

- The bore diameter
- The stator and rotor's pole height
- The stator and rotor's pole width
- The stator and rotor's back iron thickness

Another limitation appears in the assembly of the motor as the winding machine isn't capable of winding the phases of the motor with the specification to be used, set in section **??**. This meant that, after the copper wires were twisted, the stator windings will have

to be created manually. This consists of a long and slow process that can never reach the amount of symmetry that only a machine designed for the effect presents. More than that, hand made windings occupy much more area around the stator pole than those automatically made.

Since the 500 W base version of the motor has about 300 turns per pole of a single copper wire with 0.45 mm of diameter, it should be expected that the maximum of turns per pole, for three twisted copper wires with the same diameter will be around 90 100. Taking into consideration the fact that the windings are to be hand made, the design must aim for a maximum of 70 turns, since this ought to be the best case scenario.

4.1.2.3 Preliminary Design

Preliminary calculations were made considering that each of the stator poles acts as if it is a solenoid, figure 4.9 and, as previously seen, the magnetic field will have to reach the value of 1.45T, which is at the brink of saturation of the magnetic steel.

Equation 4.23 is used to calculate the magnetic field intensity in the iron of a solenoid, where μ_0 is the magnetic permeability constant, μ_r is the relative permeability of the steel, N is the number of turns of the conductor and I is the phase current. Since this motor's design is done from a previous existing motor, it was decided that the phase inductances must have a value as close as possible to the ones of the base motor. This means that L_{ratio}, the ratio of inductance between the inductance of the 500 W and the 8 kW motor must be as close to 1 as possible 4.24.

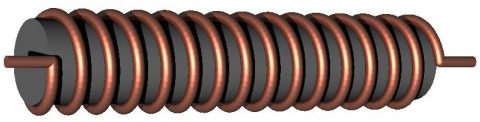

Figure 4.9: Solenoid

$$B = \mu_0 \times \mu_r \times N \times I \tag{4.23}$$

$$L_{ratio} = \frac{L_{8kW}}{L_{0.5kW}} \tag{4.24}$$

The calculations had to take in account that:

- There is space limitations, imposing a maximum number of turns per winding (70, as stated before)

- The magnetic field intensity mustn't be over 1.45T, so magnetic steel won't oversaturate
- The motor windings must be able to handle the new (superior) current that will flow there (being 8 kW, with a phase voltage of 600 V, I comes as 13.3 A, with an RMS value of 6.65 A)
- The area of the poles must be a multiple of the 0.5 kW motor, while still fitting in the space available in the ATV.

$$L = \frac{(\mu_0 \times \mu_r \times A \times N^2)}{l} \tag{4.25}$$

Equation 4.25 is used to calculate the inductance value of a solenoid, where L is the value of the inductance, l is the length of the solenoid and A is the cross sectional area of the solenoid. Here, it is important to refer that A and N are the only variables that aren't fixed, and are limited by the area available on the ATV and the area available around the stator's poles.

Taking all this into account, the author reached a solution, in which the windings have 70 turns in each coil, to create a magnetic field of around 1.5 $Tesla$, and with the fivefold of the pole's area, meaning that 300 laminations will be used for the creation of the stator and other 300 for the rotor.

4.1.3 Simulation

The motor's parameters calculated in the preliminary design are now used for a simulation on the operation of the SRM's design, as well as a simulation of the dimensions and assembly of the motor's components, using 3D CAD software.

4.1.3.1 Motor Operation

In order to validate that the motor is capable of fulfilling the requirements previously set, a simulation software of electrical machines was used. The software chosen is Infolytica's Motorsolve®, since it provides a module exclusively prepared for the design and simulation of switched reluctance machines, using either semi-analytical analysis or complete Finite Element Analysis (FEA).

The accuracy of the results are configurable by the user and, for the final design, the results have been extracted with the highest accuracy possible. Here, a report is made on the final design of the motor, with the values and graphs obtained.

Starting with the torque vs speed curve of the motor, it can be seen in figure 4.10 that, at zero speed, the developed torque is very similar to the 34.25 Nm. It can then be concluded that the motor is capable of starting the ATV's movement in the worst case

scenario, as was demanded. Another comparison that can be made is between the curve extracted from Motorsolve®and the ideal curve, presented before, in image 2.2, from chapter 2. As can be seen, the curves are quite identical.

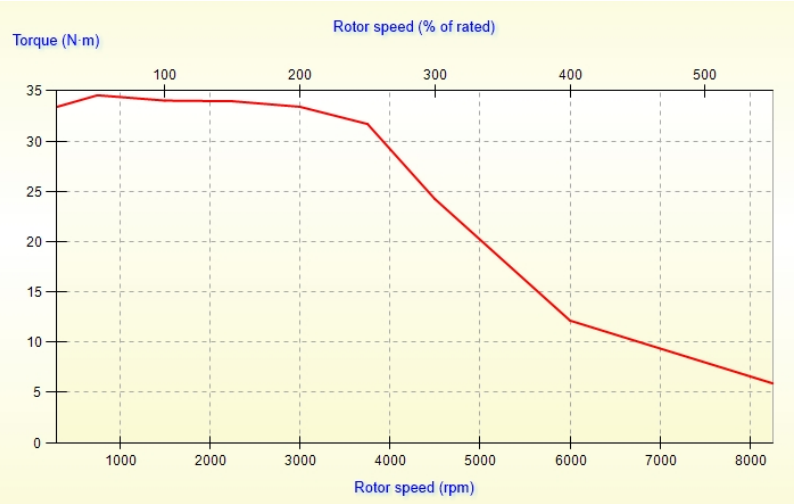

Figure 4.10: Torque vs speed characteristic of the designed motor

The next image presents the Input power, Output power and Efficiency of the motor, for the range of rotational speeds that the motor is designed to operate in.

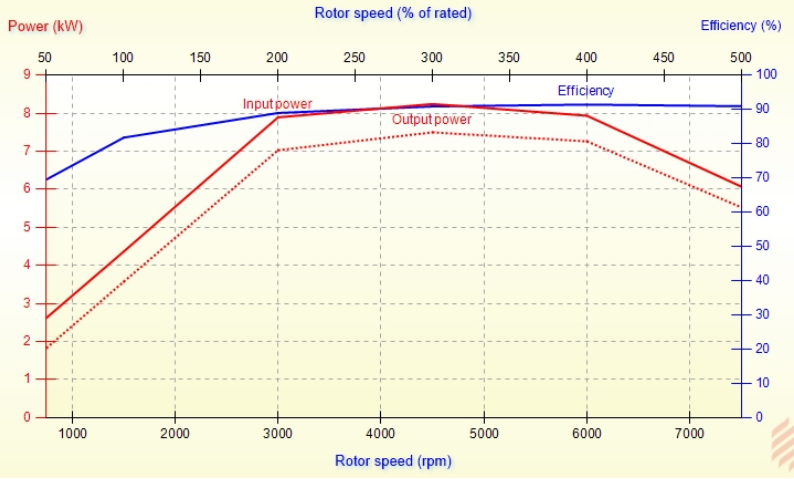

Figure 4.11: Input power, Output power and efficiency of the designed motor

In figures 4.12, 4.13 and 4.14, the inductance, torque and flux of the motor versus position of the rotor are depicted, for some values of the phase current. The data extracted from the charts that generated these curves were of the utmost importance, for the control algorithm, as will be seen in chapter 6. The shape of the curves exposed evidences the

significant difference between the ideal and real curves of the inductance, as well as the existence of saturation in the flux linkages.

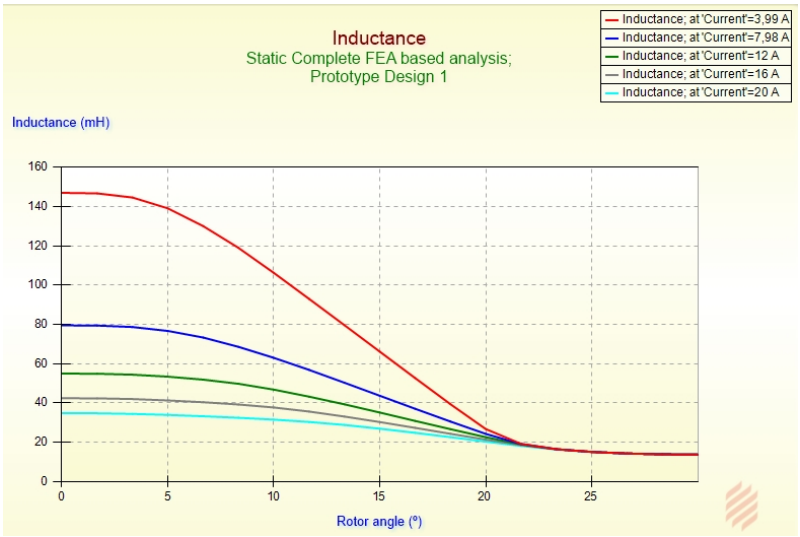

Figure 4.12: Inductance variation of the designed motor

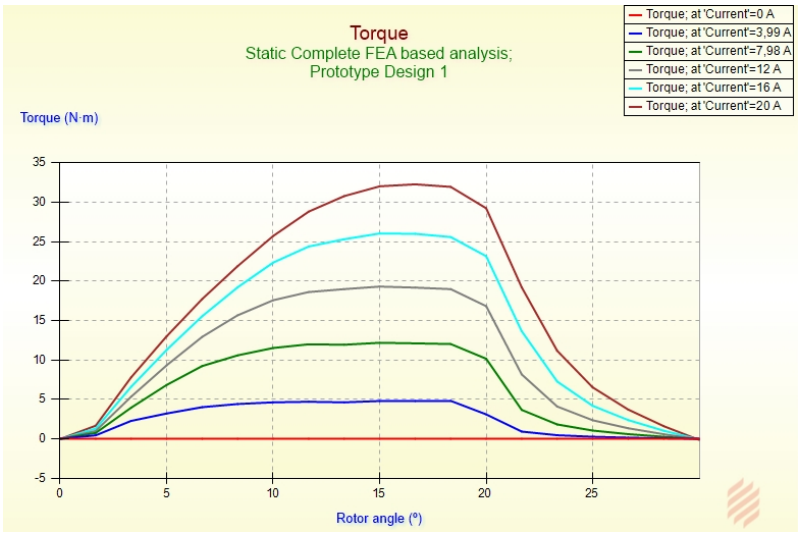

Figure 4.13: Torque variation of the designed motor

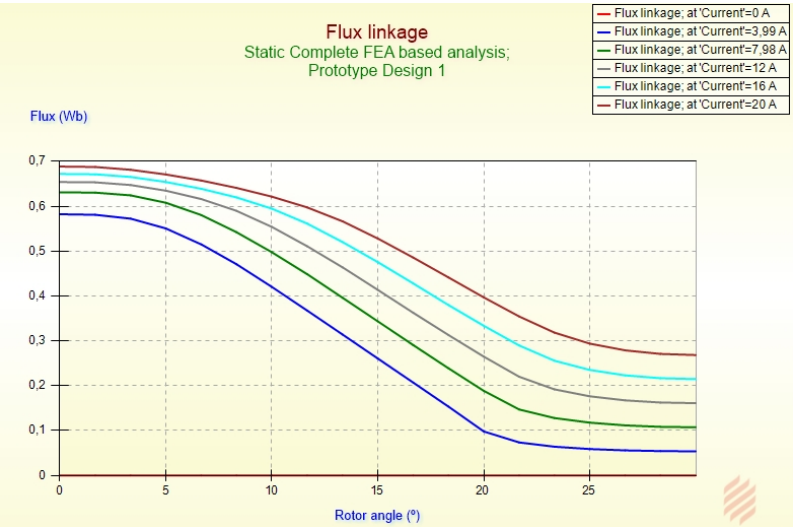

Figure 4.14: Flux variation of the designed motor

In order to verify that the motor is, indeed, reaching a saturation point near the predicted value, a probe was placed in the simulation software, in a stator pole, set to measure the magnetic flux density. The results, seen in figures 4.15 and 4.16, validate the motor's design as they show the magnetic flux density in a pole pair to be around the value calculated previously, of 1.45 Tesla.

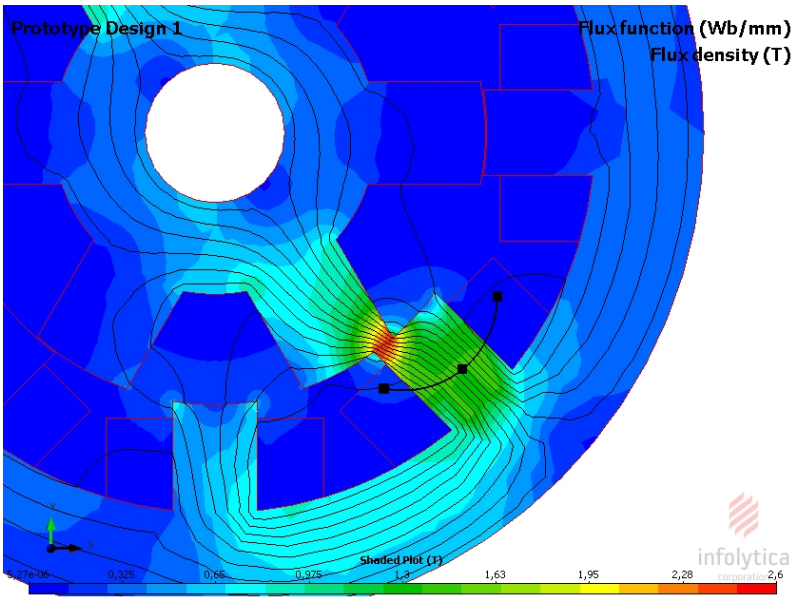

Figure 4.15: Magnetic flux density in a pole pair

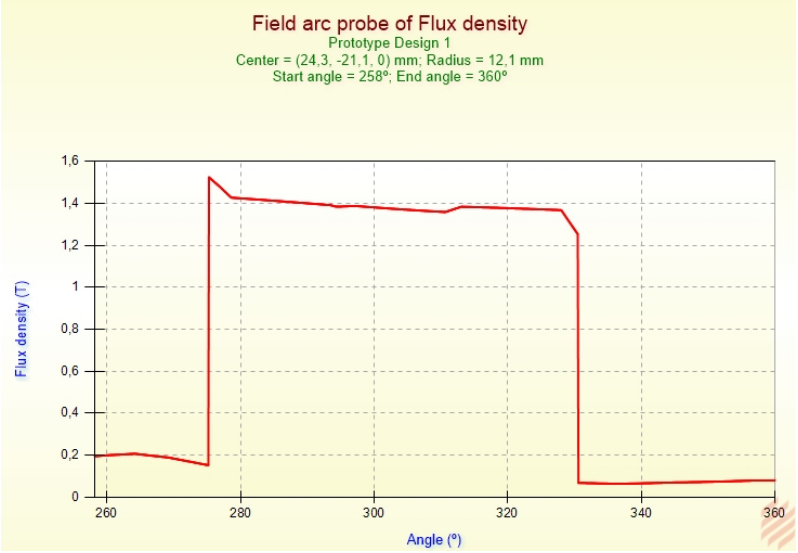

Figure 4.16: Variation of magnetic flux density in a pole pair

4.1.3.2 CAD model

In the previous subsection, the design of Scrappy, from an electrical point of view, was successfully completed. In order to advance to the manufacturing process, it was of crucial importance to achieve a complete assembly of all the 3D components that the motor is to use.

Due to difficulty in creating some parts, there was the need to redesign them tow or even three times, before the final dimensions were set.

Pieces like the covers of the motor were made using a CAM software and a CNC machine, while other, more simple parts, had only the need to be machined in a lathe and Electrical Discharge Machine (EDM), such as the shaft. The shaft design had to take in consideration some mechanical calculations, and in 4.1.3.3, those are presented. The front and back view, respectively, of the final CAD model, are presented in figures 4.17 and 4.18.

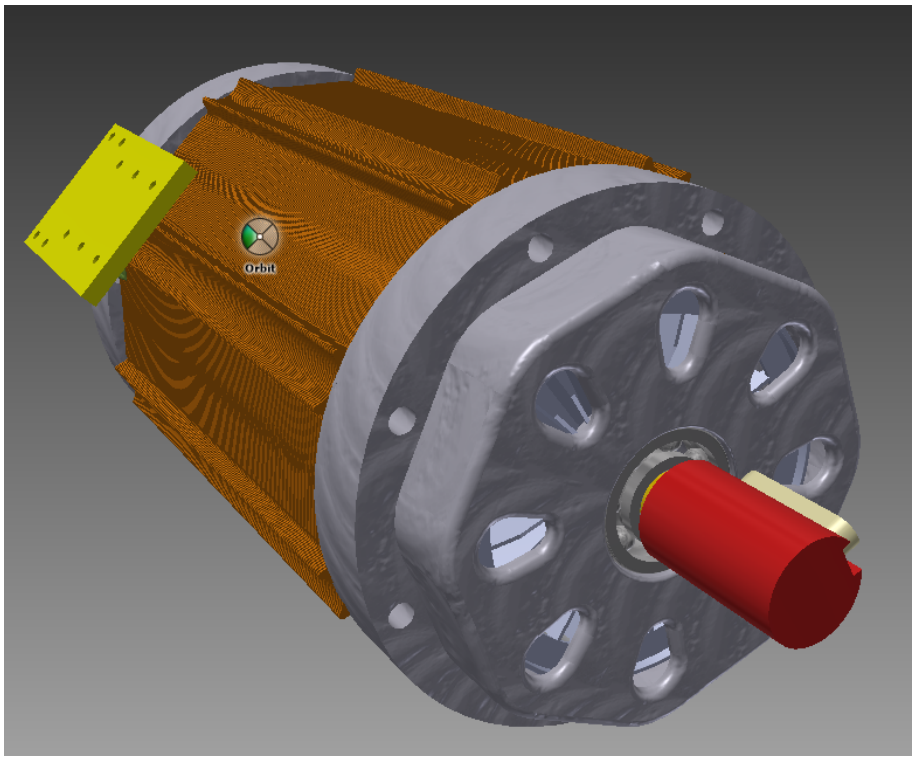

Figure 4.17: Front view of Scrappy

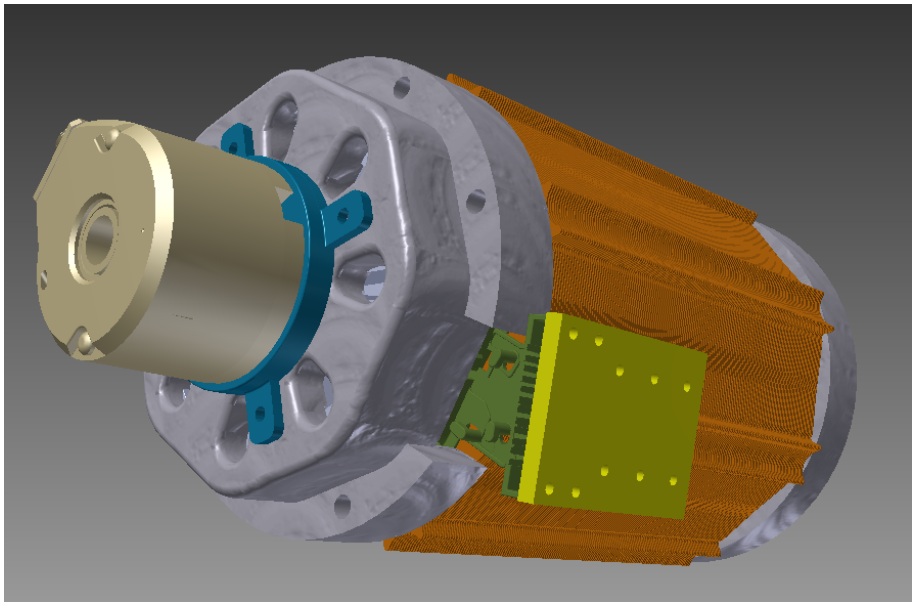

Figure 4.18: Back view of Scrappy

4.1.3.3 Shaft

The shaft is the metal element responsible for supporting the rotor pieces, bearings and coupling the movement of the rotor to the rotational element of the encoder. The shaft diameter is one key element to assure the correct operation of this system, as is through it that the mechanical power of the motor is transmitted to the vehicle.

According to [18], the shaft diameter comes as a result of the maximum value obtained from the shaft diameter calculated according to equations 4.26 and 4.27.

The first is used to calculate the shaft diameter that is needed to transmit the required torque without exceeding the maximum allowable torsional shearing stress of the shaft material.

The second equation is used to design a shaft having the consideration of the minimum diameter needed to prevent torsional deflection. Both equations are calculated using standard values for steel, with allowable stresses of 2.86 kg/mm^2.

$$D = \sqrt[2]{\frac{105 \times P_{out} \times 0.7457}{N}} mm \tag{4.26}$$

$$D = \sqrt[3]{\frac{P}{N} \times 112} mm \tag{4.27}$$

The greater value of diameter was obtained from 4.27, with a value of 147.5 *mm*. The design of the shaft was made with this in mind, having a minimum diameter value of 15 *mm*, except on the top where the encoder will be fixed, where the diameter had to obey to a maximum of 12 *mm*, imposed by this sensor.

From the shaft's point of view, the encoder is equal to a very small, constant load, so the fact that the shaft doesn't have the minimum value of diameter isn't of importance in this case.

4.2 Parts and Assembly

Having ended the design and simulation phase on the motor's project, the next step was to gather the raw materials, prepare the machinery and start the implementation of the motor, which consists of creating the pieces and assembling them in a correct manner. In this section the pieces are presented, along with a small explanation on the choices made and actions taken.

4.2.1 Structure's Covers

The SRM designed, as typical inner-rotor motors, requires two covers to be placed on the structure. One cover on each end of the stator, with a set shape so as to lodge

the rotor's bearings, allow for a good alignment of the shaft and provide good structural robustness, along with resistance to impacts and dust. The back cover of the motor also serves as a good place to append the motor's encoder. In figure 4.19, the front cover can be seen. The back cover is similar to the front one. These parts were created using CNC machinery.

Figure 4.19: Scrappy's Front Cover

4.2.2 Stator

As mentioned before, the stator of an SRM is simply formed by an amount of isolated stacked laminations, of magnetic steel, with a high magnetic permeability, so as to reduce to a minimum the core losses. The fact that the magnetic core is made of stacked laminations instead of a solid block, greatly reduces the Foucault currents induced by the variation of the magnetic flux.

The magnetic steel could be of two main types: grain oriented or non-oriented. Grain oriented magnetic steel are iron-silicon alloys that were developed to provide good magnetic properties in a certain direction. Since the magnetic flux in a SRM is continuously changing during operation, the best choice, and the type of steel to be used in this motor, is non oriented steel, so as to obtain equally magnetic properties in any direction of the material. The magnetic steel used is thyssenkrupp's PowerCore®A M400-50A, with a magnetic field saturation value of around 1.5T.

After being cut, using a pneumatic press, the laminations were given a coating of varnish around the edges, before stacked, so as to assure a complete isolation between them.

Using guiding pins, the laminations were stacked and compressed, so as to have the desired end height of 150 mm. The next step in preparing the stator was to accommodate the previously created winding plastic in between the stator poles, so as to create a path for the copper to be wounded around.

Following the 5A/mm of diameter of copper cable, and calculating the RMS nominal current as:

$$I_{RMS} = \frac{I_{avg}}{\sqrt{m}} = 6.65A \tag{4.28}$$

Where m is the number of phases of the motor. From this, one can achieve a value of 1.33 mm of diameter for the copper cable. Since the immediately next normalized value is 1.5mm, a single solid cable with this section would be adequate for the application. However, using a single solid cable would have many drawbacks, that smaller section, multiple strand cables, could reduce.

For example, in a mechanical point of view, a copper cable with 1.5mm of diameter is more difficult to bend, in order to create tight windings, than 3 cables of 0.5mm.

Looking now from an electrical point of view, the high frequency at which the voltage will be switching would create a noticeable skin effect on a 1.5mm cable, causing the current density to be much lower in the center of the conductor than it is on the surface of the cable and not allow for a complete use of all the cable's section. This leads to a higher apparent resistance of the cable and, by consequence, higher losses.

Using multiple stranded cables reduces this effect. In order to reduce the mutual inductance between the conductors, as well as reduce the space occupied by these, there was the need to twist them around each other, resulting in a final copper cable as seen in figure 4.20.

Figure 4.20: Twisted copper cable

For ease of access and connection to the phases, the end of the windings is placed on the lateral of the motor, as seen in figure 4.21. From left to right, the connectors are: A+, A-, C+, C-, B+, B-, D+, D-.

Pneumatic tube was employed, as a form of isolating the M4 threaded rod that is being used to hold the motor structure together, figure 4.22. This is recommended, since the threaded rod is made of metal and it passes through the stator's magnetic steel. Without this isolation technique, the threaded rod would shunt all the rotor's laminations and would increase the losses in the motor, due to the increased value of the Foucault currents.

M4 nuts, placed on each of the rod's endings, serve as the last fixation element of the motor's structure.

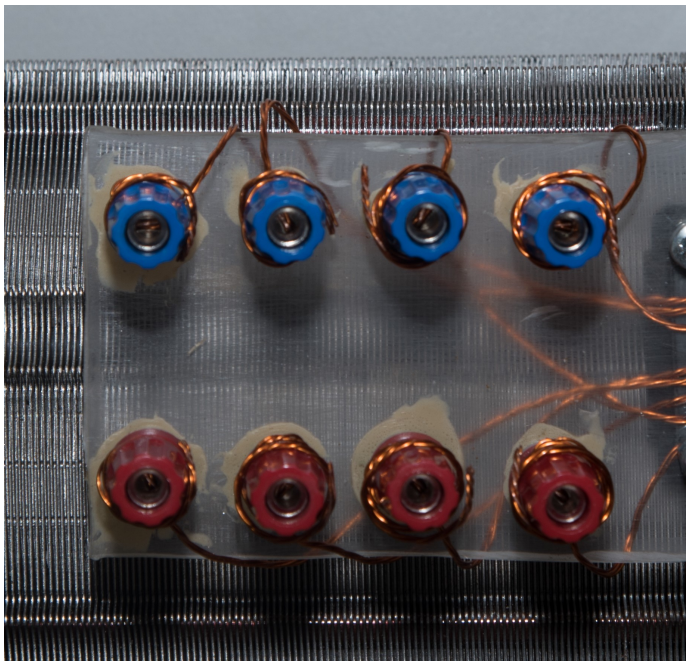

Figure 4.21: Connectors for the 4 phases of the motor

Figure 4.22: Pneumatic Tube

4.2.3 Rotor

The rotor of the SRM, like the stator, has isolated magnetic steel laminations, also created from pieces of motors that were not OK for operating. After being cut and stacked, the laminations were lined and placed on the shaft, pressed together and fixed with the piece designed for the effect (figure 4.23).

The next step in the creation of the rotor was to place the cooling fans on the shaft. The fans available are of the centrifugal type, with radial vanes. As can be seen in figure 4.25, two fans are placed, one on each side of the stacks, so as to create an air flow inside the motor's structure.

Figure 4.23: Fixer for the rotor laminations

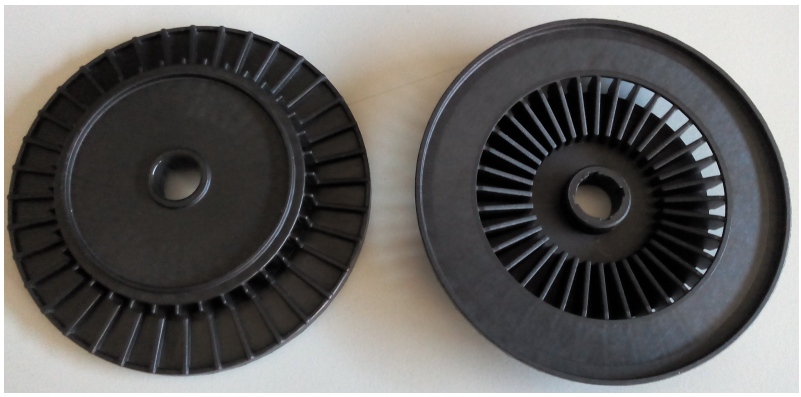

Figure 4.25: Cooling fans of the motor

The rotor was then balanced and placed inside the stator structure. The top and bottom covers of the motor were put in their final position and the bearings, after being heated, were placed on the shaft. The heating of the bearings allowed for a quick and easy placement of the bearings in the motor shaft. According to the datasheet of this component, the expansion is about $15\mu\text{m}/^{\circ}C$, with a maximum recommendable temperature of $90-95^{\circ}C$.

A specific glue for bearings was used, to place the bearings in their final location, fixed to the motor's covers.

4.2.4 Couplers

The rotary encoder is a key element in the control of the SRM, as is explained in chapter 6. It is of vital importance for the correct operation of the system that the encoder is perfectly aligned with the shaft. This is assured by a aluminium part, created in CNC, that serves as a coupler between the encoder and the motor's structure 4.26.

Figure 4.24: Rotor of the SRM

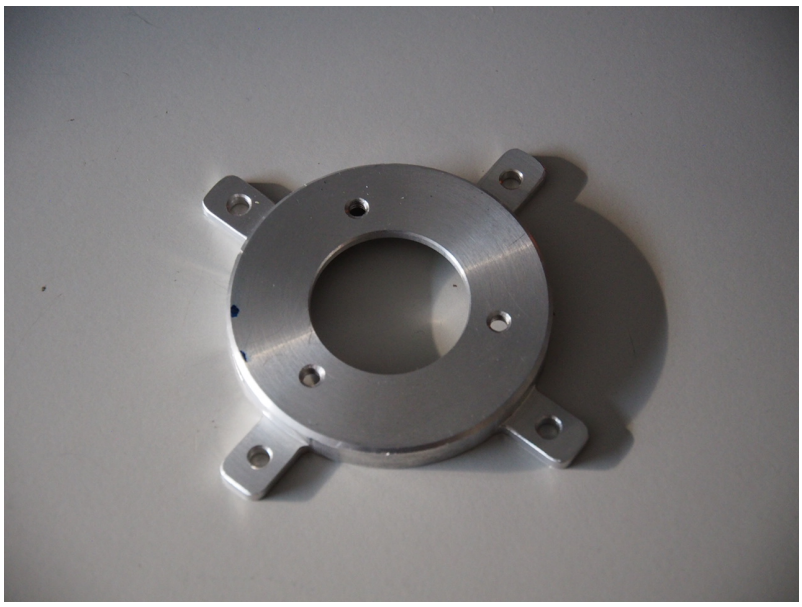

Figure 4.26: Coupler for the encoder

Another coupler necessary for the construction of the system is presented in figure 4.27. This part allows for a mechanical transmission of the rotational movement, from the shaft of the motor, to the existing ATV's transmission chain, by the use of a sprocket, seen in (figure 4.28)

Figure 4.27: Mechanical shaft coupler

Figure 4.28: Mechanical shaft coupler with sprocket

4.2.5 Final Motor

The final and totally assembled version of Scrappy is presented in figures 4.29 and 4.30. The motor seen is ready to be tested and controlled. The operation of the motor is presented in chapter 7, after the control algorithm is studied in chapter 6.

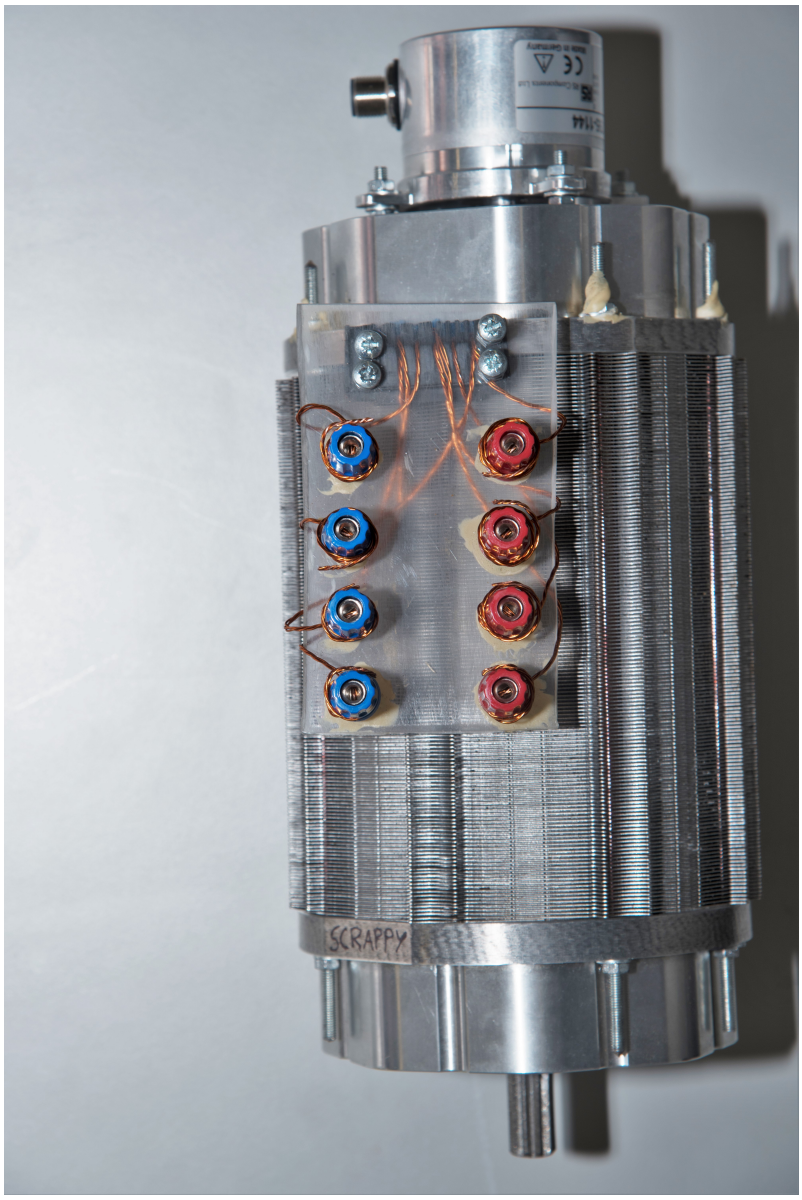

Figure 4.29: Scrappy's final version

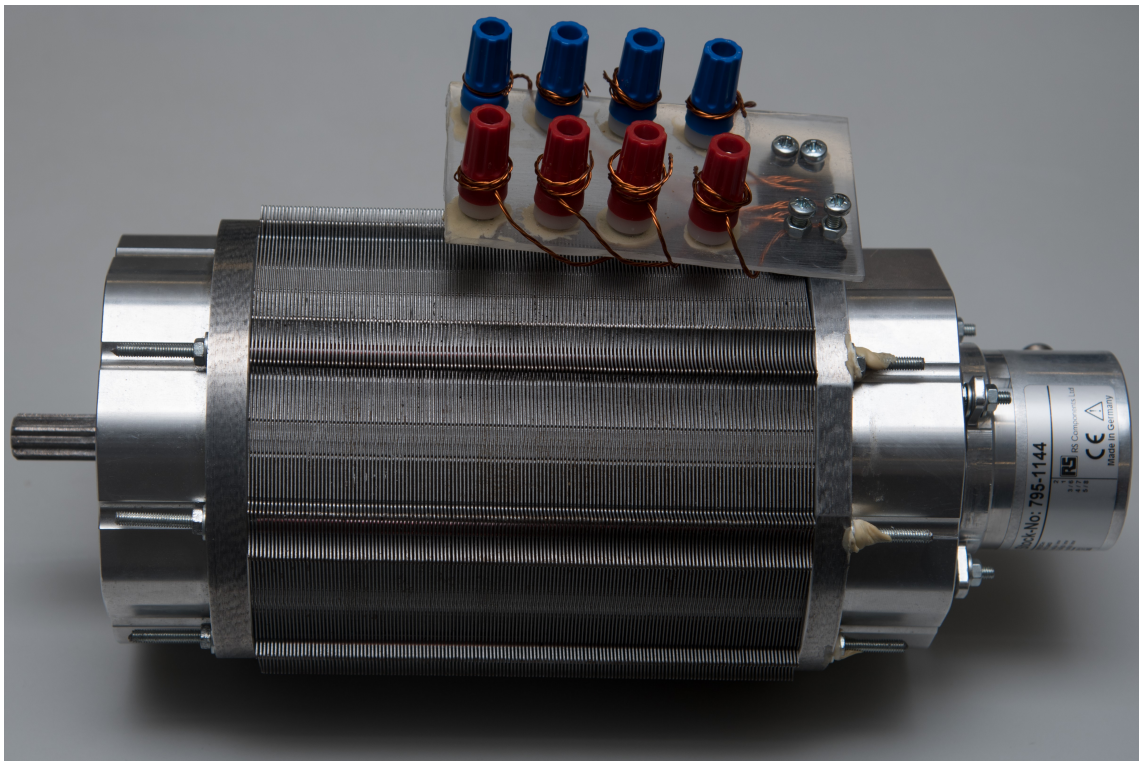

Figure 4.30: Scrappy's final version

Chapter 5

DC/DC Converter

In this chapter the DC/DC converter is designed and its operation is simulated in Simulink®. All the components of the converter are simulated with their parasitic elements, extracted from the datasheets, after the selection of components is made. These components are later presented in 7.

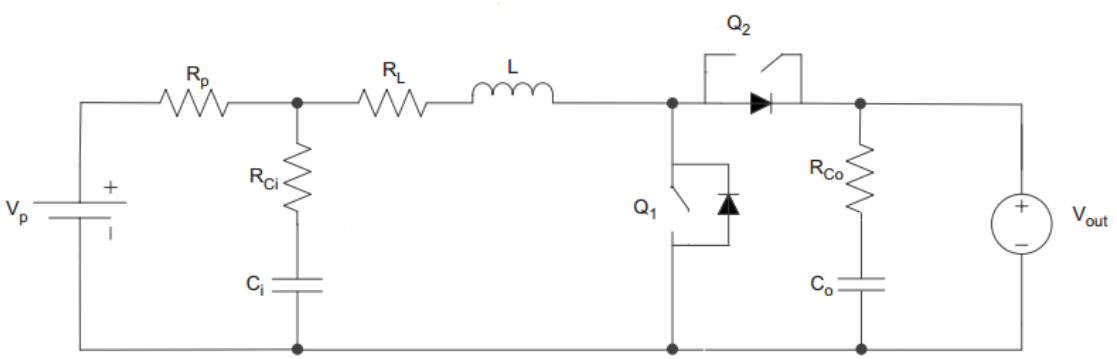

Figure 5.1: Bidirectional DC/DC converter

This converter is essentially a DC/DC boost converter, with a switch (Q2) and an anti parallel diode where a single diode is usually located. This allows for two modes of operation, either in boost mode, where Q1 is commutating and Q2 is always OFF, or in buck mode, where Q1 is always OFF and Q2 is commutating. In figure 5.2 and 5.3, a typical buck and a boost converter are shown, respectively. These are exactly the same circuit that the DC/DC bidirectional converter takes, with the control of Q1 and Q2 done as mentioned.

This operation is intended, for implementation of the motoring and regenerating modes of the motor. When the converter is in boost mode, the SRM will operate as a motor and the high DC voltage link will enhance the operation of the machine, as the phases can be

quickly magnetised and demagnetised. The buck operation of the converter allows for the operation of the machine as a generator, as power can flow from the motor to the batteries, with the implementation of regenerative braking.

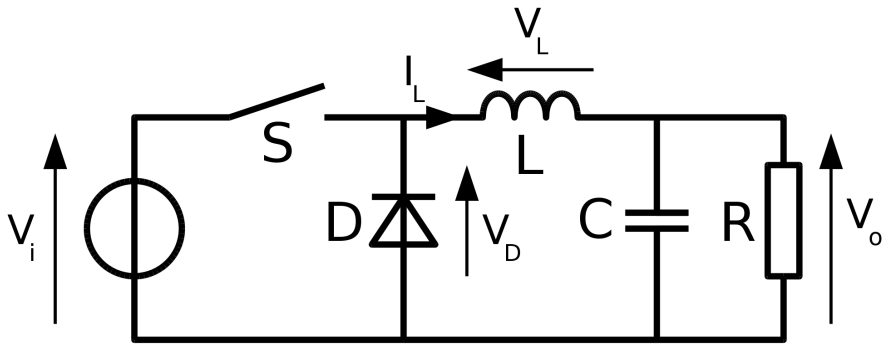

Figure 5.2: Bidirectional DC/DC converter, Buck mode

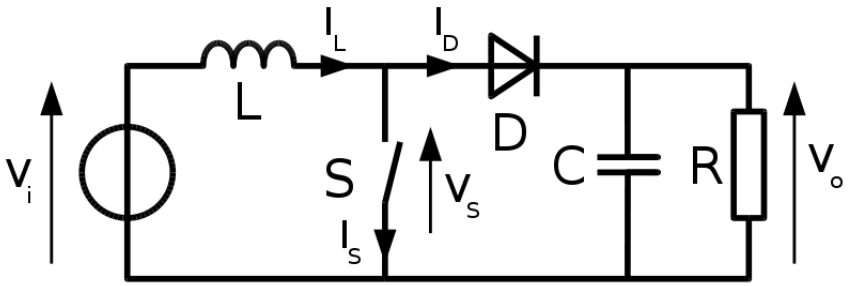

Figure 5.3: Bidirectional DC/DC converter, Boost mode

5.1 Element Calculation

As seen before, the DC/DC converter, requires at least, the following elements: two semiconductors (with anti parallel diode), two capacitors and one inductor.

The calculations for the specifications of the elements that compose the converter are exposed in this section.

As the converter acts as a boost and a buck converter in different instants, the calculations were made for both the modes, and the maximum value was used [23]. The calculations ignored the parasitic elements, for simplification. The table 5.1 shows the expressions used for the selection of the components of the bidirectional converter.

In the previous expressions of 5.1, V_{in} and $V_o ut$ are, respectively, the input and output voltages of the converter, F_{SW} is the switching frequency (25kHz), K_I is the constant that

Table 5.1: Bidirectional converter element's calculations

	Boost	**Buck**
Duty Cycle	$D_{boost} = 1 - \frac{V_{in}}{V_{out}}$	$D_{buck} = \frac{V_{out}}{V_{in}}$
Inductor	$L_{boost} > \frac{V_{in,min}^2 \times (V_{out} - V_{in,min})}{F_{SW} \times K_I \times I_{out} \times V_{out}}$	$L_{buck} > \frac{V_{out} \times (V_{in,max} - V_{out}^2)}{K_I \times F_{SW} \times V_{in,max} \times I_{out}}$
Maximum Switch Current	$I_{SW,max} = \frac{\Delta I_{max}}{2} + \frac{I_{out}}{1 - D_{boost}}$	$I_{SW,max} = \frac{\Delta I_{max}}{2} + I_{out}$
Output Capacitor	$C_{out} > \frac{I_{out} \times D_{boost}}{F_{SW} \times \Delta V_{out}}$	$C_{out} > \frac{K_I \times I_{out}}{8 \times F_{SW} \times \Delta V_{out}}$
Maximum Current Ripple	$\Delta I_{max} = \frac{V_{in,min} \times D_{boost}}{F_{SW} \times L}$	$\Delta I_{max} = \frac{(V_{in,max} - V_{out}) \times D_{buck}}{F_{SW} \times L}$

establishes the relation between the current ripple and the current in the inductor. This parameter is set as 0.3, as seen in [24]. I_{out} is the output current of the converter.

These equations allowed for a design of a converter with an inductor of around $320\mu\ H$, capacitors with a minimum capacitance of around $100\mu\ F$, semiconductors with a current rating of above 70 A. Since the converter will operate with a maximum DC voltage of 600 V, the recommendable voltage rating of the elements is around 1200 V.

In chapter 7, the exact elements used are presented, but for now, only some parameters are of interest, in order to approximate the simulation of the system as much as possible with the implementation.

5.2 Control

The control of the converter's output voltage and it's response to load variations is of extreme importance for enabling a later good operation of the SRM. This control is done with PWM signals, connected to the semiconductor's gates, by action of the driver circuit.

The control of the commutation of the switches for this converter is done according to the same control diagram, whether the converter is functioning in buck or boost mode. The only differences in control between the two modes of operation are the change in transistor that is being controlled (Q1 or Q2) with the PWM signals and the parameters of the PI controllers.

In figure 5.4, the control diagram implemented in Simulink®is shown. It consists in two feedback loops, one for the control of the output voltage of the converter and another for the output current [25]. The error of the output voltage is given to a PI controller, that in turn creates a reference signal that is used for the generation of the current error. This

current error is delivered to another PI controller, which has a much quicker time constant than the previous. Typically, the poles of this compensator appear at least, one decade before the poles of the previous [26].

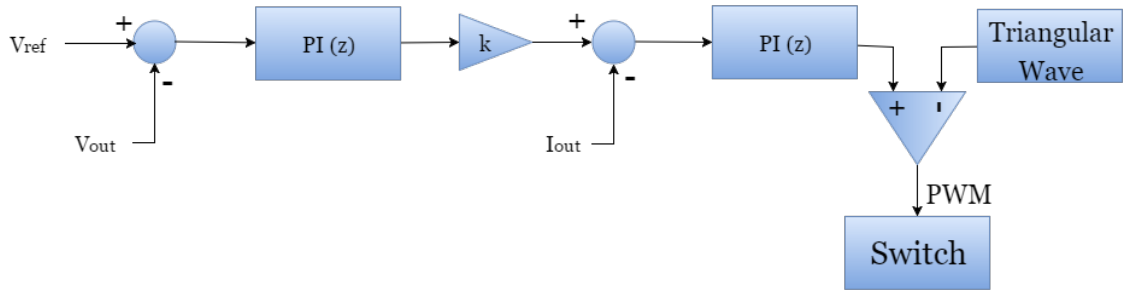

Figure 5.4: Control diagram of the converter

5.3 Simulation

In this section, the Simulink's®simulation executed is presented. The elements used have the same value of the ones that were used in the implementation (see chapter 7). The tuning of the PI controllers was done following the Ziegler Nichols method, which implies the following actions [27]:

- Set the Integral gain to zero
- Increase the Proportional gain, from zero until this gain is equal to the gain at which the output consists of a sustained, periodic oscillation (K_l).
- Use the gain previously obtained and the period of oscillation (T_l) to reach the values of the controller's parameters, through the existing tables.

The table for PI controllers uses the following values for it's parameters: $K_c = 0.45 \times K_l$ and $T_c = \frac{T_l}{1.2}$. Reference [28] explains some of the advantages and disadvantages of this tuning method, it mentions the fact that this method doesn't require an in-depth study of the system before a first approximation is achieved, along with the fact that it leads to a low closed loop robustness of the system.

For this reason, some adjust on the parameters was done after the initial solution was found, in order to achieve a better response from the system. From the continuous time simulation, a discrete time simulation was achieved, with a fixed step of $50\mu\ s$, corresponding to 20KHz. This frequency was chosen, taking in consideration the time that the control algorithm has available to execute the computations and the losses of the semiconductors, calculated in 7.

In 5.5, an image of the system in Simulink®shows how the converter was simulated, including the control blocks. The "buck" and "boost" blocks in figure 5.5, each have

inside them implemented the control logic depicted in 5.4. In 5.6, the response of the system is shown, to a variation of load. At 1.5s, the load doubles the current it sinks, increasing the output current from 10A to 20A. Note that here, the converter is operating in boost mode, with a resistive load and a voltage reference of 600 V. It can be seen that the output voltage ripple increases with the current that is being delivered to the load, as is expected.

For the response of the buck operation, a reference of 160 V is given, since that is slightly above the battery pack's nominal voltage, for the recharging of the batteries, without damaging the pack.

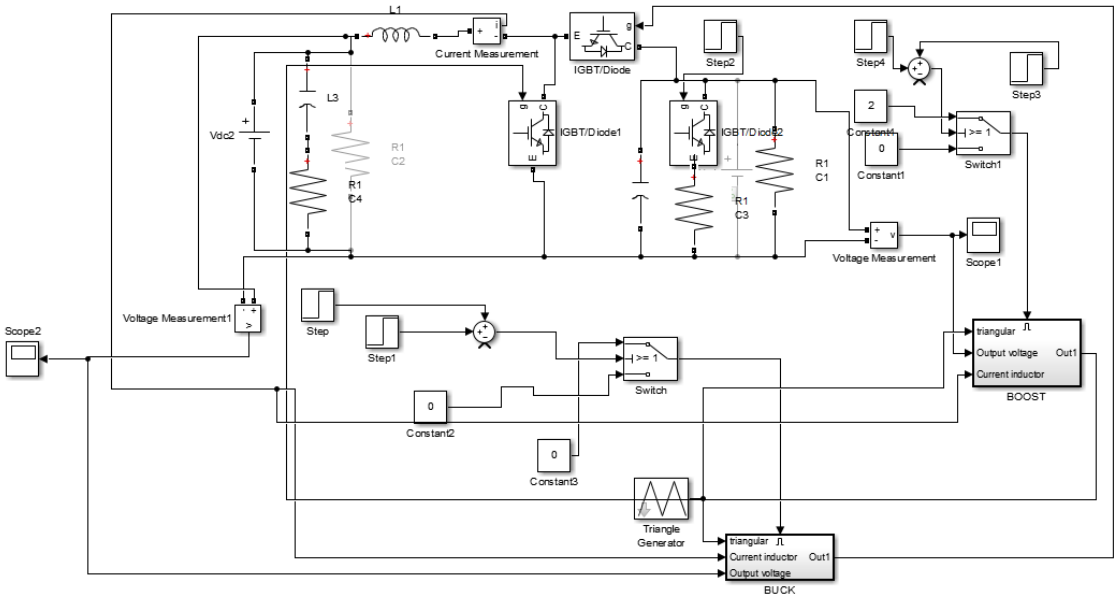

Figure 5.5: Simulation of Converter in Simulink®

The load of the buck converter is a battery pack which, from the converter's point of view, acts almost as a constant load, throughout its operation.

The input voltage of the converter, however, is in constant variation, as it is generated from the motor's back EMF, which depends, among other factors, on the speed of the rotor. Regenerative braking reduces the velocity of the rotor and, in doing so, lowers the back EMF of the motor.When employing regenerative braking, it must be taken in account the motor's zones of operation where the voltage input of the converter is superior to the battery pack's voltage.

In figure 5.8, the response of the system when operating in buck mode is presented. The input voltage is changed from 300 V to 400 at 5s. In figures 5.7 and 5.9, the start response of the converter can be seen, for both the cases mentioned.

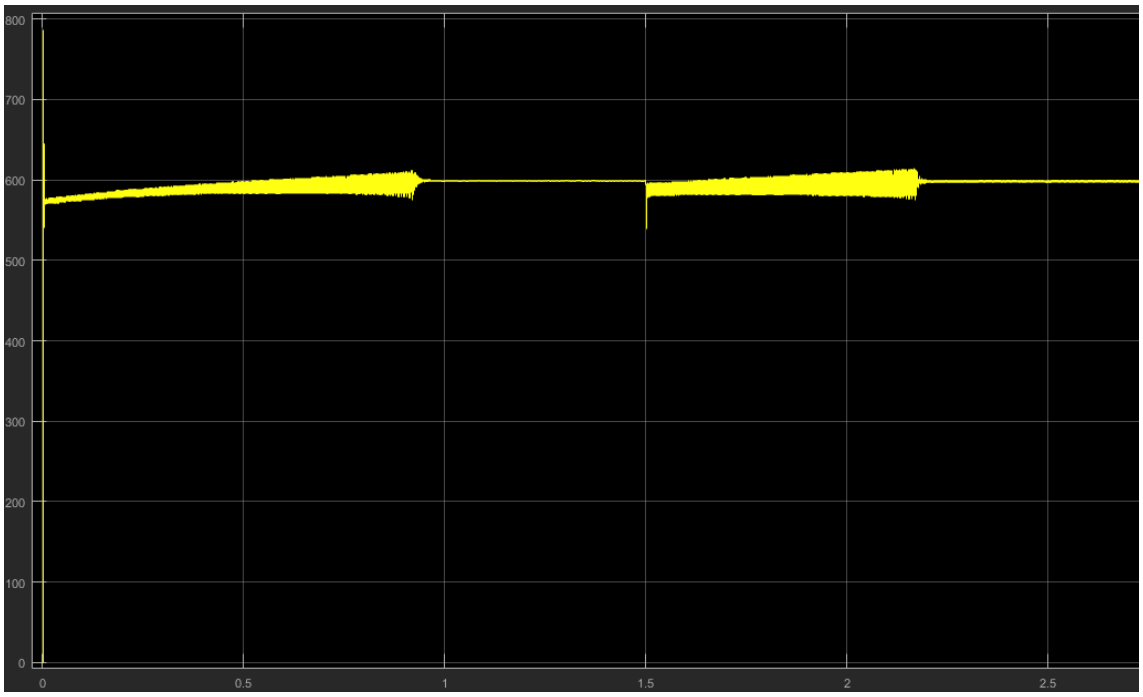

Figure 5.6: Output voltage of boost operation, with load variations

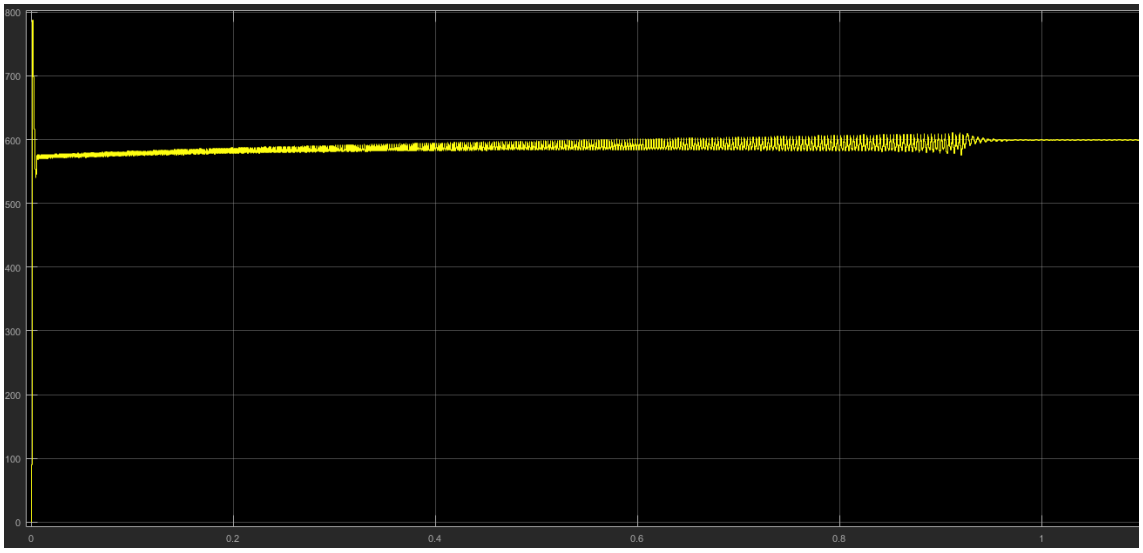

Figure 5.7: Start of operation, in boost mode

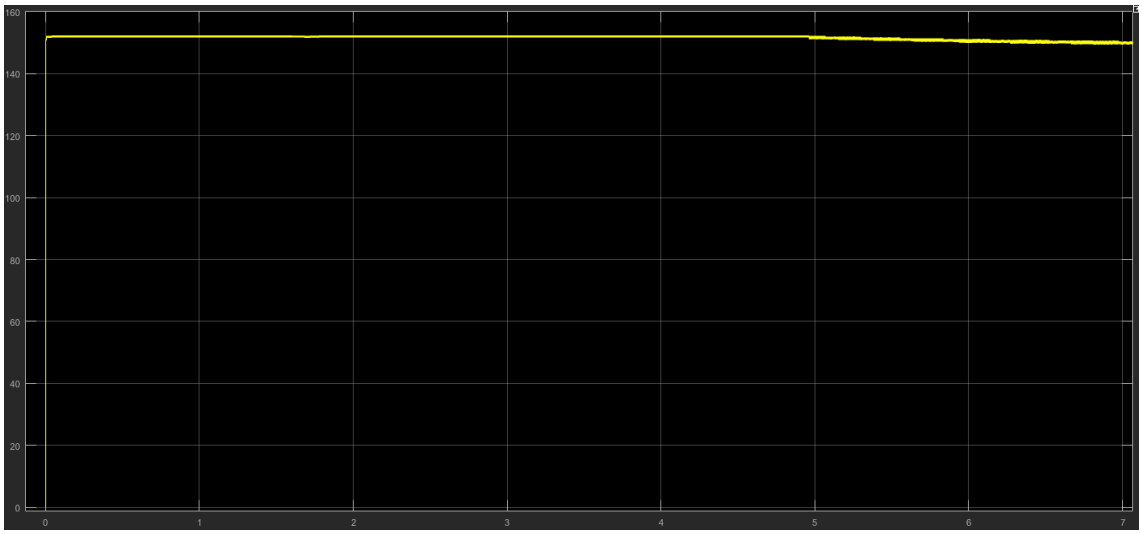

Figure 5.8: Output voltage of buck operation, with input voltage variations

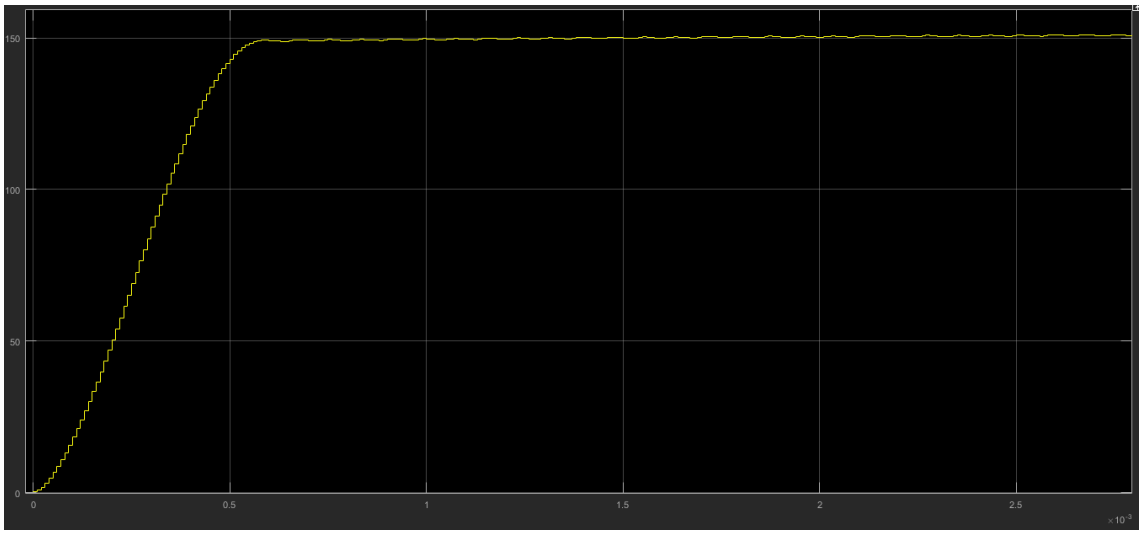

Figure 5.9: Start of operation, in buck mode

Chapter 6

Control

In this chapter, the control algorithm simulated using MATLAB's Simulink is presented. As mentioned in chapter 2, a DITC controller is used, for managing the operation of an 8/6 SRM.

6.1 DITC

As explained before in 2, the DITC is a combination of several strategies for increasing the efficiency and minimizing what is typically, the worst aspect of the operation of a SRM, the torque ripple [29].

A diagram of the blocks and connections created in Simulink®can be seen in figure 6.1. In figure 6.2, the Simulink ®environment corresponding to the implementing of the diagram is shown.

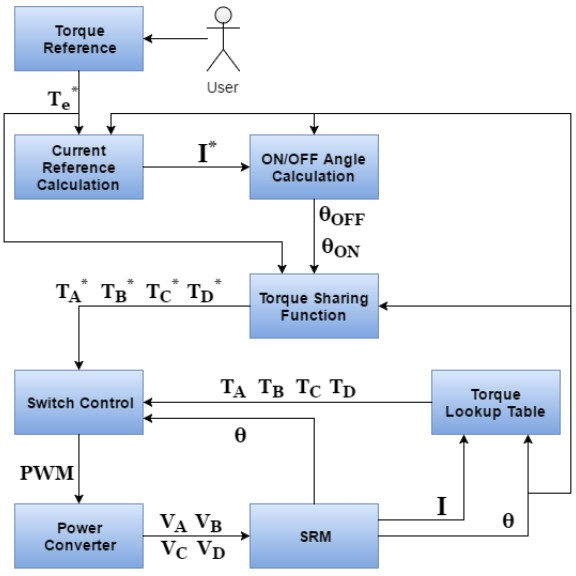

Figure 6.1: DITC Diagram

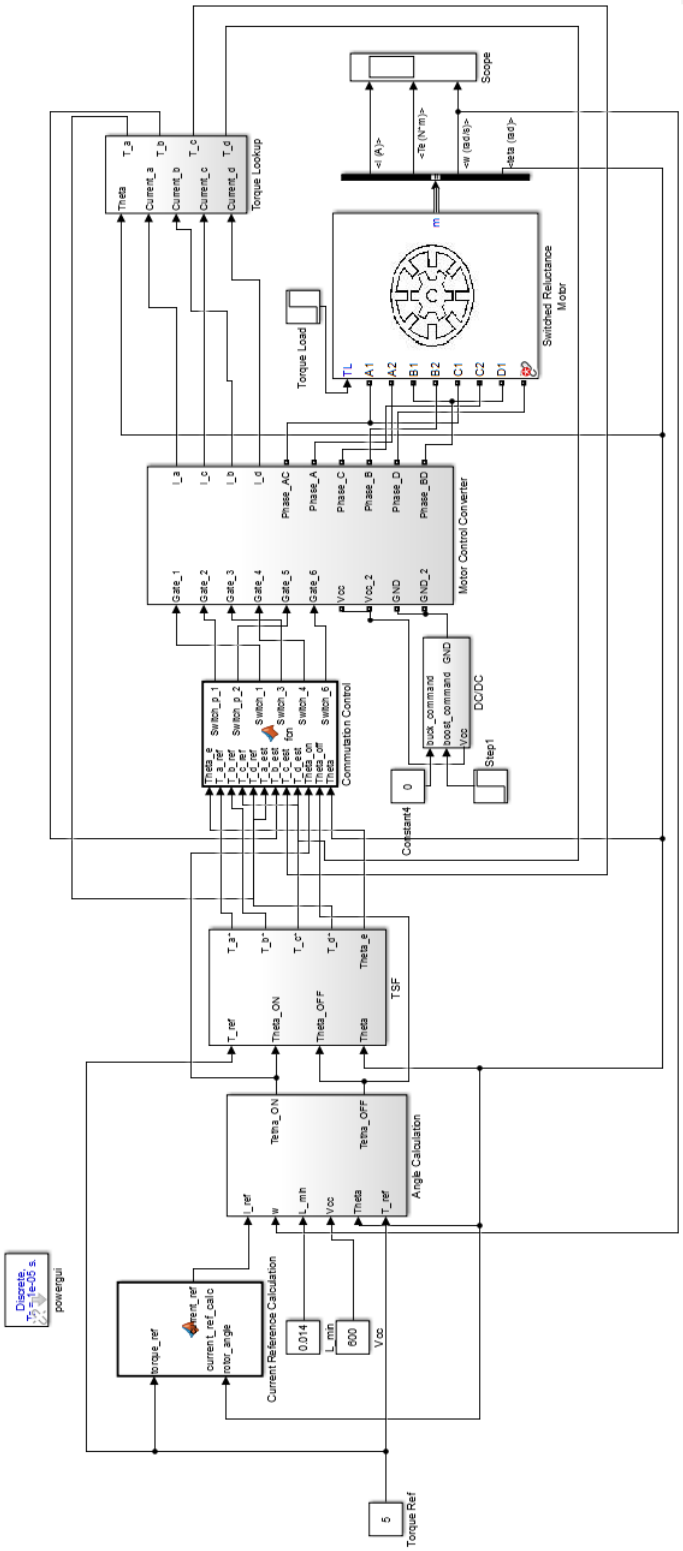

Figure 6.2: Motor simulation

6.1.1 Lookup Tables

In order to make the model of the SRM present in Simulink's library correspond to the model simulated in MotorSolve®, the flux tables had to be extracted from Infolytica's software, and, with a script specially created for the effect, import the data from the csv file to the MATLAB workspace. The data was then plotted in 3D graphs, that are depicted in figures 6.3 and 6.4.

While the lookup table of flux is used in the motor's model, the torque table is used in the control algorithm, in order to estimate the torque developed by each one of the phases, from the rotor's position and phase current. The most mentioned method in the literature for torque estimation isn't analytical. The fact that, in this motor, the torque is calculated using derivative terms, is often the reason that lookup tables are employed.

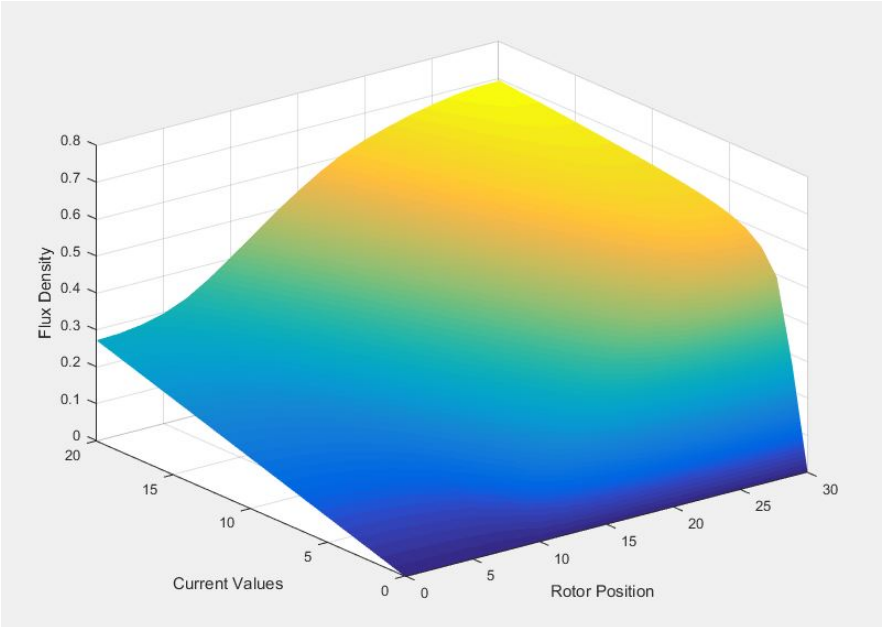

Figure 6.3: Flux Vs Position Vs Current of the motor

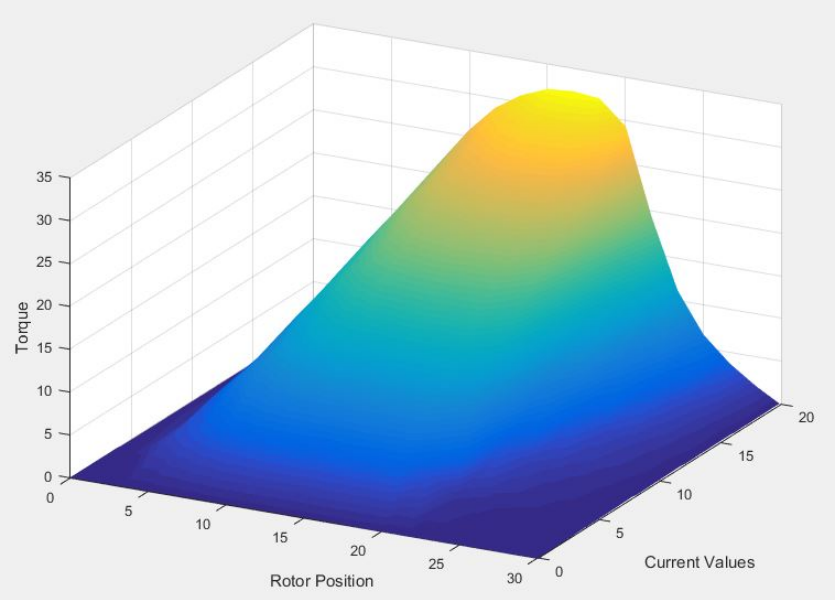

Figure 6.4: Torque Vs Position Vs Current of the motor

6.1.2 ON/OFF Angle Calculation

The block of calculation of θ_{ON} and θ_{OFF} inputs parameters and sensor measurements, in order to output the commutation angles, for the control of the SRM.

The equations used for the calculation of such angles were extracted from [30] and [31]:

$$\theta_{ON} = \theta_x - \frac{L_u \times i^* \times \omega}{V_{DC}} \tag{6.1}$$

$$\theta_{OFF} = \frac{\theta_a + \theta_{ON}}{2} \tag{6.2}$$

In the θ_{ON} calculation, θ_x is the angle at which the phase inductance starts to rise (figure 6.5). At this angle, the phase current should already be at the reference value, in order to extract the maximum torque of the machine.

L_u is the unaligned inductance, i^* is the current reference, ω is the speed of the rotor and V_{DC} is the phase voltage applied. θ_a and θ_u are, respectively, the aligned and the unaligned positions of the rotor, for each of the phases.

The current reference, needed for the calculation of θ_{ON} and, consequentially θ_{OFF}, is obtained from the Torque lookup table and the values of θ and T_e^*, the rotor's position and the torque reference given by the user.

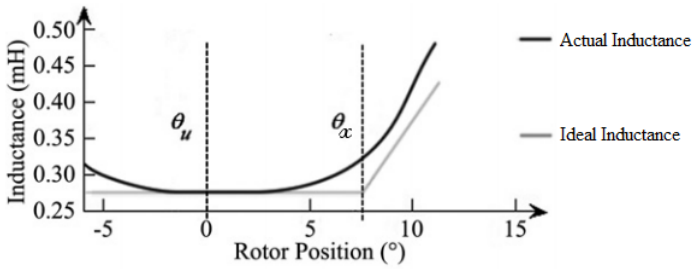

Figure 6.5: θ_x, for the ideal and real phase inductances

6.1.3 TSF

Reference [32] proposes an ideal torque sharing function for the DITC algorithm. It chooses to divide the torque references in five distinct zones, in which the references take two constant values, two quadratic and one linear expressions. This behaviour is shown in image 6.6.

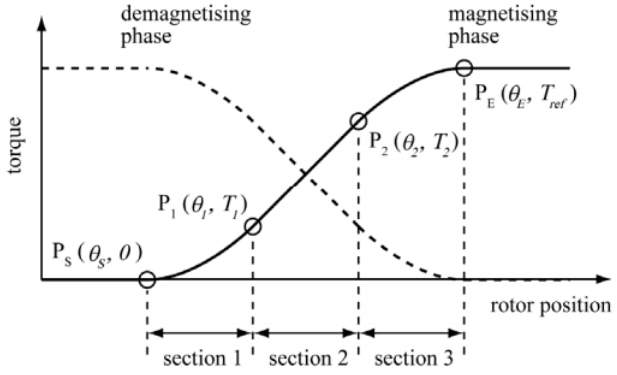

Figure 6.6: Torque reference for a magnetizing phase

In the first zone, the torque reference for the magnetizing phase is 0, since the rotor hasn't reached θ_{ON} position. When the rotor's position is in section 1, the torque reference rises, following a quadratic expression. When in section 2, a linear expression is employed, following another quadratic expression when in section 3. After the end of section 3, the torque reference is equal to the input of the user, and this constant value is the torque reference for the controller, until θ_{OFF} is reached.

For the demagnetization phase, the torque curve is calculated as being the difference between the torque reference input by the user and the torque curve of the magnetising phase.

In table 6.1, the calculations for each of the sections are corresponded with the angles in which they are used.

Table 6.1: TSF

T_{ref}	**Angle Interval**
0	$\theta_{ele} < \theta_s$
$\frac{k^2}{4\times T_1} \times (\theta_{ele} - \theta_s)^2$	$\theta_s \leq \theta_{ele} < \theta_1$
$k \times (\theta_{ele} - \theta_1) + T_1$	$\theta_1 \leq \theta_{ele} < \theta_2$
$\frac{k^2}{4\times (T_2 - T_{ref})} \times (\theta_{ele} - \theta_E)^2$	$\theta_2 \leq \theta_{ele} < \theta_E$
T_{ref}	$\theta_E < \theta_{ele}$

The parameters k, θ_s and θ_E are calculated according to the following expressions:

$$k = \frac{T_2 - T_1}{\theta_2 - \theta_1} \tag{6.3}$$

$$\theta_s = \theta_1 - \frac{2 \times T_1}{k} \tag{6.4}$$

$$\theta_E = \theta_2 - 2 \times \frac{T_2 - T_{ref}}{k} \tag{6.5}$$

Simulating the waveform generations, for a starting reference of 10 $N.m$, with two steps, one of 5 $N.m$ and another of -10 $N.m$ at, respectively, 0.15 s and 0.2 s, the TSF created the waveforms seen in figure 6.7, each of the colors corresponds to the reference of a different phase. On the first section of the image the torque waveforms are depicted and in the second, the torque reference from the user.

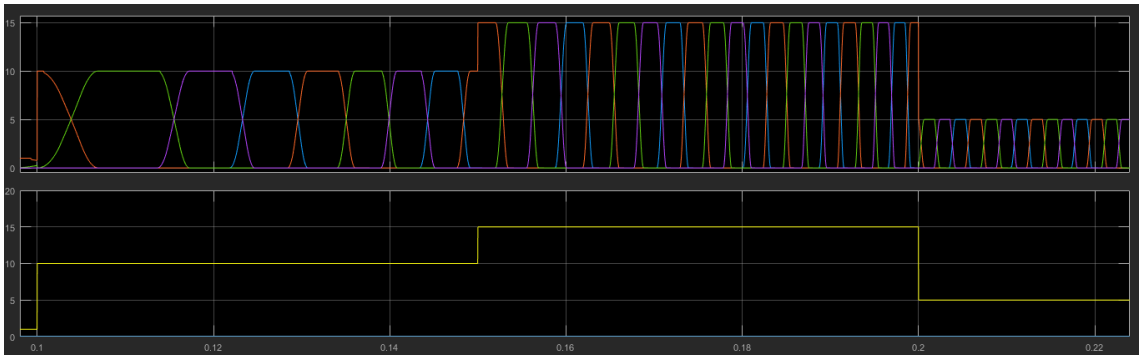

Figure 6.7: Torque input from user and waveform output of TSF

6.1.4 Switch Commutation

As presented in chapter 2, the 1.5 transistor configuration converter is used for the control of the 8/6 SRM created in this dissertation. In figure 6.8, the converter is shown and in this subsection, the switching control of the semiconductors is presented.

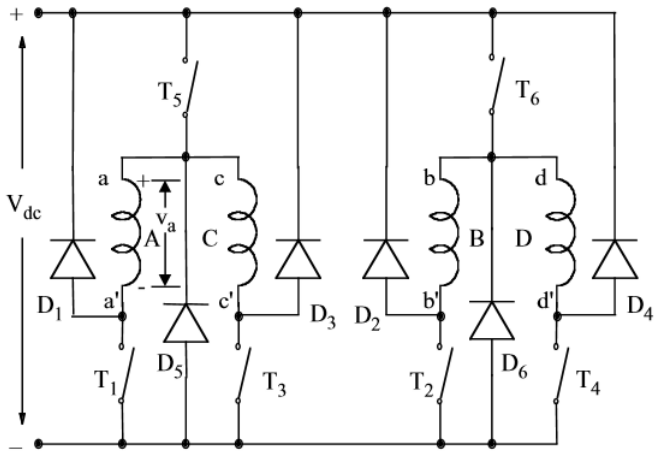

Figure 6.8: 1.5 Transistor Configuration Converter

The commutation of the phase switches is done with hysteresis control, according to diagram 6.10, so to place the converter in magnetising, freewheeling and demagnetising operation, for each one of the phases. The 1.5 transistor configuration converter has one transistor that is shared by two phases. For this semiconductor, an "OR" logic is implemented, that is, the semiconductor is commutated ON if either one of the phases that it feeds commands it to.

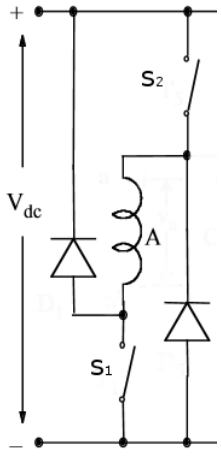

Figure 6.9: Electrical schematic of the converter, for phase A

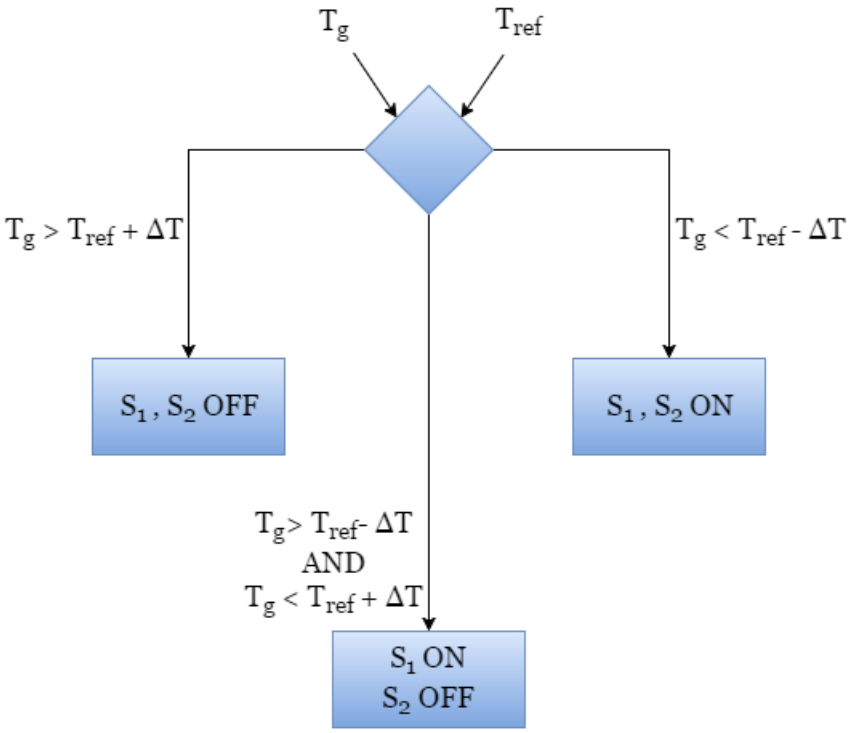

Figure 6.10: Diagram for Switch Control of a phase

6.1.5 SRM Operation

In this section the simulation's results of the operation of the motor are presented, as the motor is given several torque references, simulating the inputs from the user, as well as a load, placed instantaneously on the shaft. All the simulations shown are already in discrete form, being run with a constant time step of 50 microseconds (corresponding to 20kHz). In figure 6.11, it can be seen that the previously mentioned torque estimation outputs values very identical to the actual torque generated by the motor, which validates the data from the torque table, as well as the motor's model defined in Simulink®.

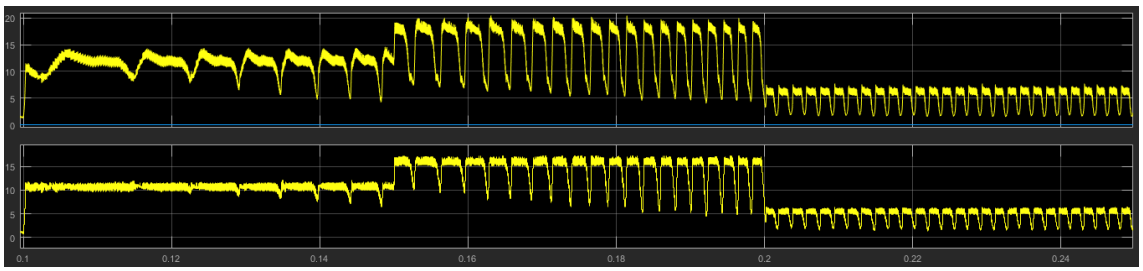

Figure 6.11: Torque estimator Vs Actual SRM torque

In figure 6.12, the operation of the SRM is presented, for a constant torque reference

of 6 $N.m$. From top to down, the currents of the motor are shown, followed by the torque developed by the motor and the rotor's speed. A load variation is made at 0.07 s, with a value of 6 $N.m$. As can be seen, the velocity of the rotor stops increasing when the step load is placed, and, since the torque generated by the motor is the same as the load, the velocity stabilizes.

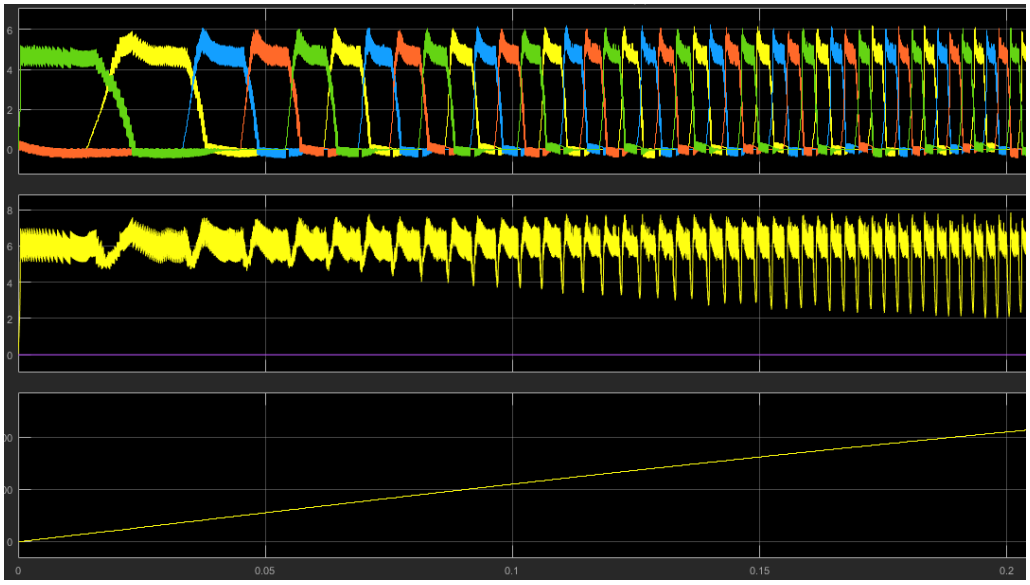

Figure 6.12: SRM operation with constant torque reference (6N.m)

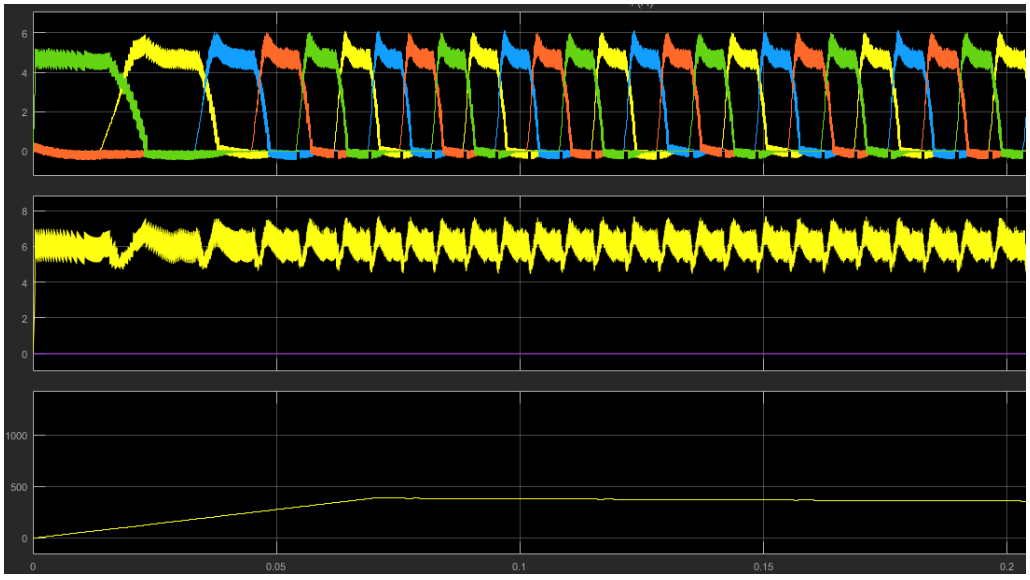

Figure 6.13: SRM operation, with torque load of 6N.m, at 0.07s

The operational simulation of the SRM, with the same input from the user as in the TSF section (6.1.3), outputted the graphs seen in 6.14. The torque ripple is notorious when

the machine is exchanging excitation phases, but it is completely expected. Since the simulation isn't being run in continuous simulation, but in discrete time, with a frequency of 20kHz, the control of the system isn't as effective, and torque ripple increases. The 20kHz frequency comes as a choice of the author, based on the pros and cons of increasing the commutation frequency of the semiconductors.

The higher the frequency of operation, the higher the frequency at which the semiconductors have to commutate. Besides the semiconductor's limits of commutation frequency, the losses will increase with the increase of frequency. A limit in the operation frequency is also imposed by the control platform, that needs to run the algorithm in the period defined.

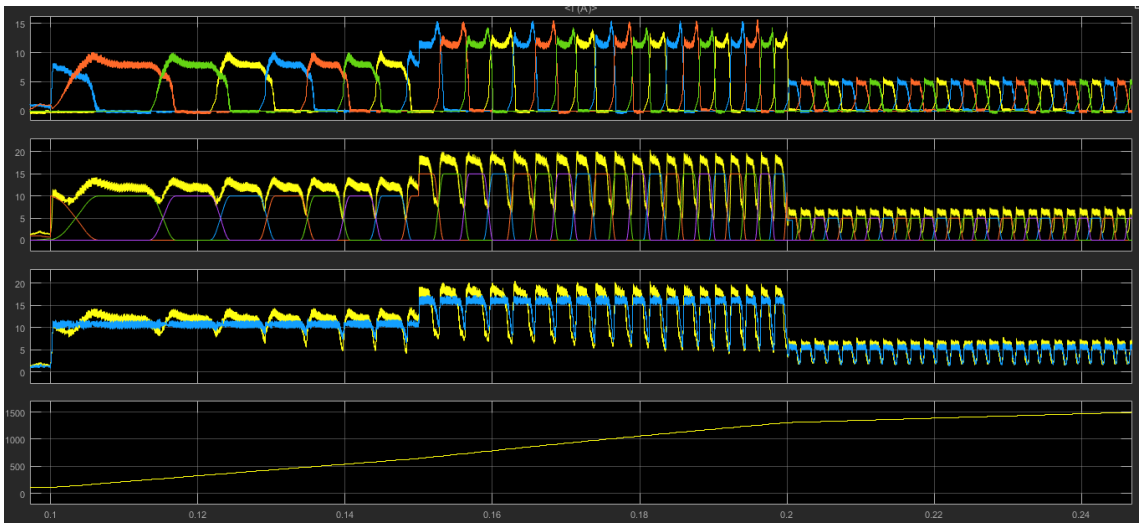

Figure 6.14: Motor Operation Simulation

In 6.14, the first graph corresponds to the phases' currents in the SRM, each color being of a different phase. In the second graph, the torque response of the motor is compared to the torque references. The third graph is the comparison of the torque generated with the torque estimated and the last graph is the SRM's speed.

Chapter 7

Implementation

In the chapter that is now introduced, the systems mentioned previously are given form. The converters are modelled and assembled, and all the necessary auxiliary circuits are created and presented. In the final sections, the final system and experimental results are exposed and discussed.

7.1 Passive Elements

The DC/DC Buck Boost converter requires passive components in order to operate. These components are one inductor and two capacitors. The inductor was chosen first, because of the small number of solutions existing in the market for such a specific use. To have a custom made inductor would be a great risk in the project, due to delays that could occur in the manufacturing process, so that option was only considered as a last resort. Typically, inductors available in the market with the necessary inductance aren't fit for operating with such high RMS currents. The best option was found to be the H1305-301 model, 7.1 , from MPS Industries. It is an inductor with a current rating of $60A$ and a nominal inductance value of $300\mu H$.

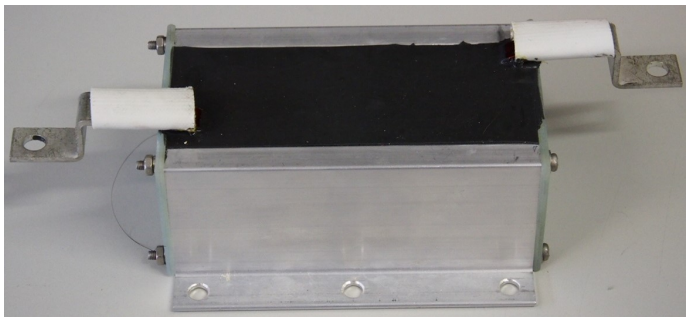

Figure 7.1: Inductor

The capacitor chosen, besides having a capacity higher than the value calculated in 5, has to be able to cope with the high peak currents requested by the SRM, so it must present low ESR and low inductance. The capacitor used for the DC-link is shown in figure 7.2. The capacitor chosen is from Cornell Dubilier ®, reference 944U141K102ACM.

Figure 7.2: Capacitor

7.2 Semiconductors

There exists the necessity to purchase semiconductors both for the motor control converter and the DC/DC Buck Boost. Associated with these semiconductors, there are gate driver modules that also need to be requested. These modules were bought according to the suggestion given by the manufacturer of the semiconductors, in order to achieve perfect compatibility and easy of physical assembly. In this case, SEMIKRON®is the manufacturer.

7.2.1 DC/DC Buck Boost

The DC/DC Buck Boost converter must contain 2 transistors, connected in half bridge topology 7.3, capable of operating with $2 \times V_{max}$, being V_{max} the maximum voltage to appear in the circuit, meaning, in voltage terms, the transistors must have a V_{CES} rating of 1200 V. In current terms, I_C must be able to operate with the maximum collector current that will appear on the circuit. In a case scenario where there are no losses, and the output current is constant and equal to the maximum motor current, the equation 7.2 approximates fairly well the current expected in the semiconductor. D is the duty cycle of the converter, set as 0.75, in order to convert 120 V, in a worst case scenario, from

the battery pack into almost 600 V in the output of the converter and f_s is the switching frequency.

$$\Delta I_L = \frac{V_{IN,min} \times D}{f_s * L} = 30A \tag{7.1}$$

$$I_{SW,max} = \frac{\delta I_L}{2} + \frac{I_{out,max}}{1-D} = 68.2A \tag{7.2}$$

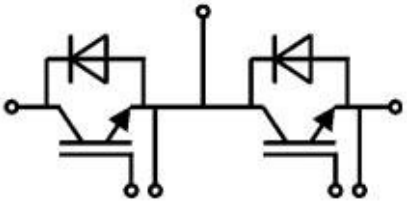

Figure 7.3: Semiconductors in Half Bridge construction

The chosen semiconductors have a nominal collector current of 100 A and were chosen taking in consideration the ON resistance (R_{CE}), as well as the voltage drop across the semiconductor and the energy required in the commutation. The reference of the semiconductors is "SKM100GB12V", seen in figure 7.4.

Figure 7.4: Half Bridge Semiconductors

7.2.2 Motor control converter

For the motor control converter, the same principle used before is employed, being the V_{CES} rating of the semiconductors 1200 V and the I_C rating superior to the maximum current at the output of the DC/DC Buck Boost converter, which was seen before to be approximately 20 A. This leads to a choice of two semiconductor devices, in two different

construction methodology, one, the so called ”GAL” topology and the ”GAH” topology, that can be seen in figures 7.5 and 7.6, respectively. Two of these packages allow the creation of the mentioned before ”1.5 Diode and Transistor Configuration”.

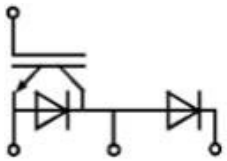

Figure 7.5: Semiconductors in GAL construction

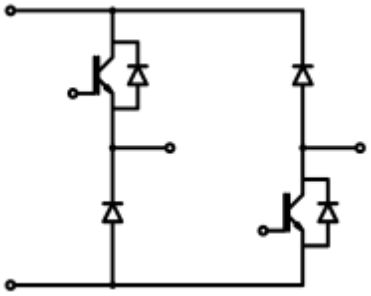

Figure 7.6: Semiconductors in GAH construction

The chosen semiconductors:

- GAL: SK35GAL12T4 (figure 7.7)

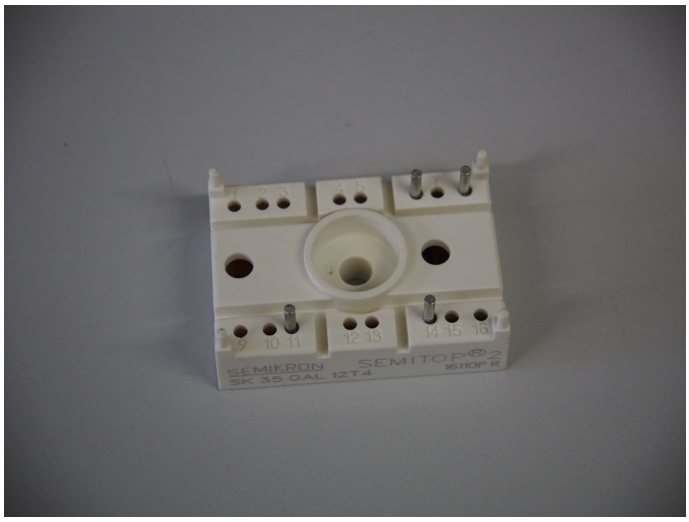

Figure 7.7: GAL semiconductor used

- GAH: SKM25GAH125D (figure 7.8)

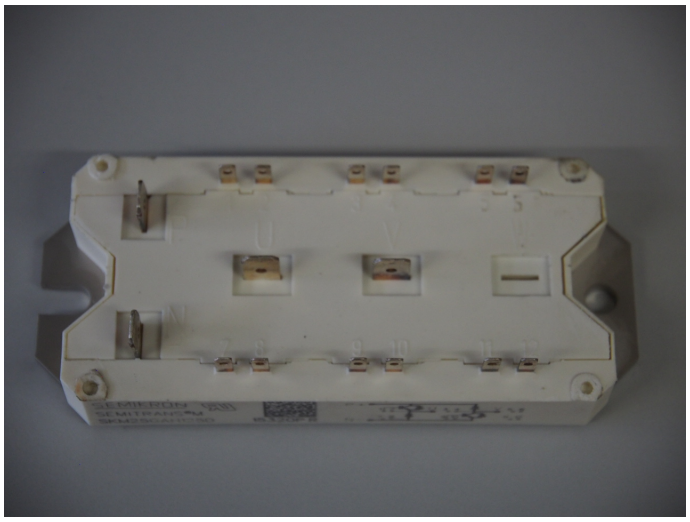

Figure 7.8: GAH semiconductor used

7.3 Power Losses and Heat Sink

Inherent to electronics, especially power electronics, are power losses. There is no perfect system, capable of presenting a 100% efficiency. The power losses cause the rise of the temperature of the electronics and, in order to assure the correct operation of the components or the longest period possible, power losses must be calculated and heat sinks must be designed for assuring the best possible working conditions for the electronics.

INFINEON ®and FUJI®offer manuals ([33], [34] and [35]) on how to calculate the major losses in IGBTs and design of heat sinks. Such calculations were made for both the DC/DC buck boost converter and the motor control converter. The losses in inductors and capacitors weren't taken in account, as the decision on the components to purchase was not concluded at the time that this report was elaborated. The worst case scenarios were carefully analysed in order to reach the worst possible outcome of power being dissipated and the values found are as follows:

- Maximum losses for the semiconductors on DC/DC Buck Boost: $P_{max} = 442W$
- Maximum losses for the semiconductors on motor control converter: $P_{max} = 381.56W$

Meaning that the power converters, in a worst case scenario, will have losses around 10% of the nominal power.

It is expected that the efficiency of the power train, in reality, will be lower than expected, as there are many factors that these calculations don't account for. However, these losses, along with the thermal resistances mentioned in the several datasheets, enabled the selection of a heat sink for the converters. The heat sink's reference is ABL Components 164AB2000B and it's thermal resistance is of 0.12ºC/W (figure 7.9).

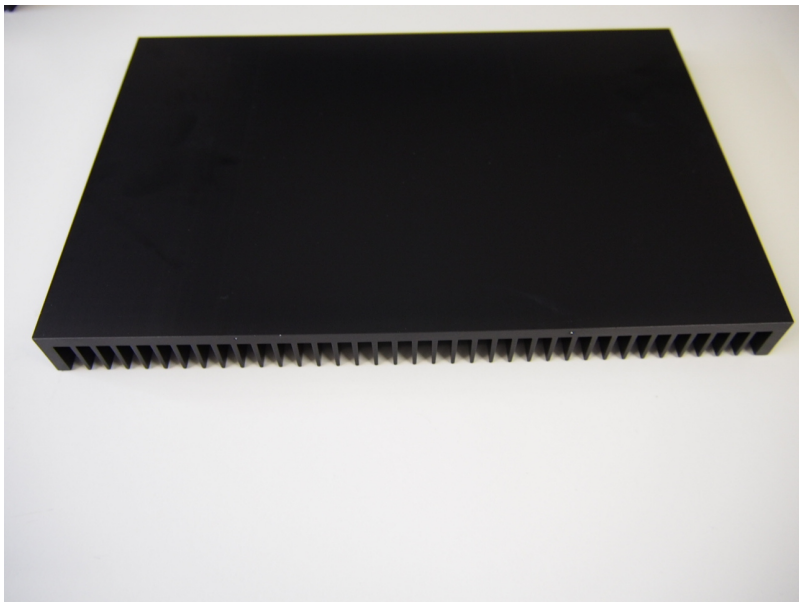

Figure 7.9: Heatsink used

7.4 Sensors

7.4.1 Voltage Sensor

In order to establish feedback in the system, so as to control it's operation, one must resort to sensors, in several points of the power train.

To control the operation of the DC/DC bidirectional buck boost converter, a voltage sensor will be required, to assure the correct response of this subsystem. For this, a voltage sensor was requested, capable of measuring the high DC voltage and provide isolation from the power electronics of the converter. The reference of the sensor is ACPL-C87BT-000E and it can be seen in figure 7.10. This sensor is then placed in a Printed Circuit Board (PCB), with a circuit similar to the recommended by the manufacturer in the sensor's datasheet. In figure 7.11, the PCB is presented, placed on top of a capacitor, as it will be used in this project.

Figure 7.10: Voltage sensor

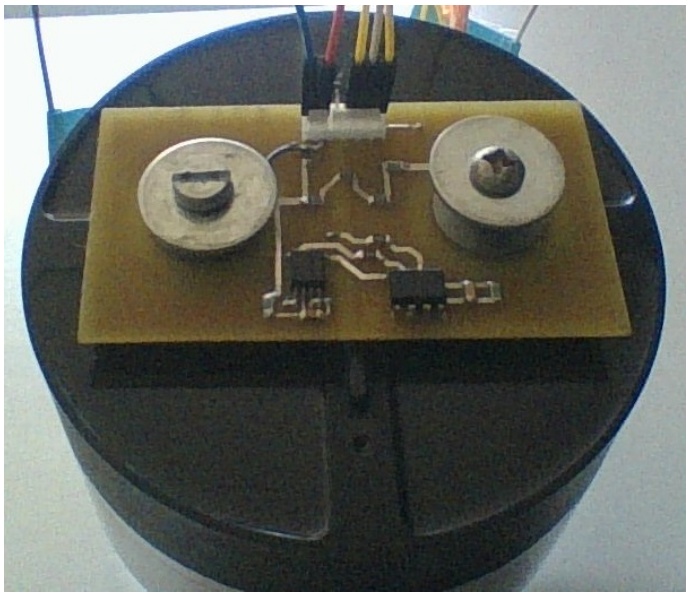

Figure 7.11: PCB used for the voltage sensor

7.4.2 Current Sensors

As mentioned before, the correct control of the phase currents in SRM is vital for a good operation of the electric machine. With that in mind, four current sensors, one for each phase, with good accuracy and linear response to a measured current are to be used, in order to provide feedback to the control platform on the operational status of the SRM. The reference of the sensors chosen is ACS759LCB-50B and are similar to the one present in figure 7.12, with capacity to measure from $-50A$ up to 50 A. The DC/DC converter also employs a current sensor, with a higher current rating, from -100 A to 100 A.

Figure 7.12: Current sensor

7.4.3 Shaft Position Sensor

Another sensor that is required is a rotor position sensor, in order to deliver to the control platform the information that enables it to compute the next phase to be turned ON and the moment when to commute. This information is given by an optical incremental encoder. The encoder available is RS®reference 795-1144 and has 5000 points per revolution, a maximum speed of 6000 rpm. It can be seen in figure 7.13. It outputs 3 signals that enable the position calculation: two square waves, with a phase shift of 90 degrees between them, and an index signal, that is generated once per rotation cycle of the encoder.

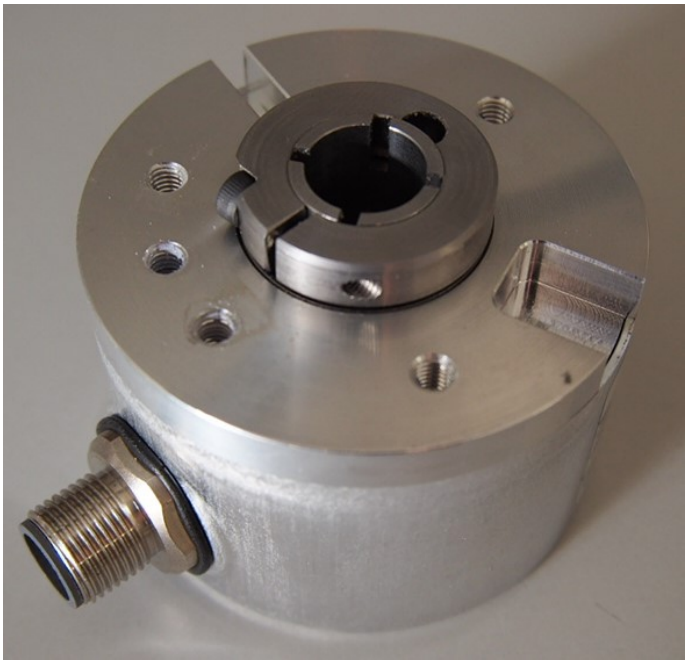

Figure 7.13: Encoder used

7.5 Assembly

The assembly of the previously mentioned components had to be done with a step sequence similar to the assembly of the parts of the motor 4.2. First, the CAD of the different components is created, according to the dimensions indicated in the datasheet, or using existing models, given by the manufacturer. Then, a study on the fixation elements and space constraints was done, having as motive the fact that parasitic elements of the connection cables can be diminished if the space is optimized and components that need to the connected are close to one another. Another factor that was taken in account was the placement of the fixation holes in the heat sink, once these can cause a lower capacity

of heat dissipation. Figure 7.14 shows the 3D CAD model created, for prediction of space usage and component distribution, on the heatsink.

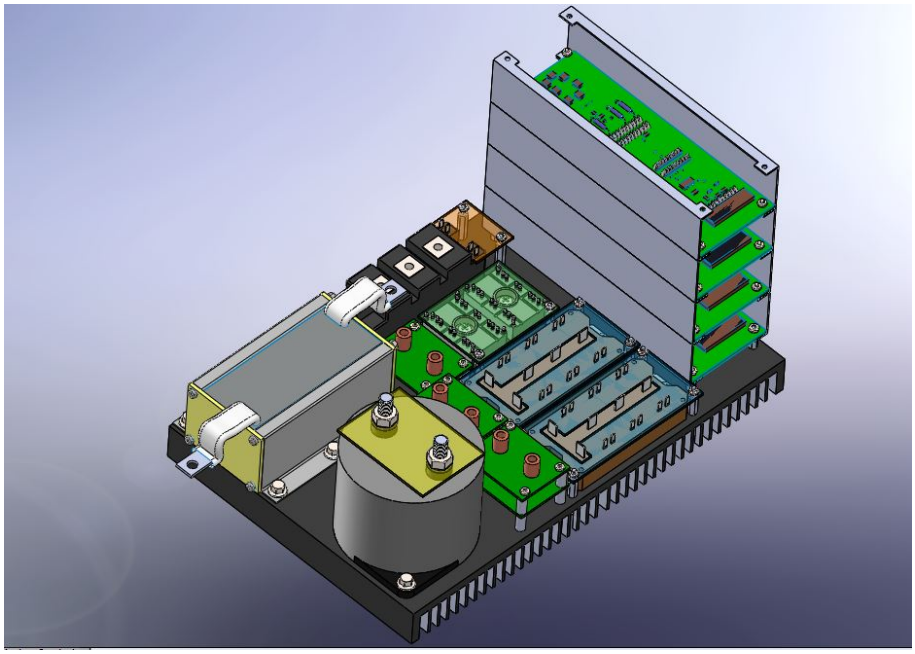

Figure 7.14: CAD component assembly

The heat sink was then computed in CAM software and, using a CNC machine, the holes for the fixation of the several elements to be placed on the heat sink were made. The final result of the assembly is in figure 7.15.

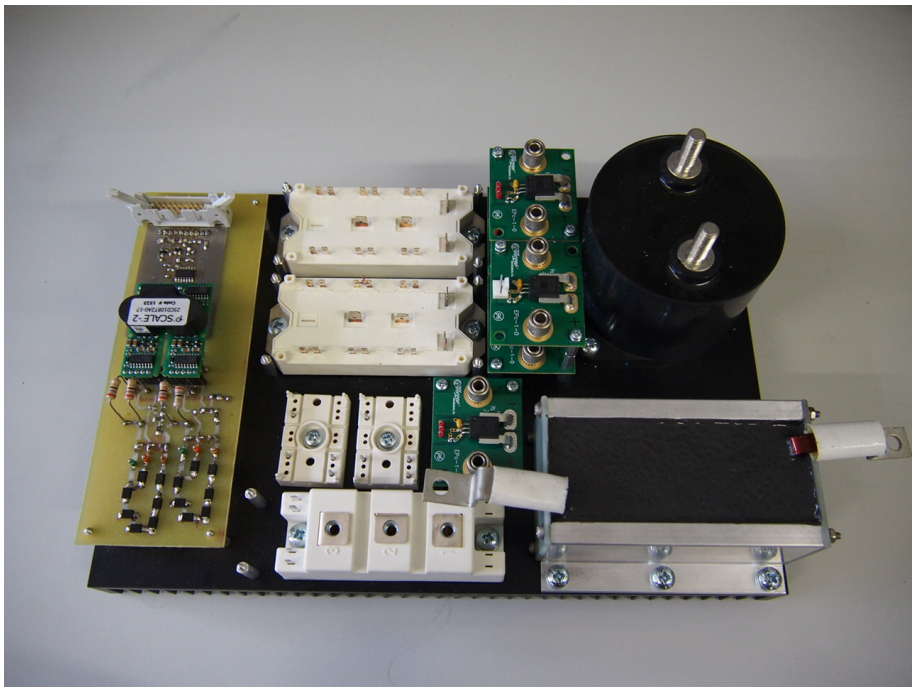

Figure 7.15: Converter′s component assembly

7.6 Printed Circuit Boards

Several PCB had to be designed for the implementation of the system, using National Instrument's Ultiboard®. Excluding the previously mentioned voltage sensor board, essentially, the boards created can fit into three groups:

- **Driver boards**

  The driver boards are used as a bridge between the control platform and the semiconductors. They are created to lodge the driver module 7.16 and some passive elements, including the gate resistors, so as to attack the gate of the transistors and force their commutation in the time calculated. First, a prototype board was created (figure 7.17), and, after testing and validation of the board's operation, final boards were sent to manufacturing. The result without components, can be seen in figure 7.18. In figure 7.19, the final driver board can be seen.

- **Interface boards**

  The interface boards are needed for an easy and secure connection of the semiconductor's control pins to the control board. They hold connectors and are specifically made to fir in each of the semiconductor's modules employed in the project (figures 7.20, 7.21, 7.22).

- **Control board**

The control board is by far the most complex board designed. It holds three DC/DC converters, so to feed all the electronics it possesses. It is composed by two levels. It has a place to connect the control platform, the XMC4500 (in figure 7.23), several connectors to take the signals from the sensors to the control platform and it includes buttons, for enabling/disabling parts of the system, such as the DC/DC or the motor converter. For debugging purposes, it also hosts many LEDs (Light Emitting Diodes), associated with status or errors, such as short circuits detected by the driver board on the semiconductors. The board can be seen in figure 7.24, where the two levels are assembled and in their final position.

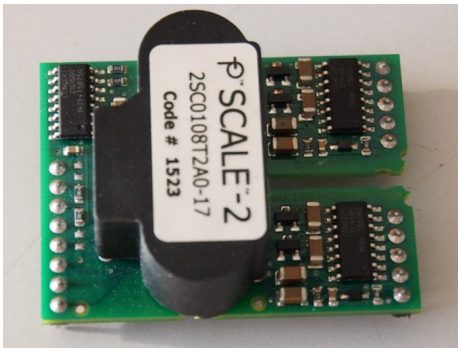

Figure 7.16: Driver Module

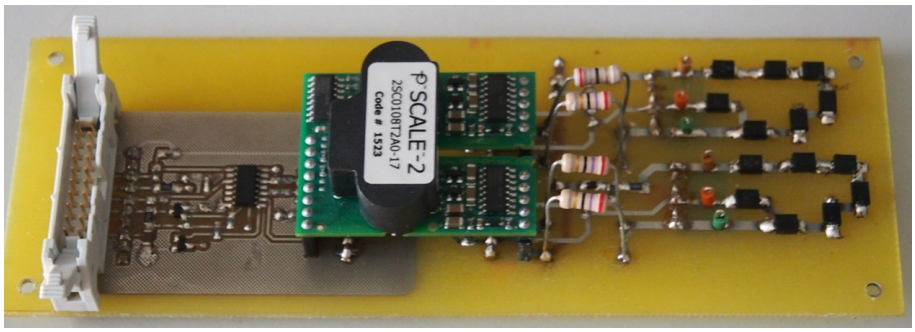

Figure 7.17: Driver prototype board

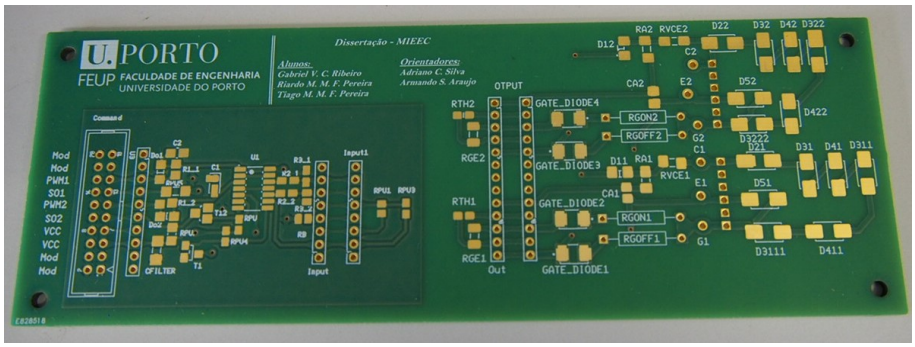

Figure 7.18: Final driver board (without components)

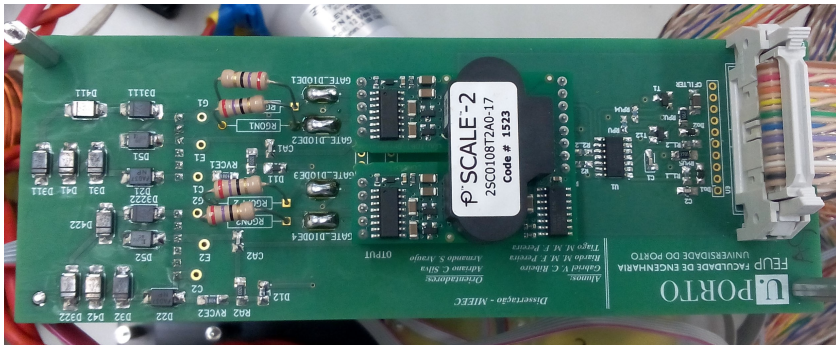

Figure 7.19: Final driver board (with components)

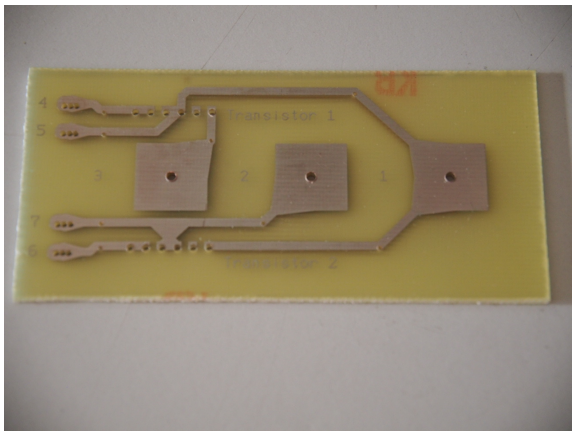

Figure 7.20: Interface board for SKM

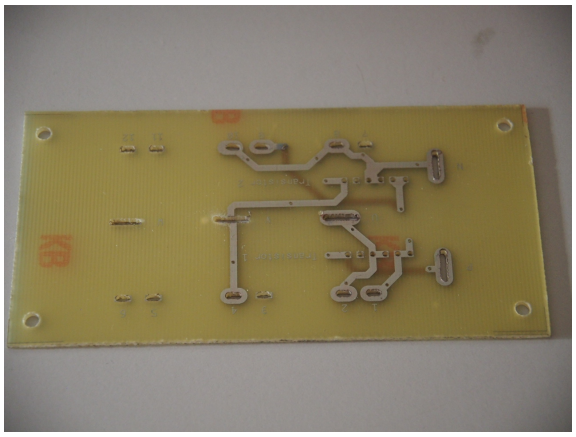

Figure 7.21: Interface board for GAH

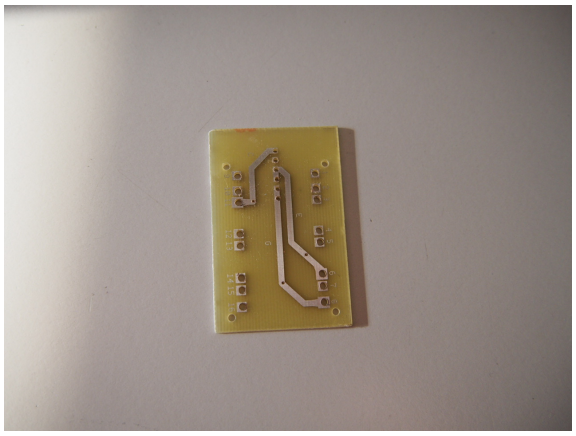

Figure 7.22: Interface board for GAL

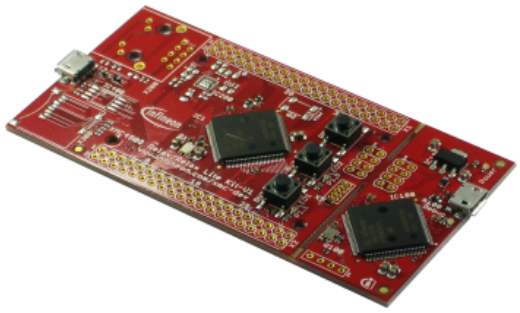

Figure 7.23: Control platform, the XMC4500

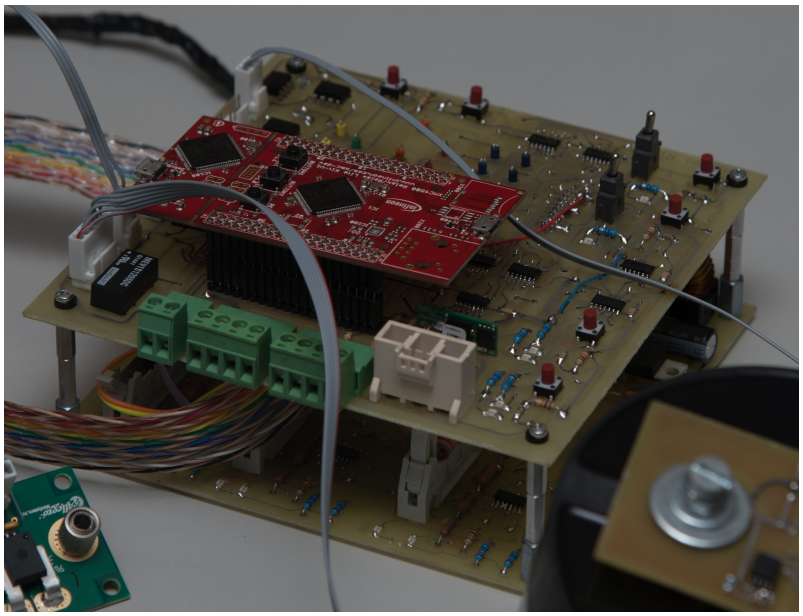

Figure 7.24: Control board

7.7 XMC4500 Programming

Infineon's ®XMC4500, can be programmed using an Eclipse-based IDE with a GNU C-compiler, named DAVE. DAVE's programming is based on the use of applications (APPs), often configured using specific GUI. For this dissertation, several instances of some APPs were used, each one with its purpose, as follows (APP name : Usage):

- ADC002: Used for analog to digital conversion, of signals created by current and voltage sensors.
- IO001: Used for configuring a pin in analog mode, where the sensors will be connected.
- IO004: Used for configuring a digital pin as a GPIO, for diagnosis purposes.
- PWMSP002: Used to generate a single phase PWM waveform, in order to control the commutation of the semiconductors in the system.
- POSQE001: Used for analysing the signals created by the quadrature encoder, for position tracking of the motor's rotor. It outputs the angle of the rotor in degrees and the speed, in rpm.
- NVIC002: Used to generate user defined interrupts. Useful for executing certain parts of the code with a certain frequency.

- CCU4GLOBAL: Capture Compare Unit 4, is used to configure the sharing of the global resources of the CCU4 module between APPs [36].

- CCU8GLOBAL: Same as CCU4, only it is used for the CCU8 module [37].

- DBG002: Used for debugging the code. Allows a complete overview on the values of the variables used. In this case it is used with serial communication.

- ADCCH001: Used to configure the ADC channel and result register.

- ADCGLOB001: APP responsible for setting the ADC clock and configure ADC's global registers.

- ADCGROUP001: Used to configure each specific ADC group.

Most of the APPs have dependencies on other APPs in order to proper operate, such as clock and reset signals. These APPs are generated automatically and their behaviour results as a consequence of the configuration made for the parent APP. In figure 7.25, it can be seen the final connectivity software diagram of all the APPs used for the control of the system.

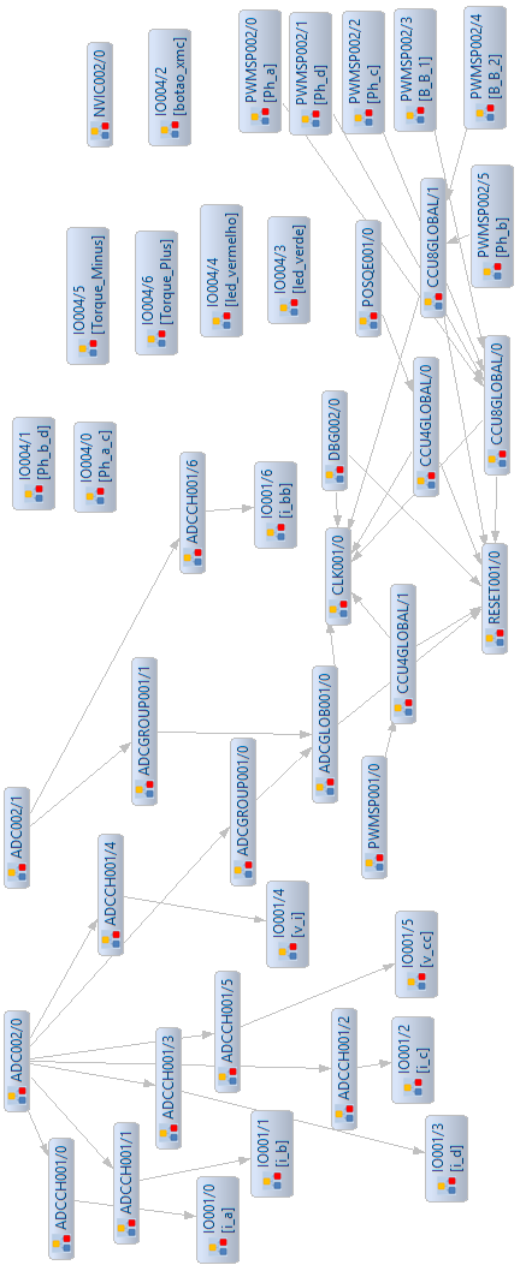

Figure 7.25: Network of connection of the DAVE APPs

7.8 Results

Upon assembling and connecting all of the subsystems, several tests were run, in order to validate the functioning of the system. In figure 7.26, the final assembly is presented.

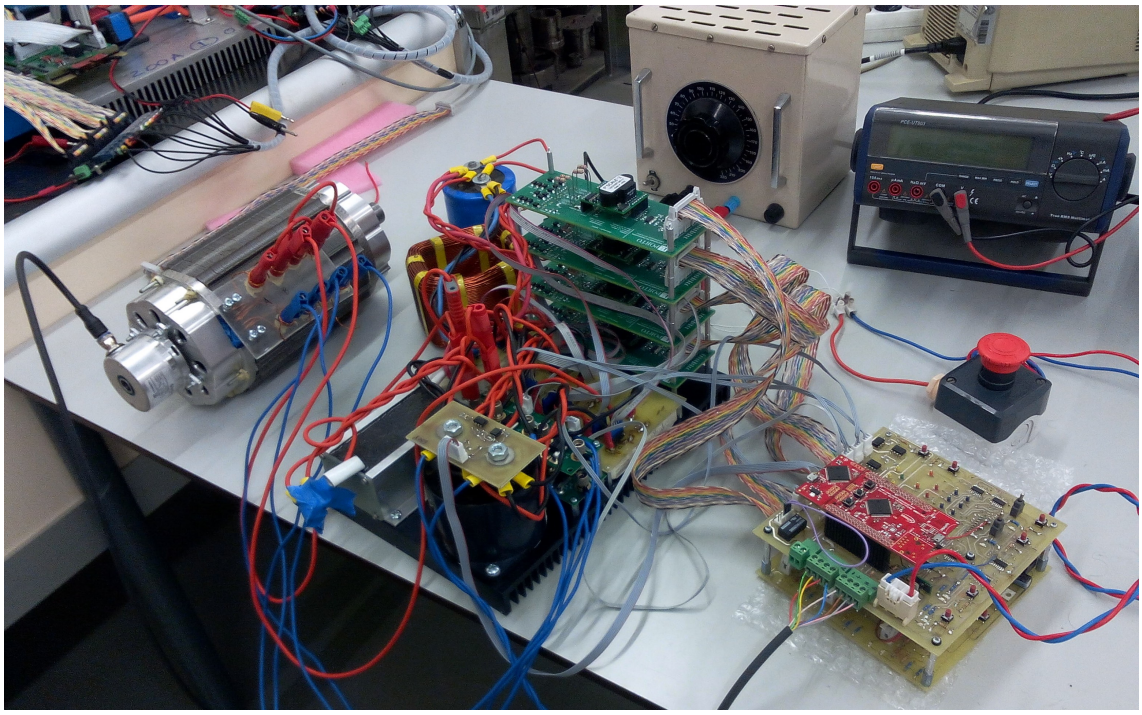

Figure 7.26: Bench assembly of the system

7.8.1 DC/DC

In figure 7.27, it can be seen the conversion of the input voltage, in green, around 30V, to the output voltage, blue, of 115V. Since this test was made with a fixed duty cycle of 75 % and load, it can be concluded that the DC/DC converter is achieving a satisfactory conversion ratio (output voltage should be 4 times the input voltage, it is 3.8 times higher). The test was done with a load that was sinking 10A approximately.

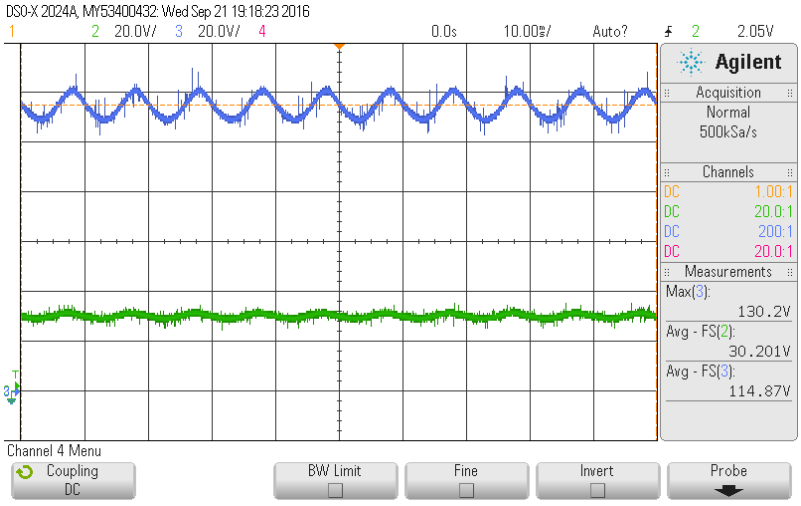

Figure 7.27: Result on the conversion ratio verification

7.8.2 SRM

Due to the lack of a torque sensor, the torque response of the motor couldn't be accurately measured. The results of the tests made can be seen in figures 7.28, 7.29 and 7.30. In these print screens of the oscilloscope, it can be seen, respectively, the commutation of the transistors of each of the phases, the current of one phase and the sum of the current in all of the motor's phases. All these values were extracted when the motor was rotating, without load, at a near constant speed. The results serve as a start to validate the operation of the SRM, since they appear very similar to those obtained in the chapter where the control simulation is made (chapter 6). The control used was the presented in chapter 6, based on a DITC algorithm.

Figure 7.28: Gate signals of the asymmetrical bridge's semiconductors

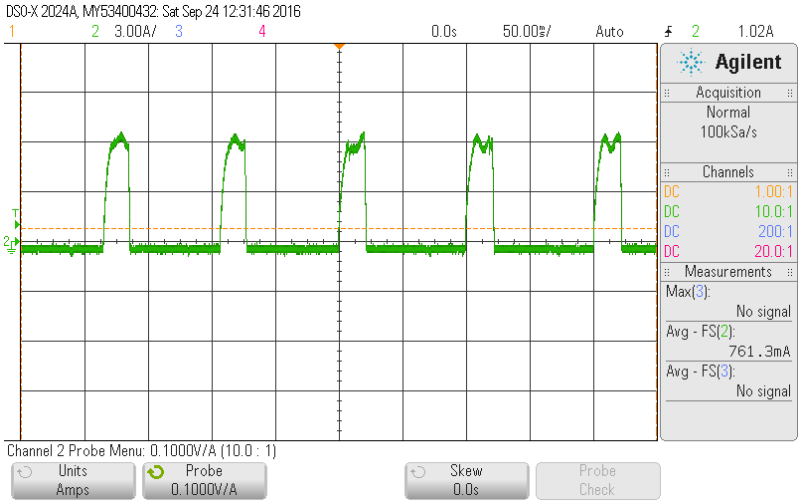

Figure 7.29: Current of one phase

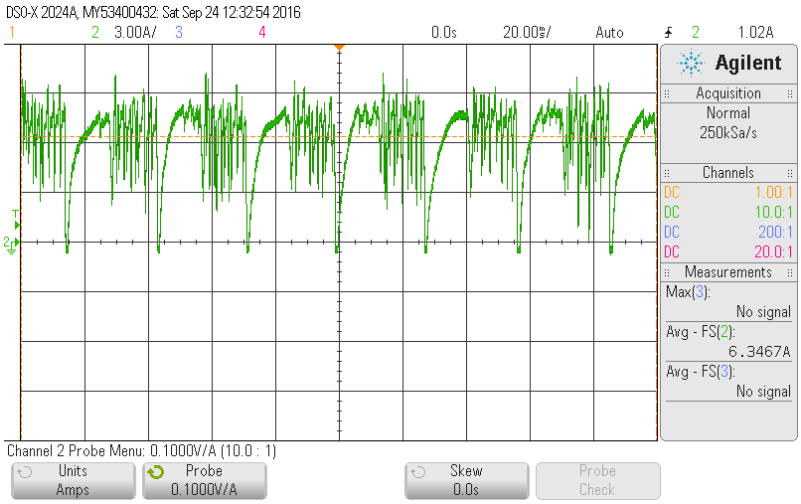

Figure 7.30: Sum of the currents from the four different phases

Chapter 8

Conclusion

In this chapter, a summary of the dissertation's report is made. The work that took place is briefly reviewed and the results are discussed. The incomplete parts of the work are analysed and from there, the future work is proposed.

As stated, the project is composed by several subsystems. In a very general point of view, the project of each of the subsystems went through a phase of research in the state of the art, followed by a simulation experiment, in several different softwares (Matlab ®, Simulink ®, MotorSolve ®, Inventor ®, Solidworks ®). When the simulation was complete, the next logical step was to search the market for the best solutions for the application, either it was on semiconductors or in mechanical components for the assembly of a bench test. The implementation took place after the arrival of the components and several unpredicted incompatibilities had to be dealt with, the best way possible.

The weeks spent assembling the system and testing all the connections and logic circuits made it impossible to run all the tests and extract all of the results needed. Some tests were even impossible to make due to the lack of instrumentation, such as an adequate torque sensor, for measuring the torque and torque ripple of the SRM. However, all the results that could be obtained from the operation of the system meet the expectations and appear to be correct, such as the phase semiconductor's commutation and driver circuitry, current, voltage and position sensor's operation, XMC programming and control algorithm.

In this thesis, a control algorithm typically used in high efficiency SRM drives is tested and implemented. All of the circuits needed for testing the electrical machine are operational. At this point, is it possible to say that all the work developed for the dissertation made it possible to have an operational bench, where one can have access to a new, 8kW switched reluctance machine. Projects of research and development in the control of these machines can now be taken into the implementation phase. The same can be said for the DC/DC bidirectional converter.

8.1 Future Work

To complete the objectives set at the start of the dissertation, this is, to place the system in the ATV and verify that the requirements are correctly fulfilled, several tasks still have to be done. Starting with exhaustive tests to the operation of the motor and DC/DC converter, with a correct measurement of torque ripple and torque response. The battery pack will have to be created and prepared for placement in the ATV's structure. All the prototype boards will have to be substituted by their final version and all the cables will have to be made again, this time with the length needed to connect the subsystems in the ATV. The input from the user needs to be adjusted to allow an easy use while driving the ATV and several mechanical metallic parts have to be designed and machined in CNC to allow a correct and reliable fixation of the subsystems to the ATV, never forgetting the need to make the system resilient to dust and humidity. It is predictable that then, the ATV will be completely ready for operation and will meet the requirements set.

References

[1] John Lowry James Larminie. *Electric Vehicle Technology Explained*. John Wiley and Sons, Ltd, 2003.

[2] Rony Argueta. A technical research report: The electric vehicle. Technical report, University of California Santa Barbara College of Engineering, 2010.

[3] R Krishnan. Whither motor drives: A case study in switched reluctance motor drives. 2007.

[4] Tausif Husain Md Wasi Uddin. Design of a switched reluctance machine for off-road vehicle applications based on torque-speed curve optimization. *IEE*, 14(3):342–351, 2014.

[5] Ali Emadi Mehrdad Ehsani, Yimin Gao. *Modern Electric, Hybrid Electric, and Fuel Cell Vehicles*. CRC Press, 2010.

[6] Mohammad Naser Hashemnia; Behzad Asaei. Comparative study of using different electric motors in the electric vehicles. 2008.

[7] TJE Miller. *Electronic Control of Switched Reluctance Machines*. Newnes Power Engineering Series. Elsevier Science, 2001.

[8] R Krishnan. *Switched Reluctance Motor Drives: Modeling, Simulation, Analysis, Design, and Applications*. Industrial Electronics. CRC Press, 2001.

[9] Dr. R. Dhanasekaran S.Muthulakshmi. Performance analysis of current controlled three phase switched reluctance motor. *Recent Trends in Engineering and Technology, Vol. 10, No. 2*, 2014.

[10] Qingguo Sun Shiyou Yang Yihua Hu Lebing Jin Chun Gan, Jianhua Wu. Low-cost direct instantaneous torque control for switched reluctance motors with bus current detection under soft-chopping mode. *IET Power Electronics*, 2015.

[11] S.L. Ho X. D. Xue, K.W.E.Cheng. A control scheme of torque ripple minimization for srm drives based on flux linkage controller and torque sharing function. *International Conference on Power Electronics Systems and Applications*, 2006.

[12] So-Yeon Ahn Dong-Hee Lee and Jin-Woo Ahn. Advanced torque control scheme for the high speed switched reluctance motor. 2011.

[13] T. J. E. Miller, editor. *Electronic Control of Switched Reluctance Machines*. Newnes, 2001.

[14] Sanzhong Bai Yu Du, Xiaohu Zhou. Review of non-isolated bi-directional dc-dc converters for plug-in hybrid electric vehicle charge station application at municipal parking decks. 2010.

[15] Salvador P. Litran Maria Bella Ferrera. A converter for bipolar dc link based on sepic-cuk combination. *IEEE transactions on Power Electronics*, 2015.

[16] Mirza Qutab Baig Suhail Ashraf Tamim Ahmed Khan Syed Murtaza Ali Shah Bukhar, Junaid Maqsood. Comparison of characteristics - lead acid, nickel based, lead crystal and lithium based batteries. *UKSIM-AMSS International Conference on Modelling and Simulation*, 2015.

[17] *HONDA FOURTRAX 250 OWNER'S MANUAL.*

[18] James Carvill. *Mechanical Engineers Data Handbook*. Butterworth Heinemann, 1993.

[19] Sandeep Dhameja. *ELECTRIC VEHICLE BATTERY SYSTEMS*. Butterworth-Heinemann, 2002.

[20] Sergio Baptista Claudio Magalhaes, Joao Nogueira. Estudo e desenvolvimento de um veiculo hibrido tendo como plataforma de base uma moto 4 honda fourtrax. Technical report, FEUP, 2012.

[21] Li Yuren Zhang Zhihui. Numerical and analytical modeling of switched reluctance machines. *Journal of Computers, vol.7, no.12*, 2012.

[22] C. Chellamuthu R. Jayapragash. Development of analytical models for switched reluctance machine and their validation. *Electrical Engineering Technology*, 2015.

[23] Hamid Gualous Monzer Al Sakka, Joeri Van Mierlo. *Basic Calculation of a Boost Converter's Power Stage*. InTech, 2011.

[24] Shraddha Deogade Apekshit Bhowate. Comparison of pid tuning techniques for closed loop controller of dc-dc boost converter. *International Journal of Advances in Engineering & Technology*, 2015.

[25] Rames C. Panda V. Vijayan. Design of pid controllers in double feedback loops for siso systems with set-point filters. *ISA Transactions*, 2012.

[26] Derek P. Atherton Dingyu Xue, YangQuan Chen. *Linear Feedback Control*. Society for Industrial and Applied Mathematics, 2007.

[27] T. Hagglund K.J. Astrom. Revisiting the ziegler-nichols step response method for pid control. *Process Control 14*, 2004.

[28] Alireza Zomorrodi Mohammad Shahrokhi. Comparison of pid controller tuning methods.

[29] JIn-Woo Ahn. *Switched Reluctance Motor, Torque Control*. InTech, 2011.

[30] L. Chen S.L. Lu Y.Z. Xu, R. Zhong. Analytical method to optimise turn-on angle and turn-off angle for switched reluctance motor drives. *IET Electric Power Applications*, 2012.

[31] C.Renuka V. Vasan Prabhu, K.S.Mahesh. Simulation of switched reluctance motor/generator with optimum turn-on and turn-off control for the application of variable speed drives. *Second International Conference on Sustainable Energy and Intelligent System*, 2011.

[32] Haitham Abu-Rub Omar Ellabban. Torque control strategies for a high performance srm drive system. *IEEE GCC Conference and exhibition*, 2013.

[33] Calculation of major igbt operating parameters. Technical report, INFINEON Technologies, 1999.

[34] Marco Purschel Dusan Graovac. Igbt power losses calculation using the datasheet parameters. Technical report, INFINEON Technologies, 2009.

[35] *FUJI IGBT MODULES APPLICATION MANUAL.*

[36] *INFINEON - Application Note - Capture Compare Unit 4 (CCU4).*

[37] *INFINEON - Application Note - Capture Compare Unit 8 (CCU8).*